T-3057

ADSORPTION OF COPPER AND LEAD ONTO GOETHITE AS A FUNCTION OF PH, IONIC STRENGTH, AND METAL AND TOTAL CARBONATE CONCENTRATIONS

by

Kathleen S. Smith

T-3057

A thesis submitted to the Faculty and the Board of Trustees of the Colorado School of Mines in partial fulfillment of the requirements for the degree of Master of Science (Geochemistry).

Golden, Colorado

Date Nov. 3, 1986

Signed: Kathleen S. Smith

Approved: Dr. Donald Langmuir,
Thesis Advisor

Golden, Colorado

Date 11/3, 1986

Dr. George H. Kennedy
Department Head,
Chemistry and Geochemistry

ABSTRACT

Aqueous copper and lead adsorption onto a well-characterized synthetic goethite was investigated at 25°C in batch experiments. Initial total metal concentrations were varied from 10^{-4} to 10^{-6} M for copper and 10^{-5} to 10^{-7} M for lead. Ionic strength (I) was adjusted to either 0.01 or 0.1 M with KNO_3 or $KHCO_3$. Final pH values ranged from about 5 to 9 in experiments with varying amounts of total dissolved carbonate (C_T). Surface area of the goethite was 31 m^2/g. Rate studies indicated that adsorption attained equilibrium within about one hour.

Nearly complete adsorption of copper and lead took place at pH values below the point of zero charge of 7.6, indicating that specific adsorption occurs. Copper is more strongly adsorbed than lead. Fractional adsorption was greater at lower metal concentrations. Differences in ionic strengths up to I=0.1 M (as KNO_3), and changes from C_T=0 to atmospheric conditions ($P_{CO_2}=10^{-3.5}$ atm.) had no effect on adsorption.

Above-atmospheric C_T conditions inhibited copper and lead adsorption. This inhibition is proportional to C_T, and is a function of pH and total metal concentration. The inhibition is probably due to copper and lead carbonato

complexing, which becomes important at pH's above 6.5-7, for C_T=0.01 M, and total metal concentrations of 10^{-4} to 10^{-5} M. This reflects the relatively weak adsorption by goethite of neutral and anionic metal carbonato complexes in contrast to strong adsorption of free ion and/or cationic copper and lead hydroxo complexes. This study indicates that the mobility of copper and lead in soil and groundwater systems is a function of their pH and C_T content.

Adsorption was successfully modeled with the surface complexation site-binding model assuming either outer or inner sphere adsorption of metal ions. Assumption of outer sphere adsorption indicates that hydroxo species are adsorbed whereas assumption of inner sphere adsorption indicates that free ions are adsorbed. It is not clear from this study which of these approaches is preferable.

Addition of reactions and intrinsic complexation constants for the adsorption of HCO_3^- and CO_3^{2-} onto goethite does not improve model fits of experimental data, and results in an overestimation of lead adsorption when previously determined copper and lead intrinsic complexation constants are used.

The surface complexation site-binding model was not able to adequately model metal adsorption inhibition at elevated C_T conditions. However, change from C_T=0 to

atmospheric conditions was successfully modeled. Adsorption density changes were qualitatively and semi-quantitatively modeled. The model gave good fits for varied ionic strengths.

TABLE OF CONTENTS

FIGURES

Figure Page

Figure Page

TABLES

ACKNOWLEDGEMENTS

I thank my advisor, Dr. Donald Langmuir, for his guidance and helpful insights. Appreciation is extended to the members of my committee, Dr. Stephen Daniel, Dr. Ronald Klusman, Dr. James McNeal, and Dr. Ronald Severson, for their patience, advice, and thoughtful comments on my work.

I gratefully acknowledge the following persons for their help and analytical expertise: P. Briggs, J. Crock, D. Dickerhoof, W. Ficklin, J. Fitzpatrick, R. Hamilton, B. Hatfield, J. Herring, R. Keil, R. Malcolm, J. McHugh, M. Ripp, P. Russell, P. Sliva, J. Taggart, and D. Updegraff.

Special thanks go to Laurie Balistrieri, John Catts, Dan Hsi, John Mahoney, Jim Ranville, Sandy Riese, and Rich Wanty for their insights and helpful discussions.

I am indebted to Lori Filipek and Jim McNeal for their support of this undertaking.

I thank Bonnie Erwin and Laurie Temple for the endless hours of drafting they put in on this thesis.

Finally, sincere appreciation goes to my husband, Steve Gebhard, for his love and encourgement at the times I needed them most.

Initial funding was provided by the U.S. Department of Interior, Office of Surface Mining, Mining and Minerals Resources Research Institute grant number G5195011.

INTRODUCTION

Trace metals in the natural environment follow a complex network of migrational pathways in which the atmosphere, lithosphere, hydrosphere, and biosphere are all involved. Basic understanding of the mechanisms which govern trace metal mobility is essential to the determination and predictive modeling of environmental pathways. This research pertains to copper and lead mobility in aqueous systems which contain mineral substrates.

It has long been noted that solubility reactions do not provide an adequate explanation for the low trace metal concentrations found in natural waters. Hence, the effect of mechanisms other than solubility control must be evaluated to explain these low concentrations. Trace metal mobilities in natural water/rock systems are usually dominantly controlled by adsorption-desorption reactions (Jenne, 1968; Hem, 1970; Leckie and James, 1974). This control is partially due to the often rapid equilibration times of sorption reactions as compared to the often longer equilibration times of water-mineral solubility reactions. Rapid equilibration rates for sorption reactions reflect the fact that sorption is predominantly a surface phenomenon.

Solubility reactions equilibrate at relatively high metal ion concentrations (dependent upon specific mineral solubilities), whereas adsorption-desorption reactions will equilibrate at any metal ion concentration below that corresponding to mineral saturation. Adsorption-desorption tends to be very effective at the low concentration levels typical of trace metals in natural waters. This tendency is illustrated by the adsorption isotherms in Figure 1. As indicated by this plot, there is significant trace metal adsorption at low dissolved metal concentrations. At these concentrations in excess of 99% of the dissolved metal is often adsorbed onto the solid phase. Such low metal concentrations are typical in the natural environment, yet little is known about adsorption mechanisms at such diminutive concentrations.

There is a pressing need to study, and so to understand and model these sorption processes and their role in the mobility of trace metals. Interest in sorption studies and their implications has been expressed by researchers in such disciplines as agronomy, geochemistry, physical chemistry, environmental sciences, medicine, and engineering. Successful predictive modeling of trace metal sorption processes has extensive applications in: (1) trace metal pollution and water treatment processes; (2) geochemical

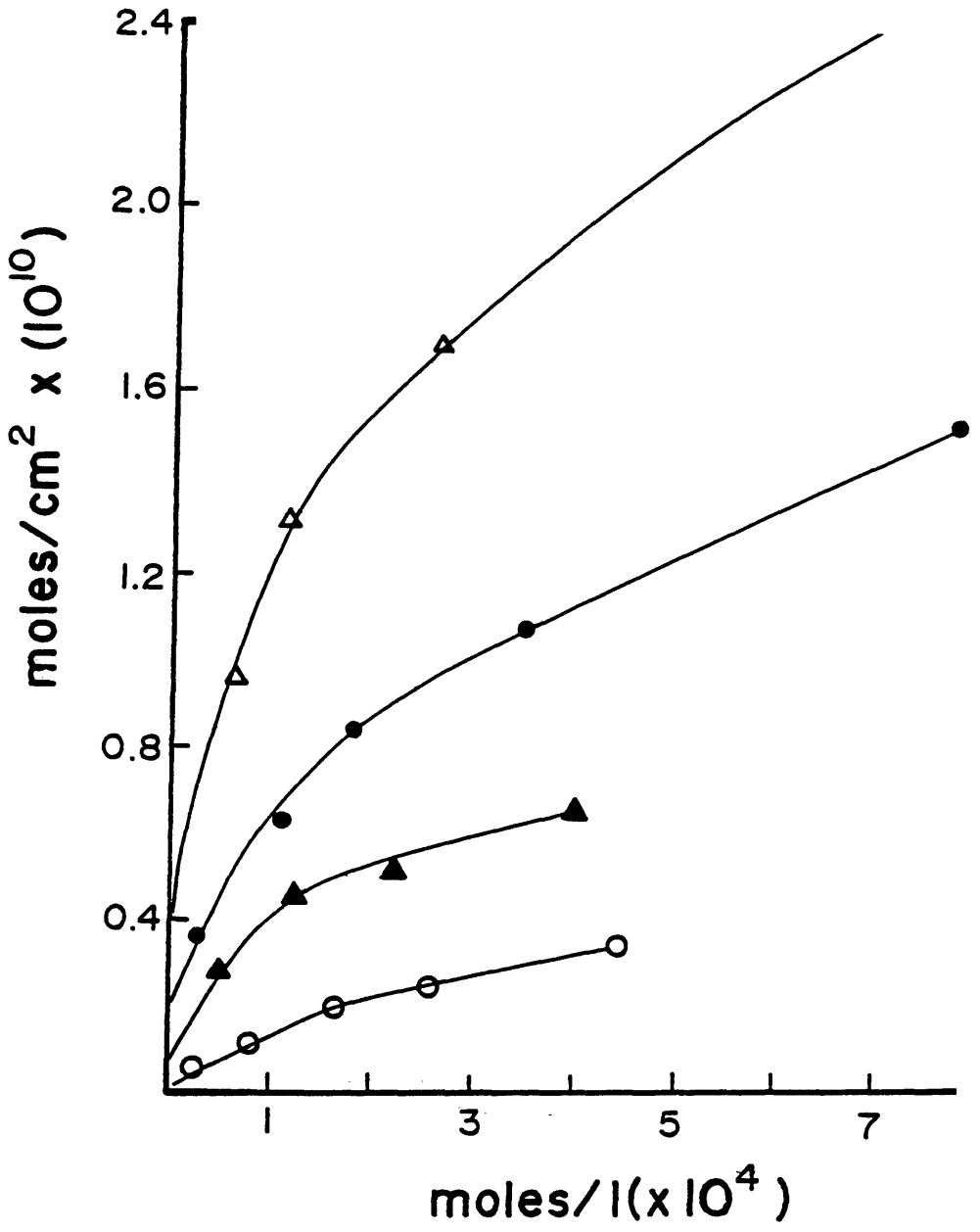

Figure 1: Adsorption isotherms of zinc on goethite in 0.1 M NaCl (after Bowden and others, 1973). Open circles are for data at pH 5.5, closed triangles for pH 6.0, closed circles for pH 6.5, and open triangles for pH 7.0.

exploration; (3) the understanding of trace metal accumulations; (4) plant and animal nutrition; and, (5) environmental health and disease.

There are two principal objectives of this study: (1) to examine the adsorption of aqueous copper and lead onto well-characterized synthetic goethite under a variety of aqueous conditions; and, (2) to model the adsorption data using the surface complexation site-binding treatment of Davis and others (1978) as applied with the computer program MINEQL (Westall and others, 1976). Goethite was chosen because it occurs naturally and is often a major component of soils, sediments, and suspended matter in streams and aquifers. It is known to have a high adsorptive capacity for heavy metals and is active in the attenuation and transport of these metals, especially at neutral to alkaline pH's (Jenne, 1968).

Sorption was studied in batch laboratory experiments using the sorbent phase in suspension. Copper and lead sorption were measured as a function of pH, ionic strength, total carbonate carbon, and metal concentration. The pH was adjusted to values between 5.0 and 9.0 using HNO_3 or KOH. Ionic strength was adjusted to either 0.01 M or 0.1 M with either KNO_3 or $KHCO_3$. The experiments were conducted at initial metal concentrations of 10^{-4} M, 10^{-5} M, and 10^{-6} M

for copper and 10^{-5} M, 10^{-6} M, and 10^{-7} M for lead. These concentration levels were chosen to simulate concentrations found in natural systems.

Thermodynamic data for Cu and Pb aqueous hydroxo and carbonato complexes and minerals were collected and used in computer program models to determine Cu and Pb speciation and solution-mineral equilibria.

BACKGROUND INFORMATION AND LITERATURE

ELECTRICAL DOUBLE LAYER THEORY

Solid surfaces acquire an electrical charge when in contact with an aqueous phase. This surface charge produces a microenvironment of electrical potential imbalance which influences the distribution of neighboring ions such that ions of opposite charge, counterions, are attracted toward the charged surface and ions of like charge, coions, are repelled away from that surface. The total net charge of the substrate and solution must be balanced to preserve electroneutrality. Under most natural conditions, the surfaces of particles in solution exhibit a net negative charge and, as a result, tend to attract cations.

Upon examination of charged surfaces in aqueous solution, it is necessary to consider both the nature of the electrical potential at the solid/solution interface and the distribution of the neighboring ions in solution. The situation is often described as a double layer of charge, the electrical double layer (EDL), in which one layer is localized next to the surface and the other layer is developed in a diffuse region extending out into the solution (Adamson, 1976; Stumm and Morgan, 1981). The

double layer results from an equilibrium between coulombic (electrostatic) forces and Brownian motion of the liquid molecules.

Historical development of EDL theory is discussed by James and Healy (1972a, 1972b), Adamson (1976), and Shaw (1980). This theory was proposed by Helmholtz in the late 1800's. He suggested that a charged particle behaved as a simple capacitor in solution. The Helmholtz model, sometimes referred to as the fixed layer model, proposes that, in order to retain electroneutrality, each charged surface in an aqueous medium has a fixed layer of counter-ions which serves to balance the charge on the surface. This purely coulombic approach is not realistic for high surface potentials.

During the early 1900's, Gouy (1910) and Chapman (1913) independently suggested a diffuse distribution of ions near a plane charged surface. They maintained that the ions at the charged surface are subject to the influence of thermal kinetic motion as well as the coulombic forces suggested by Helmholtz. These interactions result in a Boltzmann-type distribution of charge density of the ions in solution with distance from the charged surface. Shaw (1980) states that the Gouy-Chapman model assumes: (1) that the ions are point charges, thus neglecting ion size, ion solvation, and

specific adsorption of ions; (2) that a plane charged surface exists; (3) that a single symmetrical electrolyte exists; and, (4) that the solvent only affects the double layer through its dielectric constant. The Gouy-Chapman model is only quantitatively applicable for dilute solutions and for small surface potentials (Stumm and Morgan, 1981). Stumm and Morgan (1981) provide discussions of the mathematics and derivations of the equations used in these models.

Stern (1924) refined the Gouy-Chapman model by suggesting that the region near the surface be divided into two parts, the first part being a compact (Stern) layer of ions adsorbed at the surface and the second being a diffuse (Gouy) layer. Stern suggested that ions retain their hydration sphere during adsorption. The Stern model considers ionic sizes and surface attraction by something other than electrostatic force (specific ion adsorption). Therefore, Stern layer ions can be subject to both electrostatic forces and specific adsorption such that, if the specific interactions prevail, the Stern layer may exhibit superequivalent adsorption (i.e. the adsorption would overcompensate for the net surface charge) (Stumm and Morgan, 1981).

Figure 2 provides visual and graphical representations

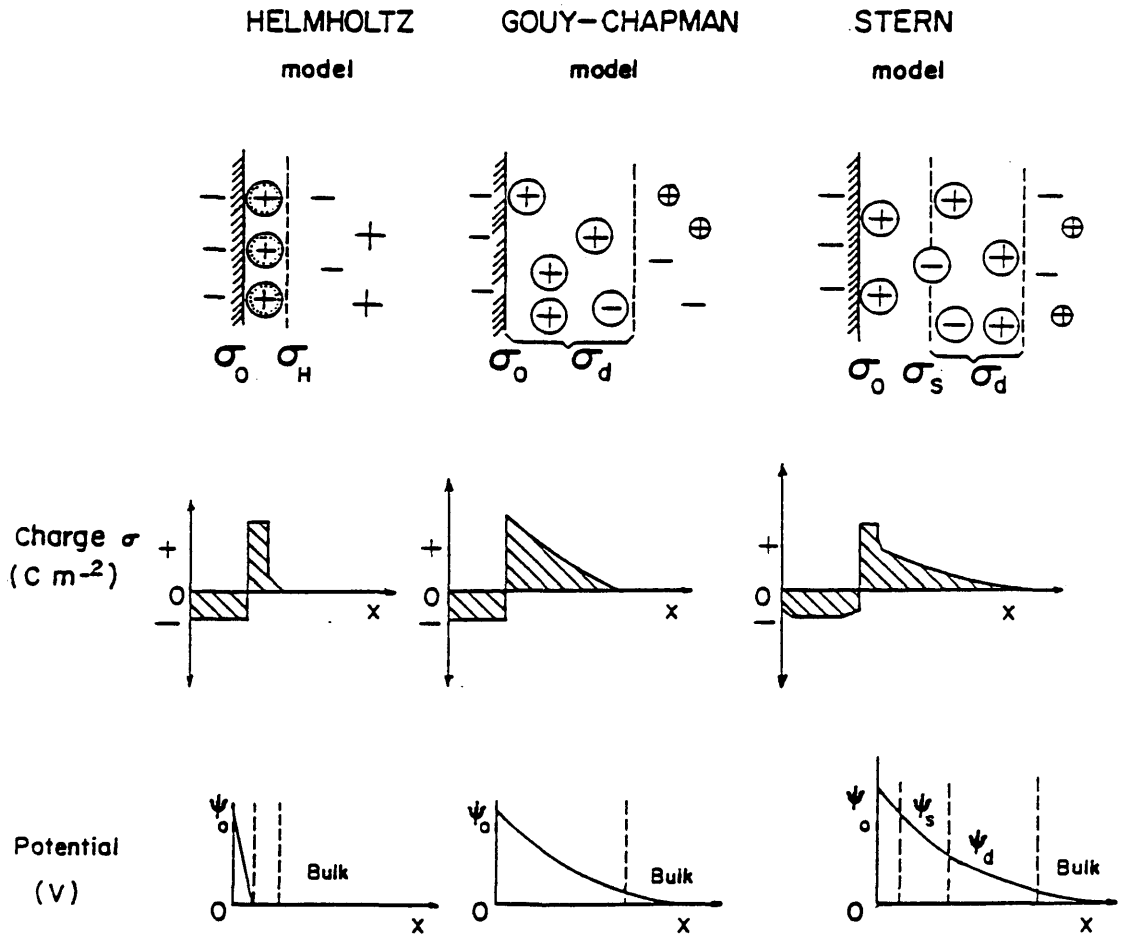

Figure 2: Distribution of charge, ions, and potential at a solid-solution interface as conceived by different models (Stumm and Morgan, 1981).

of the distribution of ions, electrical potential, and charge at the solid/solution interface as described by each of the above models for the case of a negatively charged surface where:

σ_o = (fixed) surface charge density ($\mu C/cm^2$)
σ_H = Helmholtz layer charge density
σ_d = diffuse (Gouy) layer charge density
σ_s = Stern layer charge density
ψ_o = surface potential (potential difference between the surface and the bulk solution) (V)
ψ_s = Stern layer potential
ψ_d = diffuse double-layer potential (derived from Gouy-Chapman diffuse layer theory)
x = distance from the surface of the solid (cm)

The sum of the surface charge density, the Stern layer charge density, and the Gouy layer charge density must be equal to zero in order to retain electroneutrality.

Grahame (1947) altered the Stern model with the suggestion that specifically adsorbed ions release their hydration waters from the side closest to the oxide surface. Hence, with the Grahame model specifically

adsorbed ions may approach the surface as close as a distance equal to their unhydrated radius.

James and Healy (1972a, b, c) further refined the previous models by proposing that the Stern layer is separated from the surface by at least one layer of adsorbed interfacial water molecules. Hence, the sorbed ions retain their inner hydration spheres. This model serves to preclude direct chemical bonding and, in most cases, favor the adsorption of hydrolyzed species over free ions. The James-Healy model is based on the idea that the free energy of adsorption consists of three separate terms:

$$\Delta G_{ads} = \Delta G_{coul} + \Delta G_{solv} + \Delta G_{chem}$$

where ΔG_{coul} is the coulombic term, ΔG_{solv} is the solvation term, and ΔG_{chem} is the chemical term. The coulombic term can either favor or oppose adsorption based on the net surface charge. The solvation term is related to the amount of energy required to remove the secondary hydration sheath from the adsorbing ion. The chemical term is used as a fitting parameter.

SURFACE CHARGE MECHANISMS

Stumm and Morgan (1981) describe three possible origins of surface charge including: (1) chemical reactions at the surface of the particle; (2) crystalline imperfections, broken bonds, and isomorphous replacements within the crystal lattice; and, (3) ion adsorption. These different origins of surface charge are categorized into two idealized end-member types of charge distribution: (1) constant surface potential (e.g. metal oxides and hydroxides, and edges of clay minerals) where the surface charge is dependent on the composition of the surrounding solution, but the magnitude of the surface potential is not affected by the presence of indifferent electrolytes; and, (2) constant surface charge, which is approached by smectites, where the surface charge is independent of the surrounding solution composition (van Olphen, 1977; Stumm and Morgan, 1981). Many minerals exhibit combinations of these idealized end-member types of charge distribution. A discussion of the fixed surface potential charge distribution follows.

Fixed Surface Potential
(Metal Oxides and Hydroxides)

Burns and Burns (1977) have described the structure of goethite as double chains of linked $[Fe(O,OH)_6]$ octahedra with orthorhombic symmetry obtained by cross-linkage of adjacent double chains through corner sharing of oxygen atoms. The structure of goethite lends itself to the fixed surface potential type of charge distribution.

Many oxides, hydroxides, hydrous oxides, and organic materials contain ionizable functional groups. Surface charge can originate from the dissociation of surface functional groups. For example, the OH group on the surface of an hydroxide may dissociate in a near neutral (sometimes moderately acidic) or alkaline aqueous medium in a manner analogous to a weak acid:

$$S\text{-}OH^0 \rightleftharpoons S\text{-}O^- + H^+_{(aq)}$$

where S is a part of the mineral structure and the OH group is on the surface of the mineral. By dissociation of adsorbed water molecules, oxides can obtain charged surfaces in a similar manner.

The charge on the particle surface is dependent on the pH of the surrounding medium such that neutral or alkaline

conditions will result in a negatively charged surface by loss of a proton (hydrolysis). Under acidic conditions, excess protons are adsorbed on the surface yielding a positively charged surface. These simple amphoteric ionization reactions of surface sites can be represented as follows:

$$\underset{\text{(low pH)}}{S\text{-}OH_2^+} \rightleftharpoons S\text{-}OH^o + H^+ \rightleftharpoons \underset{\text{(high pH)}}{S\text{-}O^-} + H^+$$

where S is a part of the mineral structure. At some intermediate pH, termed the point of zero charge (PZC), the net surface charge will be equal to zero such that:

$$[S\text{-}OH_2^+] = [S\text{-}O^-]$$

The PZC for Fe oxides varies from below 6 to 9, so natural Fe oxides are usually near their PZC in natural waters (Parks, 1965). Because the charge on the surface is controlled by the amount of H^+ and OH^- in solution, these ions are considered to be the potential determining ions (PDI's).

Davis and others (1978) state that, in addition to the reactions involving protons and hydroxide ions, there can be

complexation reactions; the word "complexation" in this context does not imply any particular type of bonding. In these complexation reactions, counterions are able to interact directly with the surface and adsorb to neutralize specific sites. The formation of surface complexes readjusts the acid-base equilibria and affects the proton balance (Davis and others, 1978).

Uptake of cations by oxides and hydroxides is strongly pH dependent. In the case of nonspecific adsorption, there is essentially no cation adsorption (other than H^+) at low pH's (positive surface charge) but, at high pH's with extensive ionization of surface functional groups and an increasingly negative surface charge, virtually all cations are strongly adsorbed. For most monovalent cations (except H^+), adsorption is usually nonspecific (bonding by electrostatic force) (Kinniburgh and Jackson, 1981). In the case of divalent cations, specific adsorption can occur, particularly at trace cation concentrations. Different substrates have different affinities for such cations.

There is a narrow pH region, known as the adsorption edge, in which the transition from essentially no adsorption to essentially complete adsorption (>99%) takes place (James and Healy, 1972b; Kinniburgh and Jackson, 1981). This pH region is characteristic of the particular adsorbing metal

ion, its concentration, and to a lesser extent on the particular substrate. The rapid increase in percent metal uptake is accompanied by a net release of H^+ (or a net uptake of OH^-) (James and MacNaughton, 1977; Kinniburgh and Jackson, 1981). It should be kept in mind that these proton exchanges involve specific adsorption of multivalent cations (Kinniburgh and Jackson, 1981). It is not clear if the protons released come from ion exchange reactions with surface OH groups or from the preferential adsorption of hydroxo complexes, or both.

DISCUSSION OF SORPTION MODELS

Many researchers have endeavored to model and predict the behavior of metals in soil and ground water systems. The numerous modeling approaches can be separated into three general categories: (1) Adsorption isotherm equations (Posselt and others, 1968; Soldatini and others, 1976; Riffaldi and others, 1976; Garcia-Miragaya and Page, 1976; Harmsen, 1979); (2) Mass action models (Krishnamoorthy and Overstreet, 1949, 1950; Garrels and Christ, 1965; Truesdell and Christ, 1968; Bittel and Miller, 1974; Maes and others, 1975; Langmuir, 1981); and (3) Double layer and surface complexation models (Menzel and Jackson, 1950; Dugger and

others, 1964; James and Healy, 1972a, 1972b; Huang and Stumm, 1973; Steger, 1973; Hildebrand and Blum, 1974; Yates and others, 1974; James and others, 1975; Schindler and others, 1976; Hohl and Stumm, 1976; Bowden and others, 1977; Davis and others, 1978; Davis and Leckie, 1979; James and Parks, 1982; James and others, 1981; Westall, 1980). Each of these categories is discussed in following sections and examples of some of the models are given.

Adsorption Isotherm Equations

Several theoretical and empirical mathematical equations have been formulated to describe adsorption density. Adsorption density is defined as the number of moles of adsorbate C adsorbed per unit mass of adsorbent. Two of the adsorption isotherm equations are discussed below.

The Langmuir isotherm was originally developed to describe gas molecule adsorption by tungsten at high temperatures with only one type of adsorption site and a single adsorption energy potential. It has since been applied to adsorption from solution. Several assumptions are inherent in the Langmuir isotherm: (1) the energy of adsorption must be constant and independent of surface coverage; (2) adsorption takes place on localized sites; and

(3) total adsorption is limited to a monolayer coverage of the surface. The Langmuir isotherm can be expressed as:

$$X = \frac{X_m \, bC}{1 + bC}$$

where X is the amount of sorbate adsorbed by a given mass of sorbent (micrograms/gram), C is the equilibrium concentration of sorbate in solution (micrograms/liter), X_m is the adsorption maximum at monolayer coverage (micrograms/gram), and b is an empirical constant related to the free energy of adsorption. The isotherm equation can be linearized, by first inverting, to give:

$$\frac{1}{X} = \frac{1}{X_m} + \frac{1}{X_m bC}$$

for graphical evaluation of the constants X_m and b.

The Freundlich isotherm may be written:

$$X = KC^{1/n}$$

where X and C are as defined above, and K and 1/n are positive empirical constants (n >1.0 in most cases). Log transformation of the equation allows estimation of the constants via a linear plot of empirical adsorption data:

$$\log X = \log K + 1/n \log C$$

The Freundlich isotherm can describe extreme cases of the Langmuir isotherm where C is very large or very small. At low concentrations of C, the Freundlich equation does not express X as a linear function of C thereby predicting infinite surface coverage at infinite concentration (Rubin and Mercer, 1981). The simple Langmuir and Freundlich isotherms are restricted in use to constant pH conditions when protons compete for adsorption sites with cations or anions.

Mass Action Models

The reaction for homovalent ion exchange involving monovalent cations may be written:

$$A^+_{(aq)} + BX = AX + B^+_{(aq)}$$

where A^+ and B^+ are exchangeable cations, and X represents the negatively charged sorbent framework. Where a monovalent and a divalent cation are competing for exchange positions, the reaction may be written:

$$A^{2+}_{(aq)} + 2BX = AX_2 + 2B^{+}_{(aq)}$$

Ion exchange takes both valence and other properties of the individual ions into account. It allows for the possibility that one ion might be preferred over another due to size or the character of chemical bonding (Ozsvath, 1979). For the case of monovalent-monovalent exchange, ion exchange may be written as:

$$K_{ex} = \frac{[B^+]\ (AX)}{[A^+]\ (BX)}$$

A specific condition of ion exchange is Donnan exchange (K_{ex}=1) which considers only valence effects and relative solution concentrations but not ion size. For the case of monovalent-monovalent exchange it can be expressed as:

$$K_{ex} = \frac{[B^+]\ (AX)}{[A^+]\ (BX)} = 1.0$$

and for monovalent-divalent exchange:

$$K_{ex} = \frac{[B^+]^2\ (AX_2)}{[A^{2+}]\ (BX)^2} = 1.0$$

where $[A^{n+}]$ and $[B^{m+}]$ represent the amounts in solution (molal concentrations) and (AX) and (BX) are the amounts

adsorbed (mole fractions).

A more general mass action model is the n-power exchange function of Langmuir (1981). This function is a general empirical model to relate activities of dissolved species to their adsorbed mole fractions and can be expressed as:

$$K_{ex} = \frac{[B^+]}{[A^+]}\left(\frac{(AX)}{(BX)}\right)^n$$

for the reaction

$$A^+_{(aq)} + BX = AX + B^+_{(aq)}$$

where the brackets denote aqueous molal activities of A and B, AX and BX are the mole fractions of each species on the surface, and n is a constant.

The n-power exchange function takes valence, size effects, and specific interactions into account. It corresponds to a regular solution exchange model (Garrels and Christ, 1965; Truesdell and Christ, 1968) when the mole fraction value of AX or BX lies between 0.25 and 0.75, and to the Freundlich isotherm at higher or lower mole fraction values (Langmuir, 1981).

The log form of the n-power exchange function can be

expressed as:

$$\log \frac{[B^+]}{[A^+]} = \log K_{ex} + n \log \frac{BX}{AX}$$

such that a plot of log ($[B^+]/[A^+]$) versus log (BX/AX) has a slope of n and a y-intercept of log K_{ex}.

Double Layer/Surface Complexation Models

Many models combine double layer theory (see the Electrical Double Layer (EDL) Theory section of this thesis) with a variety of other approaches for the treatment of adsorptive modeling. For example, the thermodynamic adsorption model proposed by James and Healy (1972a, 1972b) makes use of Langmuir isotherm equations. The surface complexation models proposed by Huang and Stumm (1973), Yates and others (1974), Hohl and Stumm (1976), Schindler and others (1976), Bowden and others (1977), and Davis and others (1978) all make use of mass action equations. Westall and Hohl (1980) evaluated five different models for the oxide surface/electrolyte solution interface. They found that experimental data could be described equally well by all of the models. A surface complexation type of electrostatic adsorption model will be used to model the sorption of Cu and Pb onto goethite in this study.

Surface complexation models take into account the amphoteric properties of metal oxide and hydroxide surfaces in aqueous systems. These models suggest that there is complex formation between ionized surface groups and the adsorbate. They take into account the pH dependence of the concentration of these surface functional groups (see the Surface Charge Mechanisms, Fixed Surface Potential section of this thesis).

Surface complexation models treat the reactions between solutes and solid surface functional groups as coordination reactions that obey mass action equations and mass balance equations. Hence, the concepts and mathematics of complexation processes become applicable to adsorption. The major problem with this treatment is that surface coordination reactions involve electrostatic interactions between the adsorbates and the charged surface such that the total free energy of adsorption must be separated into a purely chemical term and an electrostatic term. The various surface complexation models differ in their formulation of this electrostatic term. Also, these models differ in their description of the surface/solution interface (Morel, 1983).

The surface complexation site-binding model (or triple layer model) introduced by Yates and others (1974) and applied by Davis and others (1978) is the model used in this

thesis. It assumes the EDL to consist of two constant capacitance layers and an outer diffuse layer (see Figure 3). Protons are assumed to bind directly to surface oxides. They contribute to the surface charge, σ_0, and experience the surface potential, ψ_0.

The second layer, the inner Helmholtz plane (IHP) or "β" layer, is the mean plane of specifically adsorbed counterions. The IHP is separated from the surface by a region of capacitance C_1 (F/m^2). The ions in this second layer bind pairwise with oppositely charged surface groups by both specific chemical bonding and electrostatic bonding. These ions contribute to the charge σ_β and experience the potential ψ_β. The outer Helmholtz plane (OHP) or "d" layer is the closest that a non-specifically sorbed ion can come to the surface. These ions are separated from the surface by at least one water molecule. The IHP is separated from the OHP by a region of capacitance C_2. The potential at the OHP is ψ_d with a corresponding diffuse layer charge, σ_d.

Equilibrium mass balance reactions which contribute to surface charge through the uptake of potential determining ions and their corresponding equilibrium constants for the formation of surface species are as follows:

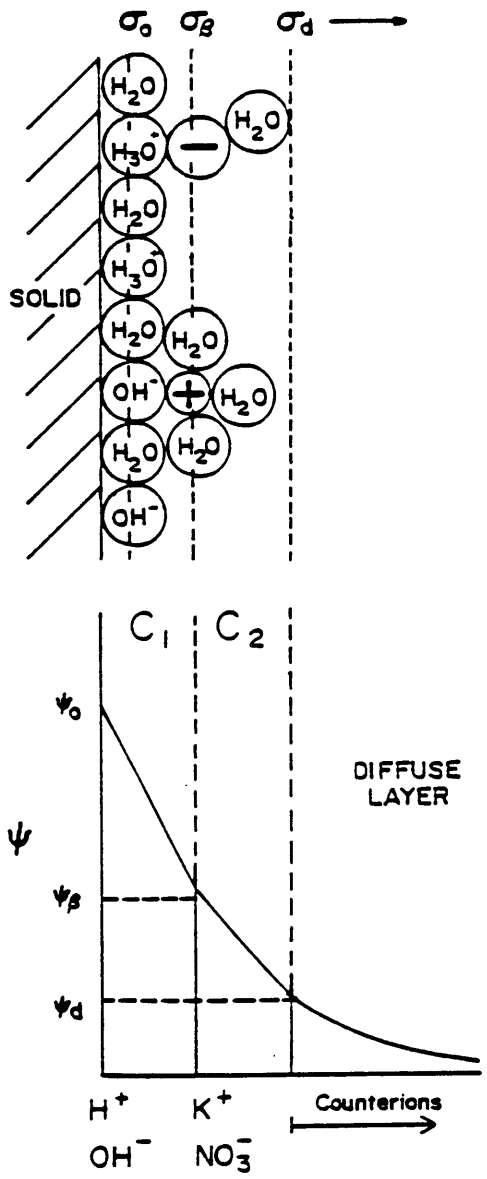

Figure 3: Schematic representation of an idealized planar oxide-solution interface and the charge distribution and potential decay away from that surface (after Davis and others, 1978). The + and - ions represent specifically adsorbed ions.

$$SOH_2^+ \overset{K_{a1}^{int}}{\rightleftharpoons} SOH + H_s^+ \qquad K_{a1}^{int} = \frac{[SOH][H^+]_s}{[SOH_2^+]} \qquad (1)$$

$$SOH \overset{K_{a2}^{int}}{\rightleftharpoons} SO^- + H_s^+ \qquad K_{a2}^{int} = \frac{[SO^-][H^+]_s}{[SOH]} \qquad (2)$$

where SOH represents a hydrated surface site, SO^- and SOH_2^+ are ionized surface sites, H_s^+ is a surface proton, and the K^{int}'s are intrinsic acidity constants determined at zero surface charge and zero ionic strength to eliminate electrostatic field effects.

The concentration of ions at some location, i, in the EDL is related to the bulk solution concentration by a Boltzmann distribution function (James and others, 1978).

$$[C^+]_i = [C^+]_{bulk} \exp^{(-ze\psi_i/kT)} \qquad (3)$$

where k is the Boltzmann constant, T the temperature (K), e the electronic charge, z the charge on the ion, and ψ_i the mean potential. With this in mind, the equilibrium constants in equations 1 and 2 can be written as:

$$K_{a1}^{int} = \frac{[SOH][H^+]}{[SOH_2^+]} \exp^{(-e\psi_o/kT)} \qquad (4)$$

$$K_{a2}^{int} = \frac{[SO^-][H^+]}{[SOH]} \exp(-e\psi_o/kT) \qquad (5)$$

Despite the high surface charge measured on oxides, studies indicate that the diffuse layer charge, σ_d, seldom exceeds 20% of the surface charge, σ_o (Yates and others, 1974). This difference in charge must be balanced by the adsorption of counterions in the IHP. To account for specific adsorption of electrolyte ions, Yates and others (1974) proposed the formation of "ion pairs" or "surface complexes" (neither term is intended to imply any particular type of bonding). These surface complexation reactions can be written as follows:

$$SO^- + C_s^+ \overset{K_{cation}^{int}}{\rightleftarrows} SO^-C^+ \qquad (6)$$

$$SOH_2^+ + A_s^- \overset{K_{anion}^{int}}{\rightleftarrows} SOH_2^+A^- \qquad (7)$$

where the subscript s denotes an ion very near the surface, A^- is an anion, C^+ is a cation, and the K^{int}'s are intrinsic complexation constants. The concentrations of these surface complexes are:

$$[SO^-C^+] = K^{int}_{cation}\,[SO^-][C^+]\,\exp^{(-e\psi_\beta/kT)} \qquad (8)$$

$$[SOH_2^+A^-] = K^{int}_{anion}\,[SOH_2^+][A^-]\,\exp^{(+e\psi_\beta/kT)} \qquad (9)$$

where ψ_β is the mean potential at the plane of specifically adsorbed counterions. It is useful to write the reactions as surface complexation reactions with uncharged surface sites:

$$SOH + C_s^+ \overset{{}^*K^{int}_{cation}}{\rightleftarrows} SO^-C^+ + H_s^+ \qquad (10)$$

$$SOH + H_s^+ + A_s^- \overset{1/{}^*K^{int}_{anion}}{\rightleftarrows} SOH_2^+A^- \qquad (11)$$

In this way the constants may be written as:

$${}^*K^{int}_{cation} = K^{int}_{a2}\,K^{int}_{cation} \qquad (12)$$

$$ {}^{*}K^{int}_{anion} = \frac{K^{int}_{a1}}{K^{int}_{anion}} \qquad (13) $$

The mass law quotients in Eqs. 1, 2, 6, 7, 10, and 11 can only be considered as thermodynamic equilibrium constants if the equilibria are expressed as surface activities. Actual surface activities cannot be directly determined. However, apparent stability quotients (Q) can be computed using solution concentrations. The quotients will not be constant (i.e. they will vary with pH and ionic strength). By use of potentiometric acid/base titration data, intrinsic acidity constants can be determined from apparent stability quotients extrapolated to zero charge and zero ionic strength. Extrapolation to zero charge and 1.0 M ionic strength will yield values for intrinsic complexation constants (James and others, 1978). This extrapolation procedure is discussed in detail in later sections of this thesis.

The equations for surface charge, σ_o, and charge in the mean plane of specifically adsorbed ions, σ_β, can be expressed as:

$$ \sigma_o = B\,([SOH_2^+] + \sum_i [SOH_2^+A_i^{n-}] - [SO^-] - \sum_j [SO^-C_j^{m+}]) \qquad (14) $$

$$\sigma_\beta = B \left(\sum_j [SO^- C_j^{m+}] - \sum_i [SOH_2^+ A_i^{n-}] \right) \quad (15)$$

where σ_o and σ_β are in terms of $\mu C/cm^2$, bracketed surface species are in mol/l, m^+ and n^- are the charge of the sorbed cation and anion, and B is a factor to convert from mol/l to $\mu C/cm^2$ ($B = 10^6$ F/Area, where F is the Faraday constant (96,500 C/mol), and Area is the surface area of the sorbent material in cm^2/l). Electroneutrality within the double layer requires that:

$$\sigma_o + \sigma_\beta + \sigma_d = 0 \quad (16)$$

The surface species are distributed among the total number of sites available (expressed as surface site density, N_s ($\mu C/cm^2$)). The surface mass balance requires that:

$$N_s = B \left([SOH_2^+] + \sum_i [SOH_2^+ A_i^{n-}] + [SOH] + [SO^-] + \sum_j [SO^- C_j^{m+}] \right) \quad (17)$$

The determination of surface site density is discussed later

in this thesis.

The site-binding surface complexation model has been incorporated into the water equilibrium computer program MINEQL (Westall and others, 1976). With this modified computer program, the concentration of surface species can be calculated from solution concentrations by use of the following equations:

$$[SOH_2^+] = \frac{[SOH][H^+] \exp^{(-e\psi_o/kT)}}{K_{a1}^{int}} \quad (18)$$

$$[SO^-] = \frac{K_{a2}^{int} [SOH] \exp^{(e\psi_o/kT)}}{[H^+]} \quad (19)$$

$$[SO^-C^+] = \frac{{}^*K_{cation}^{int} [SOH][C^+] \exp^{(e\psi_o - e\psi_\beta/kT)}}{[H^+]} \quad (20)$$

$$[SOH_2^+A^-] = \frac{[SOH][H^+][A^-] \exp^{(-e\psi_o + e\psi_\beta/kT)}}{{}^*K_{anion}^{int}} \quad (21)$$

In order to accomplish the calculation of surface species,

it is necessary to have known values for surface area, N_s, C_1, C_2, and the intrinsic acidity and complexation constants. The terms $\exp(-e\psi_o/kT)$, $\exp(-e\psi_\beta/kT)$, and [SOH] are treated as independent variables. The total number of surface sites are distributed among all the surface species such that Eqs. 1, 2, 10, 11, and 17 are satisfied. In addition, the charge balance (Eq. 16) must be satisfied where σ_o and σ_β are defined by Eqs. 14 and 15. Finally, the charge-potential relationships can be expressed through the assumption of constant capacitance values (C_1 and C_2) as shown below:

$$\psi_o - \psi_\beta = \frac{\sigma_o}{C_1} \tag{22}$$

$$\psi_\beta - \psi_d = \frac{-\sigma_d}{C_2} \tag{23}$$

The charge at the diffuse layer can be derived from Gouy-Chapman diffuse layer theory as:

$$\sigma_d = -11.74\ C^{\frac{1}{2}}\ \sinh\left(\frac{ze\psi_d}{2kT}\right) \tag{24}$$

where C is the bulk concentration of the counterion in the diffuse layer, and z is the charge of that counterion.

The modified MINEQL program solves for these parameters simultaneously in a self-consistent manner along with solution equilibria. This program can also accomodate surfaces with several types of functional groups. This is done by the definition of additional surface reactions and intrinsic constants. These additional reactions have the same form of intrinsic constant expressions as have been previously described. All the reactions can be related through mass and charge balance equations (James and others, 1978).

Summary

Langmuir (1981) points out that each of these empirical and/or theoretical approaches to adsorption modeling has some drawbacks. The isotherm and simple mass action approaches are easily manageable but are often poor predictors of natural behavior owing to their assumption of a constant surface charge and ignorance of competitive exchange effects and other properties. At the other extreme, the recently developed composite models adequately describe laboratory situations but are difficult to apply to

natural systems due to their complexity and numerous independent parameters which must be determined experimentally or estimated.

In summary, the study of sorption behavior of complex natural systems is still in its infancy. Although a variety of theoretical and empirical models have been used to explain adsorption data, their successful application to natural systems is limited or requires further testing. More research is needed to try to develop a middle-of-the-road adsorption model which can adequately describe sorption behavior in natural systems while remaining simple enough to be practical.

REVIEW OF RELATED ADSORPTION STUDIES

Several studies have examined the adsorption of aqueous metals by goethite. However, only a few researchers have sufficiently characterized the goethite for modeling with the surface complexation site-binding model of Yates and others (1974) and Davis and others (1978). Only those studies which utilized the surface complexation site-binding model to evaluate their experimental data will be discussed.

Yates (1975), and Yates and others (1974) conducted a detailed study of the structure of the oxide/aqueous

electrolyte interface. Goethite was one of the oxides studied and KNO_3 was the background electrolyte. This work introduced the surface complexation site-binding model and outlined experimental techniques to obtain required parameters for the use of this model.

Davis (1977), and Davis and others (1978) further developed the surface complexation site-binding model and incorporated it into a version of the chemical equilibrium computer program MINEQL (Westall and others, 1976). The effects of several different organic and inorganic complexing ligands on metal adsorption onto oxide surfaces were tested. Their findings show that non-adsorbing ligands decrease trace metal adsorption due to competition of the ligand with the oxide surface.

Benjamin (1978), and Benjamin and Leckie (1980, 1981a, 1981b) studied cadmium, copper, lead, and zinc adsorption onto amorphous hydrous iron oxide, lepidocrocite, α-quartz, and γ-alumina over a wide range of adsorbate concentrations, and in the presence of competing metals. Their results indicate that oxide surfaces consist of multiple groups of distinct surface sites. Furthermore, competitive adsorption experiments suggest that the group of sites which binds a metal most strongly is often distinct from that which binds another metal most strongly.

Balistrieri (1977), and Balistrieri and Murray (1979, 1981, 1982) investigated the surface properties of goethite and evaluated the effect of the major ions of seawater (H^+, Na^+, K^+, Ca^{2+}, Mg^{2+}, Cl^-, and SO_4^{2-}) on the titratable surface charge of goethite. They also examined the capacity of goethite for these ions and determined intrinsic equilibrium constants for the interactions of these ions with goethite. In addition, the adsorption of cadmium, copper, lead, and zinc onto goethite from $NaNO_3$ solutions and from major ion seawater was studied to determine the effect of the major ions of seawater on the adsorption behavior of these trace metals. Magnesium and sulfate were found to be the principal seawater ions which influence the adsorption of these trace metals. Carbonate, phosphate, and silicate were found to have little or no effect on the adsorption of cadmium and zinc onto goethite in seawater.

Hsi (1981), and Hsi and Langmuir (1985) studied uranyl adsorption onto goethite, amorphous ferric oxyhydroxide, and hematite. They emphasized the effects of carbonato and phosphato complexing, and calcium and magnesium competition on adsorption. Their results show that uranyl carbonato complexing severely inhibits adsorption. Phosphato complexing slightly enhances uranyl adsorption, and Ca^{2+} or Mg^{2+} (at 10^{-3} M) does not affect uranyl adsorption.

Tripathi (1984) examined uranyl adsorption onto goethite in the presence of carbonate, fluoride, and phosphate. As was the case in the previous study, it was shown that uranyl carbonato complexing results in a substantial decrease in uranium adsorption. However, the formation of $(UO_2)_2CO_3(OH)_3^-$ (the predominant inorganic uranyl complex in natural systems open to atmospheric CO_2) in solution did not significantly inhibit uranium adsorption. The presence of fluoride caused a slight decrease in adsorption, and phosphate resulted in a very slight decrease in adsorption.

Sanchez and others (1985) investigated the adsorption of plutonium IV and V onto goethite at high ionic strengths, varying dissolved organic carbon concentrations, and elevated dissolved carbonate concentrations. They reported that increasing concentrations of carbonate ligands decreases plutonium adsorption onto goethite. They also considered the interaction of carbonate ions with the goethite surface in their modeling calculations.

Most recently, Hayes and Leckie (1986, in press) extended the surface complexation site-binding model to include inner sphere adsorption of metal species. They used the adsorption of cadmium and lead onto goethite to test this inner sphere adsorption model for varying ionic

strengths and concluded that the assumption of inner sphere adsorption of divalent cations is more appropriate than that of outer sphere adsorption. In addition, they established the reaction stoichiometry that one proton is released per lead ion adsorbed.

This study compliments the above studies in several ways. It examines adsorption of copper and lead onto goethite under a variety of aqueous conditions including elevated dissolved carbonate. Inhibitory effects of carbonato complexing on the adsorption process have been noted by several authors (Hsi, 1981; Tripathi, 1984; Sanchez and others, 1985), but none have examined copper and lead systems. Also, attempts were made in this study to correct model calculations for the interaction of dissolved carbonate species with the goethite surface. Furthermore, the inclusion of these carbonate species in model calculations was evaluated and compared with model calculations made without these species. Finally, model calculations were performed for both inner and outer sphere adsorption of metal ions, and the two approaches compared. Hayes and Leckie (1986, in press) have also compared these two approaches, but have not carried the comparisons to changes in metal and total dissolved carbonate concentrations.

THERMODYNAMIC DATA FOR COPPER AND LEAD

Stability data for selected aquo-complexes and solids of copper and lead are given in Tables 1 and 2. Table 3 lists the free energies of formation used to calculate stability constants. These values have been incorporated into the computer program MINEQL (Westall and others, 1976) for the determination of speciation.

In order to evaluate the relative importances of precipitation and adsorption, it is necessary to determine the solid phases which would precipitate under the conditions used in this study. Figure 4 shows the predominance areas of copper species and solids as a function of pH and log P_{CO_2}. This diagram indicates that tenorite, CuO, is the thermodynamically stable cupric solid from pH 5.7 to 10 in equilibrium with atmospheric CO_2 for a total copper concentration of 10^{-4} M.

There is disagreement in the literature as to which copper phase should precipitate from solution. In order to assure that tenorite was the solid phase formed in the blank sorption solutions (no substrate present), the dark chocolate-brown precipitate was filtered and examined by X-ray diffraction and infrared spectrophotometry. The precipitate was X-ray amorphous. No carbonate, hydroxide,

Table 1: Selected formation constants for some copper aquo-complexes and compounds. Values of log K are for the cumulative formation reactions. Reactions which involve protons or hydroxide ions are written in the proton form. Complexes or compounds which contain carbonate are written as cumulative formation reactions using CO_3^{2-}.

Aqueous Species	Log K	Source and Remarks
Cu^{2+}	---	ΔG^o_f=15.67 kcal/mol (CODATA, 1977)
$CuOH^+$	-7.93	Baes and Mesmer (1981)
(for $Cu^{2+} + H_2O = CuOH^+ + H^+$)		
$Cu(OH)_2^o$	-15.3	Smith and Martell (1976) (corrected from I=1 to I=0 (Langmuir, 1984))
$Cu(OH)_3^-$	-27.5	Smith and Martell (1976)
$Cu(OH)_4^{2-}$	-39.6	Smith and Martell (1976)
$Cu_2(OH)_2^{2+}$	-10.3	Smith and Martell (1976)
$CuCO_3^o$	6.82	Byrne and Miller (1985)
$Cu(CO_3)_2^{2-}$	10.6	Byrne and Miller (1985)
$Cu(OH)_2CO_3^{2-}$	-13.0	Duby (1977)
$CuHCO_3^+$	1.8	Byrne and Miller (1985)
(for $Cu^{2+} + HCO_3^- = CuHCO_3^+$)		
$CuNO_3^+$	0.50	Smith and Martell (1976)
$Cu(NO_3)_2^o$	-0.40	Smith and Martell (1976)
Solids		
$CuCO_3$	9.63	Smith and Martell (1976)
$Cu(OH)_2$	-8.64	Baes and Mesmer (1976)
$Cu_2(OH)_2CO_3$ (malachite)	5.46	Symes and Kester (1984)
$Cu_3(OH)_2(CO_3)_2$ (azurite)	16.61	Naumov and others (1974)
CuO (tenorite)	-8.3	Barton and Bethke (1960)
(for $Cu^{2+} + H_2O = CuO + 2H^+$)		
Cu_2O (cuprite)	7.02	Robie and others (1978)

Table 2: Selected formation constants for some lead aquo-complexes and compounds. Values of log K are for the cumulative formation reactions. Reactions which involve protons or hydroxide ions are written in the proton form. Complexes or compounds which contain carbonate are written as cumulative formation reactions using CO_3^{2-}.

Aqueous Species	Log K	Source and Remarks
Pb^{2+}	---	ΔG^o_f=-5.83 kcal/mol (Rickard and Nriagu, 1978)
$PbOH^+$ (for $Pb^{2+} + H_2O = PbOH^+ + H^+$)	-7.71	Baes and Mesmer (1981)
$Pb(OH)_2^o$	-17.12	Baes and Mesmer (1981)
$Pb(OH)_3^-$	-28.06	Baes and Mesmer (1976)
Pb_2OH^{3+}	-6.36	Baes and Mesmer (1976)
$Pb_3(OH)_4^{2+}$	-23.88	Baes and Mesmer (1976)
$Pb_4(OH)_4^{4+}$	-20.88	Baes and Mesmer (1976)
$Pb_6(OH)_8^{4+}$	-43.61	Baes and Mesmer (1976)
$PbCO_3^o$	6.4	Bilinski and Stumm (1973)
$Pb(CO_3)_2^{2-}$	9.7	Determined through cerussite (using $PbCO_{3(s)}+CO_3^{2-}=Pb(CO_3)_2^{2-}$ log K=-3.10 from Bilinski and Schindler (1982)) Langmuir (1984)
$PbHCO_3^+$ (for $Pb^{2+} + HCO_3^- = PbHCO_3^+$)	2.90	Estimated by Zirino and Yamamoto (1972)
$PbNO_3^+$	1.17	Smith and Martell (1976)
$Pb(NO_3)_2^o$	1.40	Smith and Martell (1976)

Table 2 is continued on the next page.

Table 2: Continued.

Solids	Log K	Source and Remarks
$PbCO_3$ (cerussite)	12.80	Robie and others (1978)
$Pb_3(OH)_2(CO_3)_2$ (hydrocerussite)	19.14	Bilinski and Schindler (1982) (corrected from I=0.1 to I=0 (Langmuir, 1984))
α-PbO (litharge, red)	-12.68	Robie and others (1978)
β-PbO_2 (plattnerite)	-49.31	Rickard and Nriagu (1978)
Pb_3O_4 (minium)	-73.71	Robie and others (1978)

Table 3: Free energies of formation used in the calculation of equilibrium constants.

Species	ΔG^{o}_{f} (kcal/mol)	Source
$H_2O_{(l)}$	-56.687	CODATA (1976)
OH^-	-37.604	CODATA (1976)
$CO_{2(g)}$	-94.254	CODATA (1976)
CO_3^{2-}	-126.17	Wagman and others (1968)
HCO_3^-	-140.26	Wagman and others (1968)
$H_2CO_3^o$	-148.94	Wagman and others (1968)
NO_3^-	-26.64	Wagman and others (1968)

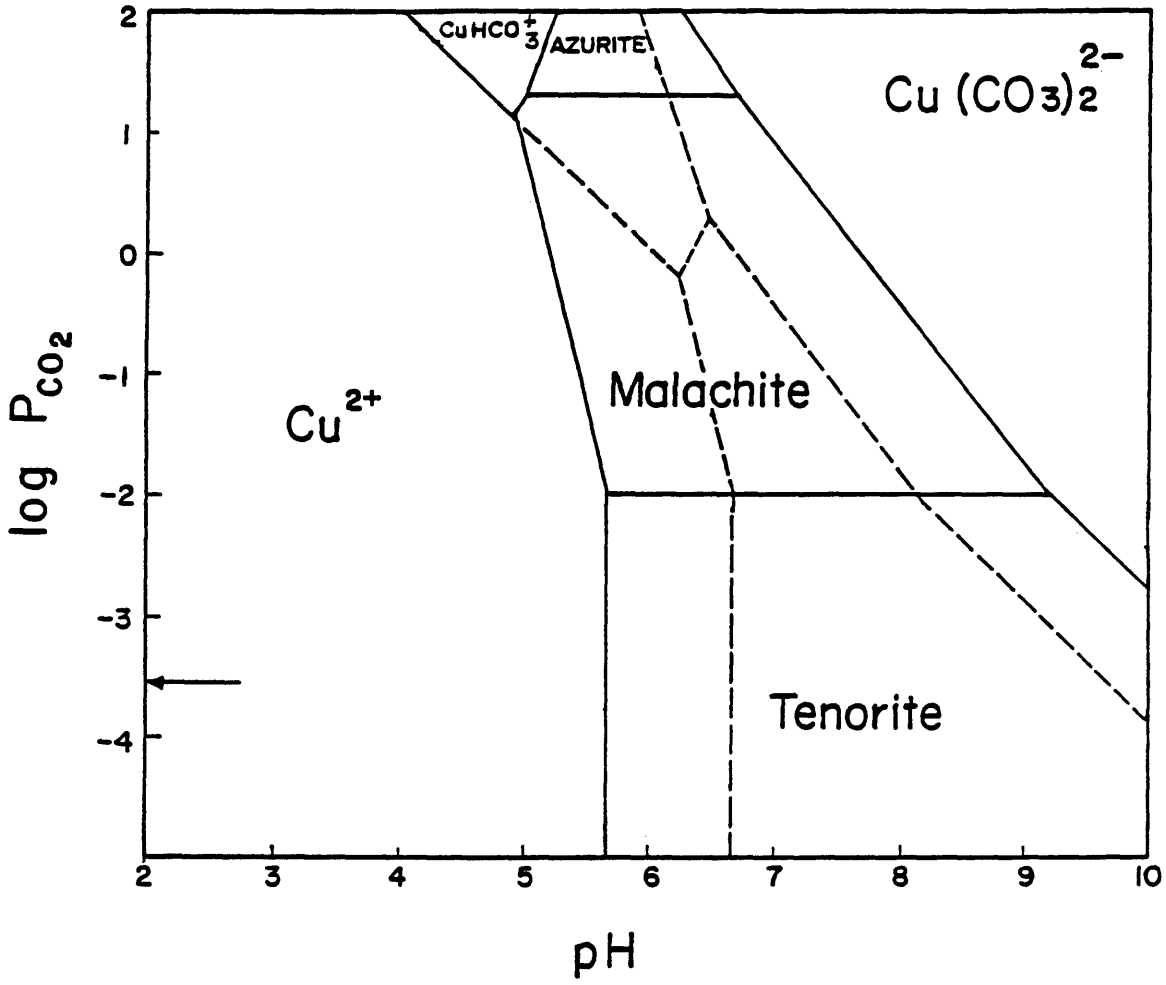

Figure 4: Predominance diagram for the Cu^{2+}-H_2O-CO_2 system at I=0 and 25°C as a function of pH and log P_{CO_2}. Solid/aqueous boundaries are drawn for total aqueous metal activities of 10^{-4} (solid lines) and 10^{-6} (dashed lines). The arrow denotes atmospheric CO_2.

or nitrate were detected by infrared spectrophotometry. Evidently, the precipitate is an amorphous form of tenorite.

The solubility of tenorite has been examined by several researchers and there is quite a bit of variability in their data. Feitknecht and Schindler (1963) and Schindler (1967) showed that CuO solubility is dependent upon its crystal structure and particle size. Schindler and others (1965) derived expressions for the solubility of CuO in 0.2 M $NaClO_4$ at 25°C as a function of surface area. Barton and Bethke (1960) reported a log K formation constant value of -8.3, apparently for poorly-crystalline CuO. The log K of -7.34 reported by Robie and others (1978) is presumably for well-crystallized CuO. The value of Barton and Bethke (1960) was used for adsorption calculations with the computer program MINEQL (Westall and others, 1976) because it is most applicable to the amorphous CuO encountered in this study.

Figure 5 gives the distribution of copper species under atmospheric conditions for a total copper concentration of 10^{-4} M, an ionic strength of 0.01 M (as KNO_3), and a temperature of 25°C. Figure 6 shows the distribution for a total carbonate carbon concentration, C_T, of 10^{-2} M with the ionic strength equal to 0.01 M (as $KHCO_3$). As seen in these figures, the Cu^{2+} ion dominates up to a pH around 7.0. The

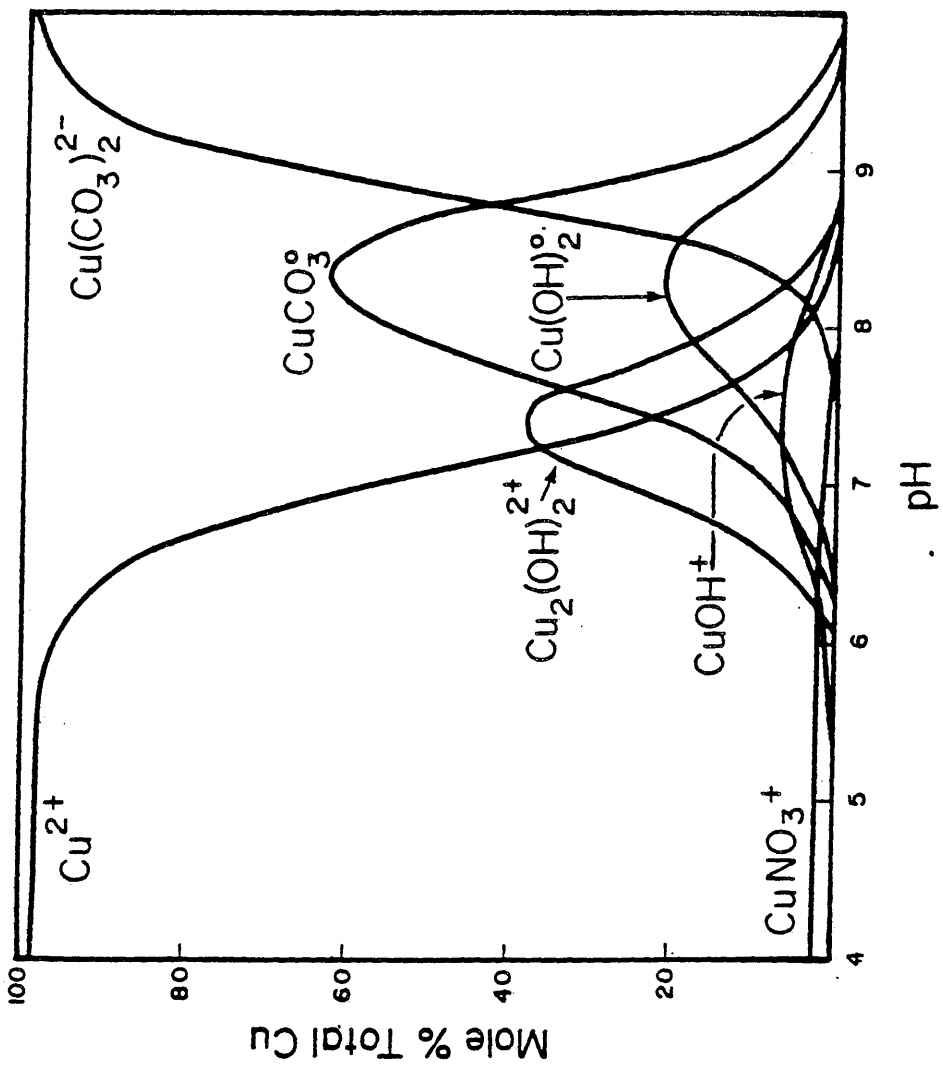

Figure 5: Distribution diagram for copper species as a function of pH for the Cu^{2+}-H_2O-CO_2 system under atmospheric conditions with I=0.01 M (as KNO_3), $\Sigma Cu=10^{-4}$ M, and 25°C.

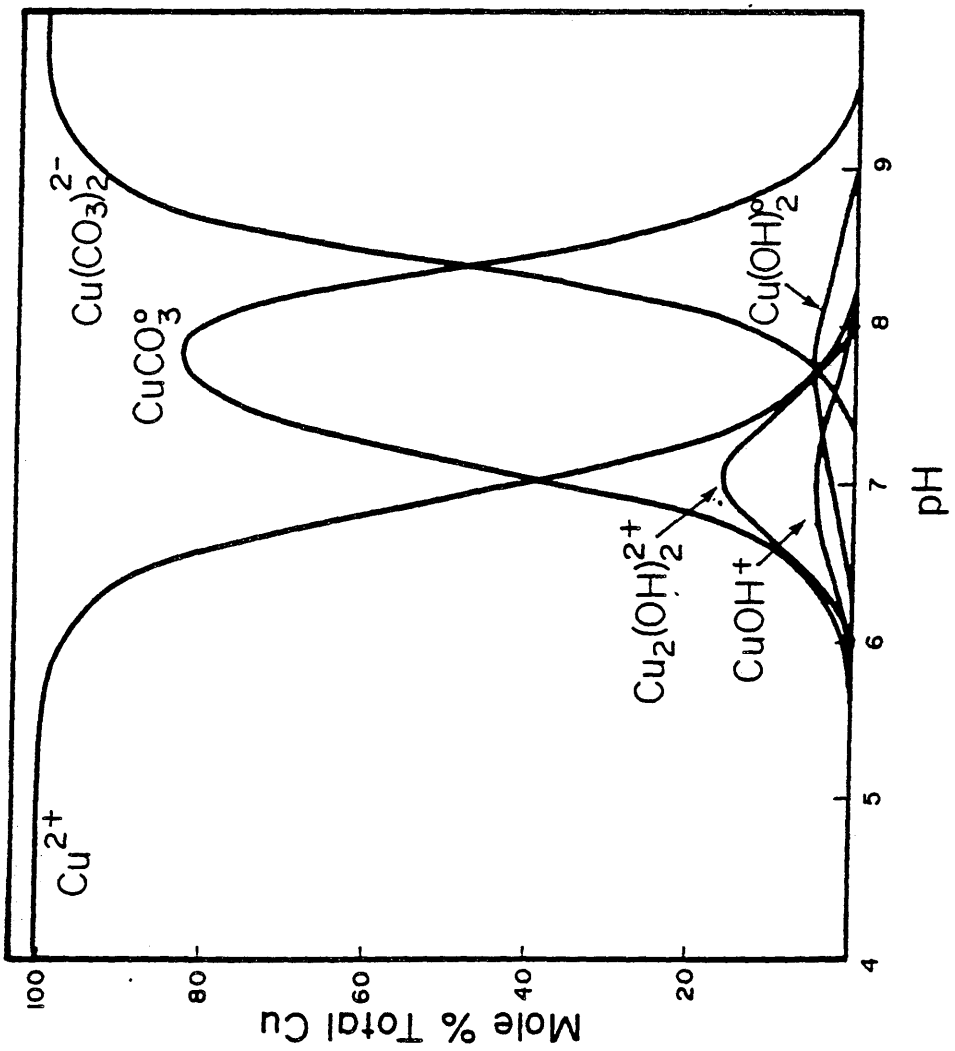

Figure 6: Distribution diagram for copper species as a function of pH for the Cu^{2+}-H_2O-CO_2 system with $C_T=10^{-2}$ M, I=0.01 M (as $KHCO_3$), $\Sigma Cu=10^{-4}$ M, and 25°C.

neutral carbonato species dominates above pH 7.0, and $Cu(CO_3)_2^{2-}$ dominates the speciation at higher pH values. The pH region of the carbonato species depends upon C_T, with higher C_T conditions resulting in a downward pH position shift.

As seen in Figure 7, the thermodynamically stable lead mineral from pH 6 to 10 under atmospheric conditions for a total lead concentration of 10^{-4} M is hydrocerussite, $Pb_3(OH)_2(CO_3)_2$. Figures 8 and 9 show the aqueous lead species distribution for atmospheric conditions and $C_T=10^{-2}$ M, respectively. Under atmospheric conditions, Pb^{2+} predominates up to pH 7.7 above which it is overtaken by the neutral carbonato species, $PbCO_3^o$. Above pH 9 the species $Pb(CO_3)_2^{2-}$ predominates. These relationships are shifted to lower pH's at higher C_T concentrations.

A solid lead hydroxide phase was not considered here due to the questions as to its existence. Rickard and Nriagu (1978) state that the precipitated gelatinous solid formed in lead salt solutions to which hydroxide has been added is probably a hydrated oxide rather than lead hydroxide.

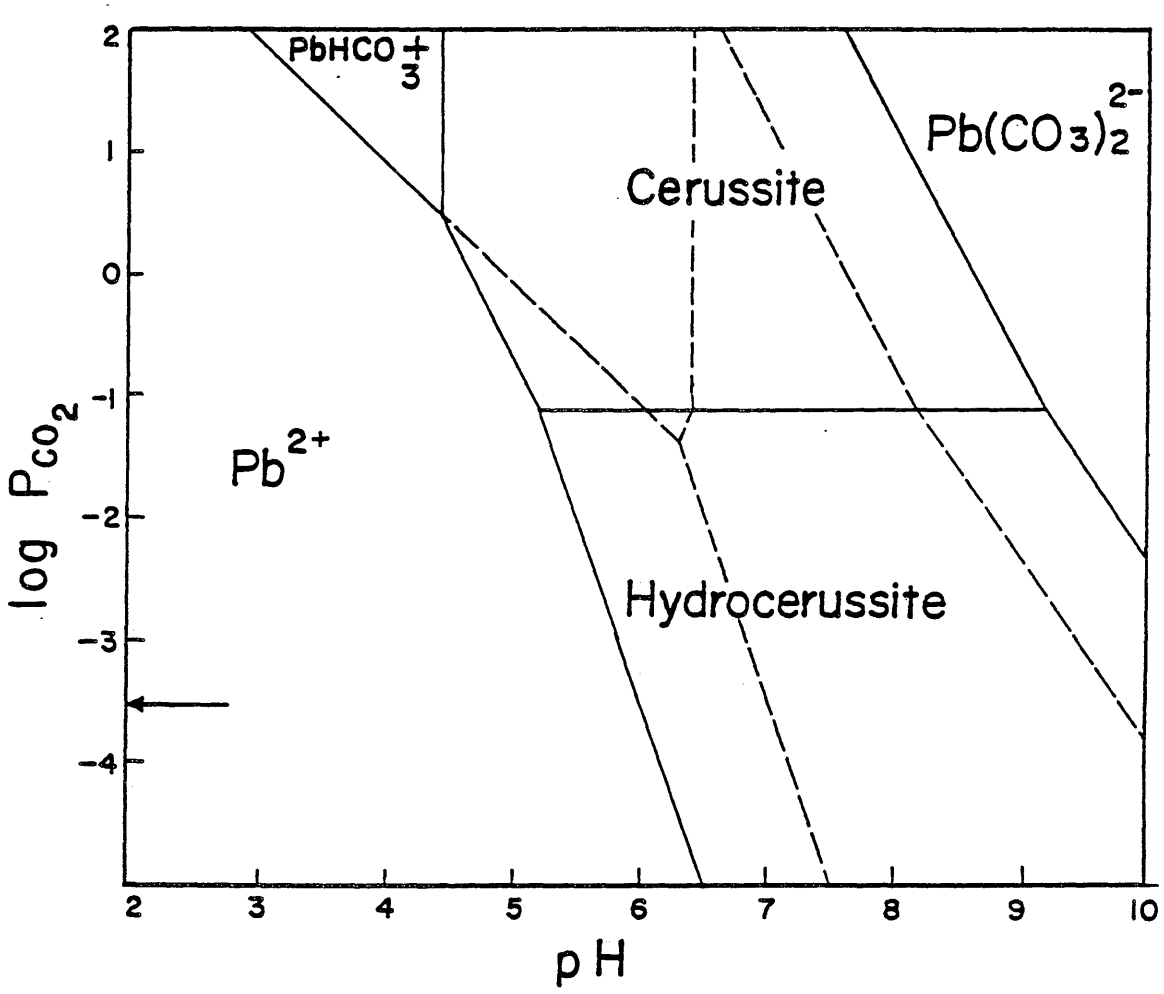

Figure 7: Predominance diagram for the Pb^{2+}-H_2O-CO_2 system at I=0 and 25°C as a function of pH and log P_{CO_2}. Solid/aqueous boundaries are drawn for total aqueous metal activities of 10^{-4} m (solid lines) and 10^{-6} m (dashed lines). The arrow denotes atmospheric CO_2.

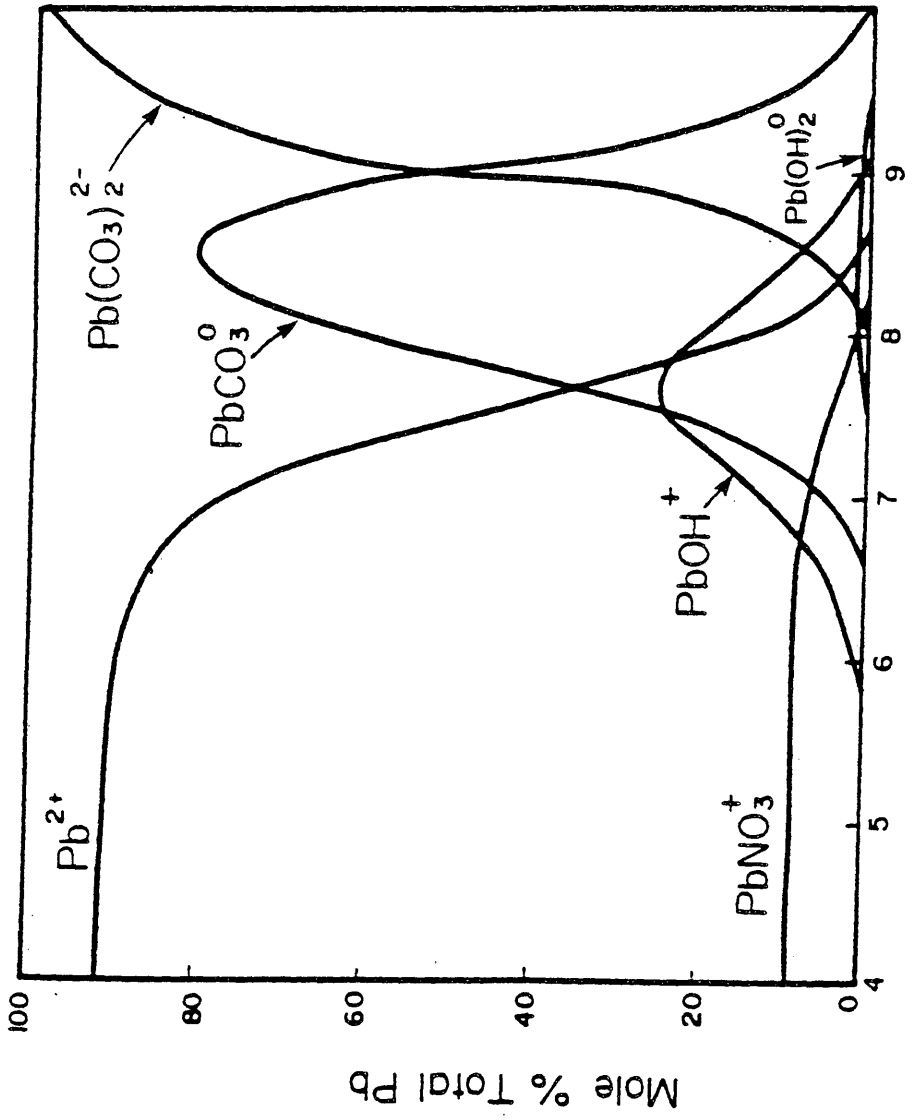

Figure 8: Distribution diagram for lead species as a function of pH for the Pb^{2+}-H_2O-CO_2 system under atmospheric conditions with I=0.01 M (as KNO_3), $\Sigma Pb=10^{-5}$ M, and 25°C.

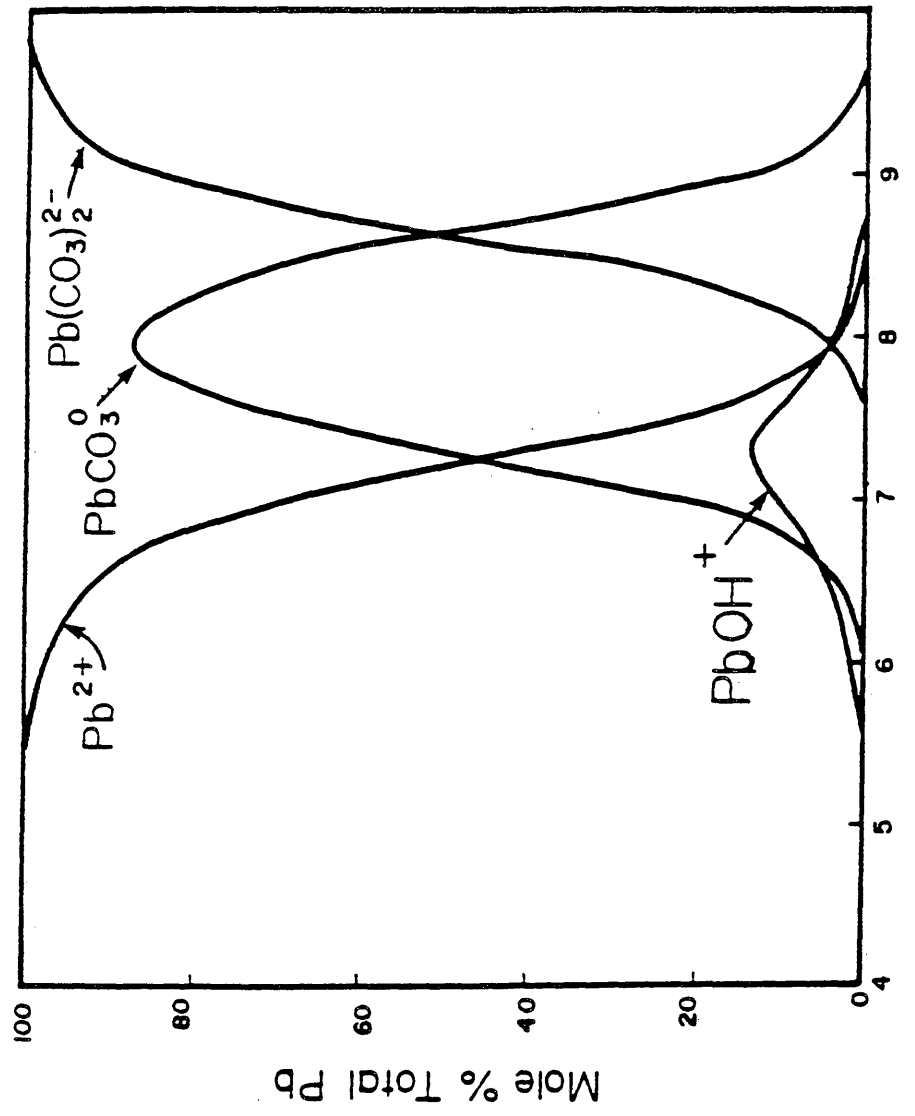

Figure 9: Distribution diagram for lead species as a function of pH for the Pb^{2+}-H_2O-CO_2 system with $C_T=10^{-2}$ M, I=0.01 M (as $KHCO_3$), $\Sigma Pb=10^{-5}$ M, and 25°C.

LABORATORY PROCEDURES

REAGENTS AND MATERIALS

All compounds used in this study were of ACS Reagent Grade or better. All solutions were prepared using doubly-demineralized water with conductivity less than 1.0 µS/cm at 25° C. The pH was adjusted with HNO_3 (Ultrex brand) or KOH (DILUT-IT brand). All standard acid and base solutions were analyzed for copper and lead by atomic absorption spectrophotometry using graphite furnace atomization. The base solutions contained less than 2 µg/l, and the acid solutions less than 1 µg/l of both copper and lead.

Acid-washed polyethylene bottles were used for storage of solutions. All glassware, glass pipets, and Eppendorf pipet tips were acid-washed before use. A special washing procedure was followed for the 40 ml polycarbonate centrifuge tubes and caps used in the sorption experiments because a small amount of residual acid can significantly affect adsorption equilibria. The tubes and caps were first washed with an Alconox solution and test tube brush. They were then rinsed with deionized water and placed in a 1% HNO_3 bath for 2 days. After the acid soak they were rinsed with deionized water and placed in a dilute Alconox bath to

remove any residual protons from the surfaces. Following another rinse with deionized water the tubes and caps were soaked in deionized water overnight after which they underwent a final rinse with doubly-demineralized water.

The analytical balance was calibrated and found to be accurate to ± 0.0001 grams. Eppendorf pipets were accurate to ± 1 %. All glassware and pipets were calibrated and found to be within the guidelines for Class A volumetric ware.

Solutions of Fisher Scientific Company certified dry buffer salts were used to calibrate the pH meter to pH 6.86 ± 0.02 and pH 4.01 ± 0.02 at 25°C. A pH 8.00 ± 0.02 MicroEssential Laboratory pHydrion sodium and potassium phosphate buffer was used to check the calibration curve at higher pH's.

Removal of CO_2 from some reagents and sorption solutions was accomplished by purging with CO_2-free O_2. The CO_2-free O_2 was obtained by bubbling O_2 through a series of vessels containing: (1) glass wool; (2) two bottles of $Ca(OH)_2$-saturated solutions with the gas bubbled through glass frits; (3) two bottles of CO_2-free demineralized water; and (4) glass wool.

SYNTHETIC GOETHITE PREPARATION

In order to obtain particles of fairly uniform shape and narrow size distribution for use in sorption experiments a synthetic goethite was prepared. The synthetic goethite (α-FeOOH) preparation method is taken from Atkinson and others (1967). A 194 ml solution of 2.5 N KOH was slowly added to a vigorously stirred ferric nitrate solution prepared by dissolving 48.48 g of $Fe(NO_3)_3 \cdot 9H_2O$ in 800 ml of doubly demineralized water. The final pH of this solution was approximately 12. Polyethylene bottles (1 liter) were used in order to prevent silica contamination from glass possible at such high pH's. The solutions were aged for 26 hrs. in a 60°C preheated oven. After aging, the suspension was cooled to room temperature and dialyzed against demineralized water until $NO_3^- < 10^{-5}$ M, as measured by a NO_3^- selective ion electrode. The goethite suspension was then washed with doubly demineralized water and centrifuged at 6,500 rpm for 30 min. followed by decanting. This process was repeated twice and the remaining particles were then freeze-dried and stored in a polyethylene bottle in a desiccator until dispersion in solution for sorption experiments.

SORPTION EXPERIMENTS

Potassium nitrate was chosen as the background electrolyte for the sorption systems. Ionic strength was adjusted to either 0.01 M or 0.1 M by the addition of KNO_3. Final pH values ranged between 5.0 and 9.0. The pH was adjusted using 0.1 N HNO_3 or 0.1 N KOH. Experiments were conducted at initial total copper concentrations of 10^{-4} M, 10^{-5} M, and 10^{-6} M, and initial total lead concentrations of 10^{-5} M, 10^{-6} M, and 10^{-7} M under conditions of both a total carbonate carbon concentration, C_T, of near zero and in equilibrium with the atmosphere. For experiments in which C_T was near zero, the reagents were purged overnight with CO_2-free O_2 and the prepared sorption solutions were bubbled for 15 min. in the centrifuge tubes and then tightly capped. Additional experiments were performed under higher C_T conditions. In these cases, both C_T and I were adjusted with $KHCO_3$.

Procedure for Sorption Experiments

Reagents were added to 40 ml polycarbonate centrifuge tubes in the sequence; doubly-demineralized water, KNO_3, pH adjustment, trace metal nitrate solution, and finally an aliquot of the goethite suspension. In the higher C_T

experiments, the $KHCO_3$ reagent was added just before the goethite suspension. The goethite suspension was prepared and ultrasonically dispersed 24 hrs. prior to use.

After preparation of the sorption solutions, the centrifuge tubes were capped and placed in a 25°C water bath for four hours. Occasional shaking of the tubes kept the goethite in suspension. The suspensions were centrifuged at 16,000 rpm for 20 min. with an International Model B20A Refrigerated Centrifuge. Fifteen milliliter aliquots of the supernatant were removed, transferred to acid-washed polyethylene bottles, and acidified with ULTREX nitric acid. The pH was measured in the remaining solution with an Orion glass combination electrode (no. 91-02) and an Orion Model 901 Research Microprocessor.

Total dissolved copper and lead in the acidified supernatant solutions were determined by atomic absorption spectrophotometry (some solutions required graphite induction furnace atomization). The supernatant solutions were analyzed in random sequence to eliminate any systematic analytical errors.

The reproducibility of the experimental adsorption isotherms is indicated by the relative positions of the data points. Each data point represents information from a single centrifuge tube, and a group of eight centrifuge

tubes were run consecutively. Each experimental adsorption curve consists of data collected from several different groups done at different times and on different days.

Analytical Error

The pH measurements were reproducible to ± 0.05 pH units for a given sorption run and ± 0.1 pH units between sorption runs. Thirty-four randomly-chosen supernatant solutions were analyzed in duplicate to test the precision of the analyses. The average standard deviation for Cu by flame atomic absorption is ± 0.018 ppm, and by graphite furnace atomization is ± 0.66 ppb. The average standard deviation for Pb by flame atomic absorption is ± 0.010 ppm, and by graphite furnace atomization is ± 2.6 ppb.

An additional estimate of analytical precision and accuracy was achieved through the analysis of stock solutions of known concentrations. At least one stock solution was analyzed with each separate analytical group of sorption solutions. Table 4 gives the results of these analyses.

Table 4: Accuracy and precision (±) of analyses as determined by analysis of stock solutions.

	Stock Solution Concentrations					
	10 ppb		100 ppb		1000 ppb	
	Cu	Pb	Cu	Pb	Cu	Pb
	10	10	90	110	900	1000
Measured	12	9	100	100	900	800
Values	10	8	100	110		
	10	11				
Mean	10.50	9.50	96.67	106.67	900	900
Standard deviation	±1.0	±1.3	±5.8	±5.8	--	--

PARAMETER DETERMINATIONS

SORPTION KINETICS

Kinetic studies were performed to determine the optimum reaction time for copper and lead sorption. Aliquots were taken at geometrically increasing times ranging from 15 min. to one week. The freeze-dried goethite was hydrated at pH 6.0, 24 hours before use. The experiments were conducted in 500 ml wide mouth acid-washed polyethylene bottles. A mixture of doubly-demineralized water, KNO_3, and metal was prepared in each 500 ml bottle and adjusted to pH 6.0 with 1 N KOH. Enough concentrated goethite suspension was added to each mixture to attain a final sol concentration of 1 g/l. The bottles were kept in a 25°C water bath with continuous stirring. Three-milliliter aliquots were removed at the specified times using B-D 10cc syringes, and filtered through Millipore filter pods containing acid-washed and sonicated Nuclepore 0.2 micrometer filters. These aliquots were acidified with ULTREX nitric acid and saved for metal analysis by atomic absorption spectrophotometry. Graphite furnace atomization was used for low-concentration samples.

The properties of the goethite suspension were: initial pH 6.0, metal concentration 10^{-5} M, and ionic

strength 0.1 M (controlled with KNO_3). The study was carried out in equilibrium with atmospheric CO_2.

The results of the kinetic studies are given in Figure 10. The data indicate that there is a two-step kinetic reaction. The first step is completed within a few minutes to one hour. The second step is much slower and takes place on a time scale of days to weeks. Similar two-step sorption kinetic reaction rates have been documented by Loganathan and Burau (1973), Davis (1977), Benjamin (1978), Hsi (1981), and Hsi and Langmuir (1985). Yates (1975) and Benjamin (1978) attribute the slower step to diffusion of sorbate ions into the solid matrix. Another explanation might be increased disaggregation of the sol over time.

A reaction time of four hours was chosen for the sorption studies to insure equilibration of the fast surface reactions and to minimize the effect of the slower uptake reactions.

GOETHITE CHARACTERIZATION

Knowledge of sorbent material properties such as particle size and shape, crystallinity, chemical composition, surface area, and numbers and types of functional groups on the particle surfaces is essential to

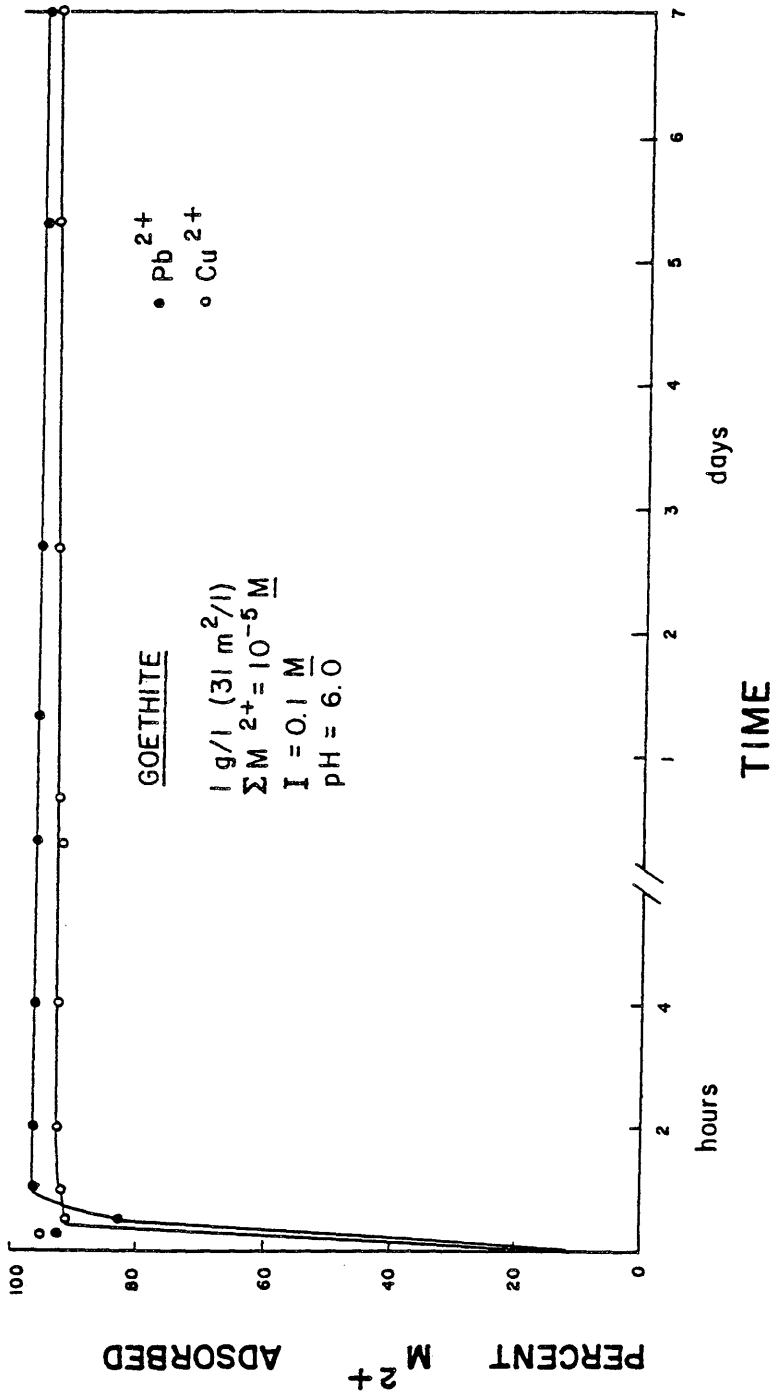

Figure 10: Kinetics of Cu^{2+} and Pb^{2+} adsorption onto goethite at 25°C in 0.1 M KNO_3. (Note the two points, at the far left of the graph, which represent an initial overadsorption at the 15-min. samples.)

the interpretation and modeling of adsorption data. The various experimental techniques used to determine these properties are briefly discussed below. The results which are detailed below were: specific surface area = 30.8 ± 1.85 m^2/g, mean cation exchange capacity = 82 ± 2 meq/100 g, and the pH at the point of zero charge = 7.6 ± 0.3 (determined by potentiometric titration).

Composition and Crystallinity

Results of the synthetic goethite chemical analysis are presented in Table 5. No evidence of Pb or Cu contamination was detected.

X-ray diffraction showed that the synthetic goethite was at least 95% pure and moderately well-crystallized.

Particle size and morphology were examined by scanning electron microscopy. The goethite particles are rod-like in structure with an average length of about 0.5 micrometers and a diameter between 0.07 and 0.1 micrometers. The preparation procedure was as follows. First, the freeze-dried powder was suspended in ethanol. Next, the suspension was sonicly dispersed and, using a syringe, deposited on a millipore filter. Upon drying, the millipore filter and sample were mounted on a stainless steel sample plate and coated with a thin film of evaporated gold/palladium alloy.

Table 5: Chemical composition of synthetic goethite.

Constituent	Chemical Analysis by XRF[1] (as percent) Synthetic Goethite
SiO_2	0.27
Al_2O_3	0.10
Fe_2O_3	90.02[2]
MgO	0.22
CaO	0.02
Na_2O	0.25
K_2O	0.08
TiO_2	0.10
P_2O_5	0.05
MnO	0.02
LOI[3]	12.34
Total	103.47

Chemical Analysis by ICP[4] (as ppm)	
Ba	<10
Cu	<10
Li	<20
Pb	<40
Sr	<20
Zn	<20

[1] X-ray fluorescence.
[2] Total iron reported as Fe_2O_3 (value for goethite is greater than the reliable upper limit of detection).
[3] Loss on ignition (925°C for 40 min.).
[4] Induction coupled argon plasma-optical emission spectroscopy (ICAP-OES).

BET Surface Area

Knowledge of the specific surface area is necessary for calculation of layer charges and potentials in the surface complexation site-binding model. The surface area was determined by Coors Spectro-Chemical Laboratory using the multipoint volumetric BET nitrogen gas adsorption method (ASTM D-3663). Gregg and Sing (1967) present a detailed discussion of this method. The freeze-dried samples were outgassed at 25°C for 72 hrs. before the measurements were taken.

The measured surface area of the synthetic goethite was 30.8 ± 1.85 m^2/g, which compares with areas of 45 and 48 m^2/g reported by Hsi (1981) and Yates (1975), respectively, 32 m^2/g reported by Hingston and others (1968), and 51.8 m^2/g reported by Balistrieri and Murray (1981).

The BET method is almost exclusively used to measure surface area. However, there are problems with applications of this method to aqueous-solid sorption studies. The most obvious of these is that the BET method involves the adsorption of vapors onto a dry sample under vacuum. Difficulties arise when attempts are made to relate trace element sorption in solution, including possible specific sorption effects, to BET surface area measurements. The BET theory (Brunauer, Emmett, and Teller, 1938), is an extension

of the Langmuir isotherm. It allows for multilayer adsorption on non-porous solid surfaces. The basic assumption behind BET theory is that the Langmuir equation applies to each of the multilayers. Hence, BET theory falls prey to the assumptions inherent in the Langmuir isotherm. These assumptions are incompatible with the fact that the highly active parts of most surfaces are heterogeneous with widely varying heats of adsorption.

Other issues arise from use of the BET procedure to determine the specific surface area of goethite. Yates (1975) observed some surface decomposition of amorphous iron oxide following outgassing at room temperature. The result of such decomposition is probably an underestimation of the true specific surface area.

Cation Exchange Capacity

Cation exchange capacity (CEC) is a measure of the quantity of readily exchangeable cations necessary to neutralize the negative charge per unit weight of solid material (Rhoades, 1982). The CEC quantity can be used as a measurement of surface site density (N_s) in modeling calculations. Results of the CEC measurements are: Ca^{2+} = 82, K^+ = 70, Na^+ = 86, NH_4^+ = 90, and the mean cation exchange capacity = 82 ± 2 meq/100 g.

Na^+, K^+, and NH_4^+ exchange capacities were determined using acetate salts of these cations, and that for Ca^{2+} determined using the chloride salt. The method used was modified from Jackson (1969) and Crock and Severson (1980). All measurements were performed at pH 7.0. Either acetic acid (HCl in the case of Ca^{2+}) or a solution of the hydroxide of the cation was used to adjust the pH of the acetate salt solutions. The starting material consisted of 1.000 gram of synthetic goethite. A blank was carried throughout the procedure.

In the first step, the saturation step, the solid particles were placed in 65 ml Kimax glass culture tubes and washed with 7 ml of 1 N acetate salt (chloride in the case of Ca^{2+}). The tubes were then horizontally agitated on a reciprocating shaker for 20 min. at 240 cycles. Afterward, the suspended material was centrifuged at approximately 2,000 rpm for 15 min. using an International Model K Centrifuge. The resulting clear supernatant was carefully decanted and filtered through a Whatman # 40 ashless filter into a 25 ml volumetric flask. The solid particles were then redispersed into another 7 ml of the acetate salt using a Thermolyne Maxi Mix. The above saturation procedure was repeated two additional times and the filtered supernatants were combined into the 25 ml volumetric flasks for each salt

and taken up to volume with the 1 N background solution. The goethite was first saturated with NH_4^+, then with K^+, Na^+, and finally with Ca^{2+}.

In the washing step, the goethite was washed with 10 ml reagent grade 2-propanol, placed on the reciprocating shaker for 10 min., and centrifuged at approximately 2,000 rpm for 15 min. The supernatant was carefully decanted and discarded. The washing procedure was performed three times.

In the replacement step, the goethite was saturated with NH_4^+ (using 1 N NH_4OAc) and washed with 2-propanol following the above procedures. After completion of the replacement step, the solid particles were saturated with another acetate salt cation.

The extracts were analyzed for K^+, Na^+, and Ca^{2+} with a Perkin Elmer 603 Atomic Absorption Spectrophotometer. The NH_4^+ extract was analyzed using an Orion Model 95-10 Ammonia Electrode. All standards were prepared with the same matrix as the extract being measured. The blank was below or near the limit of detection in all cases.

In order to calculate the CEC for each cation (as meq M^{n+} per 100 grams, where M^{n+} is the cation in question), the following formula was used:

$$\frac{\text{meq } M^{n+}}{100 \text{ g}} = \frac{100}{\text{Soil weight (g)}} \times \frac{\text{Extract volume (ml)}}{1{,}000} \times \frac{\text{meq } M^{n+}}{\text{liter}}$$

Results from an originally Ca-saturated montmorillonite, run through the procedure at the same time as the goethite, were used as a test of precision. The first NH_4^+ saturation extract of the montmorillonite was analyzed for Ca^{2+} to compare with the Ca^{2+} analysis for the extract obtained at the end of the procedure. Because Ca-saturation was the last saturation in the sequence of cations, comparison of the original Ca^{2+} value and the later Ca^{2+} value should be a good judge of the precision throughout this method. The original CEC value for Ca^{2+} was 108 meq/100g and the later CEC value was 110 meq/100g. This would indicate that there is good precision (± 2 meq/100g) for a given cation. Hence, the variation in CEC values may be due either to differences between cations or, in the case of NH_4^+, differences between analytical methods.

Potentiometric Titration

Potentiometric titration data are used to determine both the pH(PZC) and the surface charge density as a function of pH. The pH(PZC) is needed to predict intrinsic equilibrium constants. Titration data show the surface charge density to be zero at the pH(PZC). The synthetic goethite used in this study has a pH(PZC) of 7.6 ± 0.3.

Yates and Healy (1975) found pH(PZC) = 7.5 ± 0.1 for goethite in KNO_3 solutions, Balistrieri and Murray (1979) reported pH(PZC) = 7.5 in NaCl and KCl, and Hsi (1981) gave pH(PZC) = 8.5 ± 0.3 in $NaNO_3$.

The potentiometric titration method of Bolt (1957), Parks and deBruyn (1962), and Yates and Healy (1975) was used in this work. Studies have shown that protons and hydroxide ions are the potential determining ions (PDI) for the goethite surface (Parks and deBruyn, 1962). Hence, adsorption densities of these PDI's can be calculated from the amount of acid or base added to the suspension and the pH of the suspension. The following general equation illustrates these relationships:

$$\sigma_o = F(\Gamma_{H^+} - \Gamma_{OH^-})$$

where σ_o is the surface charge, F is the Faraday constant (96,500 C/mol), and Γ_{H^+} and Γ_{OH^-} are moles adsorbed per square centimeter. Titrations are performed at constant ionic strengths to fix the activity coefficients and to ensure that the PDI's do not significantly contribute to the diffuse layer charge (Yates, 1975).

The equation of Silva and others (1979) and Riese (1982) was used to calculate surface charge for each point

in the titration.

$$\sigma_o = \frac{F}{A}\left[(H^+)_i - (OH^-)_i\right]\frac{V_i}{\gamma_i} + C_a V_a - C_b V_b - \left[(H^+)_j - (OH^-)_j\right]\frac{V_j}{\gamma_j}$$

where:

σ_o = surface charge density (C/cm^2)

F = Faraday constant (96,500 C/mol)

A = surface area (cm^2)

C_a, C_b = concentration of acid or base (M)

V_a, V_b = total volume of acid or base used to a given point on the titration curve (l)

V_i = initial volume (l)

V_j = total volume at a given point on the titration curve, $V_a + V_b + V_i$, (l)

γ_i, γ_j = activity coefficients of H^+ and OH^-, respectively, used to convert activities to concentrations

$(H^+)_i$, $(OH^-)_i$ = measured H^+ and OH^- ion activities in solution at the start of the titration (m)

$(H^+)_j$, $(OH^-)_j$ = measured H^+ and OH^- ion activities in solution at a

given point on the titration curve (m)

The pH(PZC) is the point of intersection of all the titration curves obtained at different ionic strengths.

Potentiometric titrations were performed with a Metrohm-Herisau Dosimat E535 Automatic Titrator, a Beckman gel-filled combination pH electrode, and an Orion Model 901 Research Microprocessor. The titrants were approximately 0.1 M HNO_3 and 0.1 M CO_2-free KOH, standardized to ± 0.001 by the potassium hydrogen phthalate method outlined in Skoog and West (1976). Titrations were carried out under an O_2 atmosphere in a water-jacketed 50 ml titration vessel at 25° C. Approximately 24 hrs. prior to titration, a goethite suspension was placed in the glass titration vessel, with enough KNO_3 added to bring the total ionic strength to 10^{-3} M, and continuously stirred under an oxygen atmosphere. The O_2 was purified and water-saturated as described earlier.

The titrations were accomplished by adding small volumes of the standardized acid or base to the suspension. An average equilibration time of 3 minutes was allowed between each addition of acid or base. An exception to this was in the neutral pH region where additional time was necessary for the readings to stabilize. The pH was

measured with the magnetic stirrer turned off. The goethite suspension was first titrated with acid to about pH 4, then with base to about pH 10, and finally again with acid to bring it back to about the starting pH. The ionic strength was then increased and the sequence repeated. This process was sequentially performed for each ionic strength of 10^{-3}, 10^{-2}, 10^{-1} and 0.7 M. Blank titrations (without goethite) were done at the same ionic strengths under identical conditions. To test for goethite dissolution during the titration procedure, a separate vessel was prepared under titration conditions. No goethite dissolution was detected by analysis of suspension supernatant after centrifugation (for a detection limit of 20 ppb by atomic absorption spectrophotometry using graphite furnace atomization).

Titration data volumes were normalized to 0.1000 M acid and base concentrations by means of the computer program NORMV.FOR (see Appendix 1). The titration data were then plotted (Fig. 11). Blank titrations were subtracted from the goethite titration curves to correct for the amount of titrant necessary to titrate the doubly deionized water. Surface charge density was calculated with the computer program SIGMA.FOR (see Appendix 1). Figure 12 is a plot of the surface charge density (microcoulombs per square centimeter) versus pH for titration at the four different

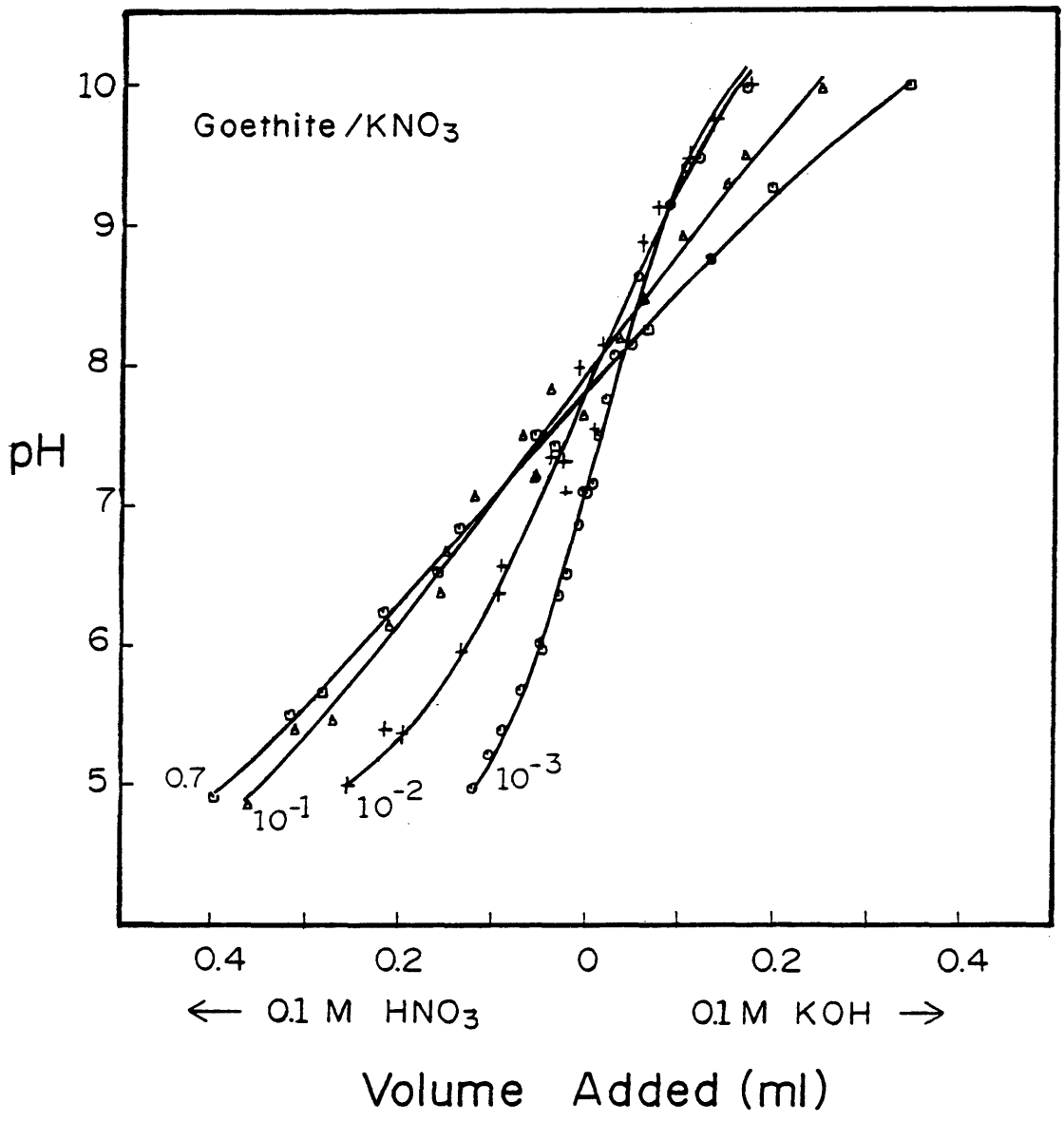

Figure 11: Potentiometric acid-base titration curves for goethite in various ionic strength KNO_3 solutions.

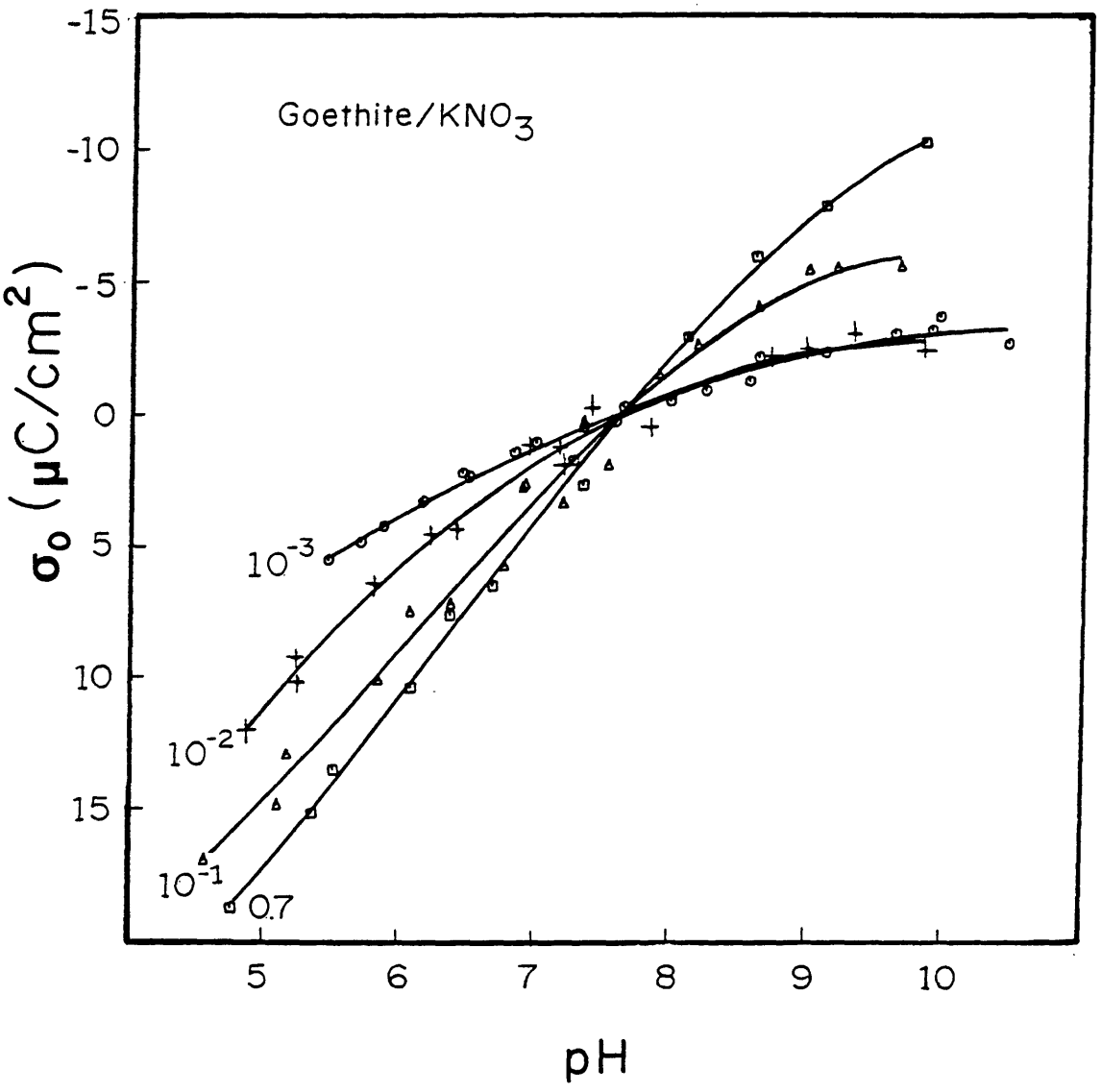

Figure 12: Variation of the surface charge density of goethite in aqueous solutions of KNO_3 as a function of pH.

ionic strengths. The curves in Figure 12 have been normalized to the pH(PZC) of 7.6. The decrease in the rate of charge development at higher pH values (>7.6) may be partially due to coagulation of the goethite suspension which was noted during the titration procedure.

RESULTS OF SORPTION EXPERIMENTS

Adsorption experiments were performed at various concentrations of copper or lead, and supporting electrolytes. In all cases the goethite surface area was 31 m^2/l.

In Figures 13 through 20, data are plotted as fractional metal adsorption versus pH. The metal scales are logarithmic and are expressed as amount of metal remaining in solution after centrifugation. This mode of presentation emphasizes the lower metal concentrations where many interactions of interest take place. The reader is referred to the Analytical Error section of this thesis for a discussion of data precision. Solid curves are free-drawn best fits of experimentally-derived data points. The best fit lines are drawn through the C_T = atmospheric conditions, I = 0.01 M (as KNO_3) data points. Data points < 1 ppb are plotted on the 1 ppb line such that there is no graphical distinction between samples at 1 ppb and samples < 1 ppb. Under atmospheric conditions (a CO_2 pressure of $10^{-3.5}$ atm.) solutions at pH 7 and 9 correspond to $C_T=10^{-4.2}$ and $10^{-2.3}$ M, respectively.

Random samples were analyzed for iron to ensure that none of the sol remained in suspension. In all cases tested

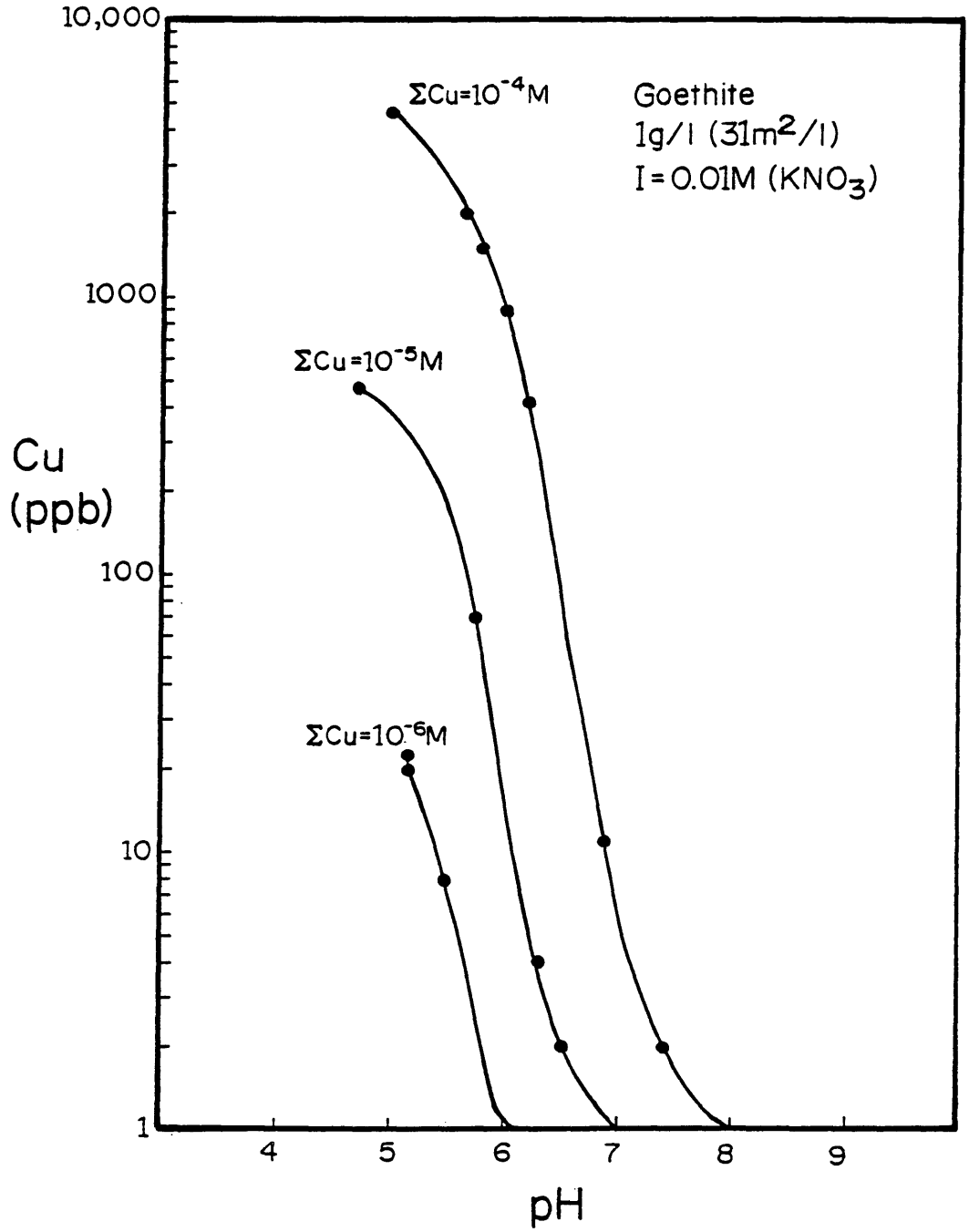

Figure 13: Effect of copper concentration on the pH adsorption edge for copper adsorption onto goethite under atmospheric conditions for I=0.01 M (KNO_3) at 25° C.

Figure 14: Adsorption of copper onto goethite for $\Sigma Cu=10^{-4}$ M under a variety of aqueous conditions. Vertical lines connect some of the analytical duplicates, with a slash at the average value. In several cases duplicate values were the same or very close and are not shown in the graphs. The following key applies to the various data point symbols:

× = $C_T=0$; I=0.01 M (as KNO_3)
⊕ = $C_T=0$; I=0.1 M (as KNO_3)
● = C_T=atmospheric CO_2; I=0.01 M (as KNO_3)
o = C_T=atmospheric CO_2; I=0.1 M (as KNO_3)
▲ = $C_T=10^{-2}$ M; I=0.01 M (as $KHCO_3$)
▲ = $C_T=10^{-1}$ M; I=0.1 M (as $KHCO_3$)
▼ = $C_T=10^{-1.3}$ M; I=0.1 M (as 50% KNO_3, 50% $KHCO_3$)

Blank data are indicated both by dashed lines and separate points.

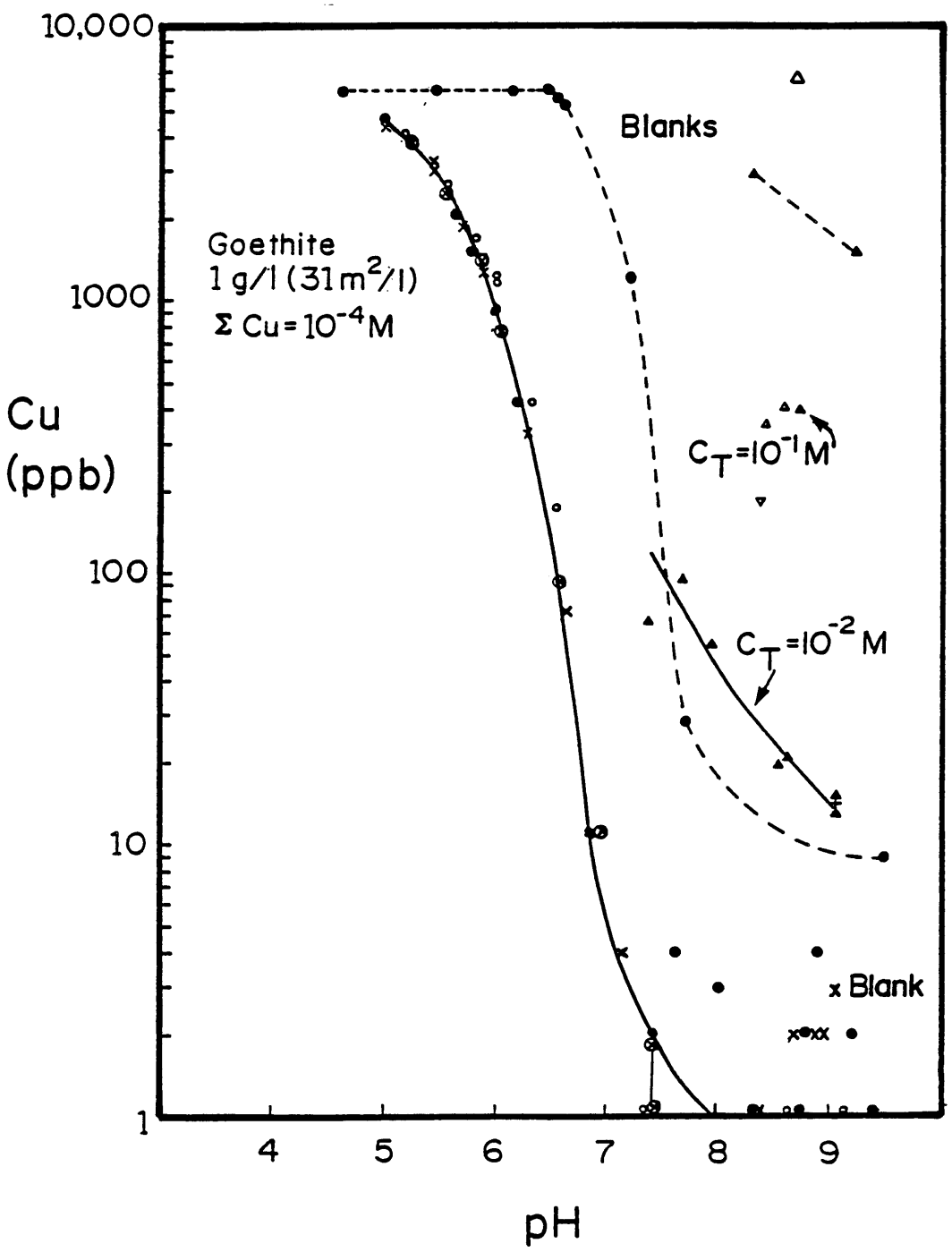
10,000
1000
100
10
1
Cu
(ppb)
Goethite
1 g/l (31 m²/l)
Σ Cu = 10⁻⁴ M
Blanks
C_T = 10⁻¹ M
C_T = 10⁻² M
x Blank
4
5
6
7
8
9
pH

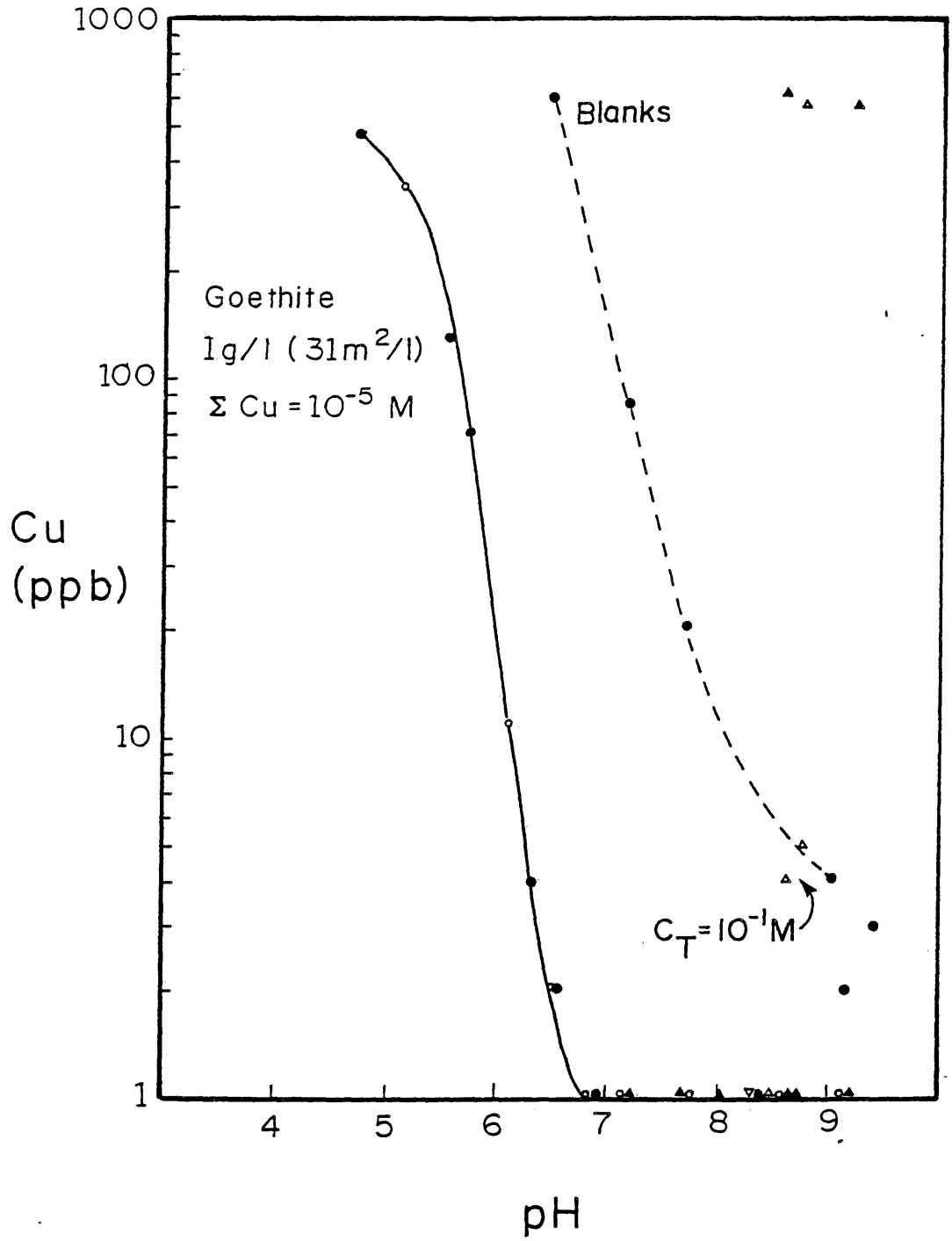

Figure 15: Adsorption of copper onto goethite for $\Sigma Cu = 10^{-5}$ M under a variety of aqueous conditions (see Fig. 14 for key to data symbols).

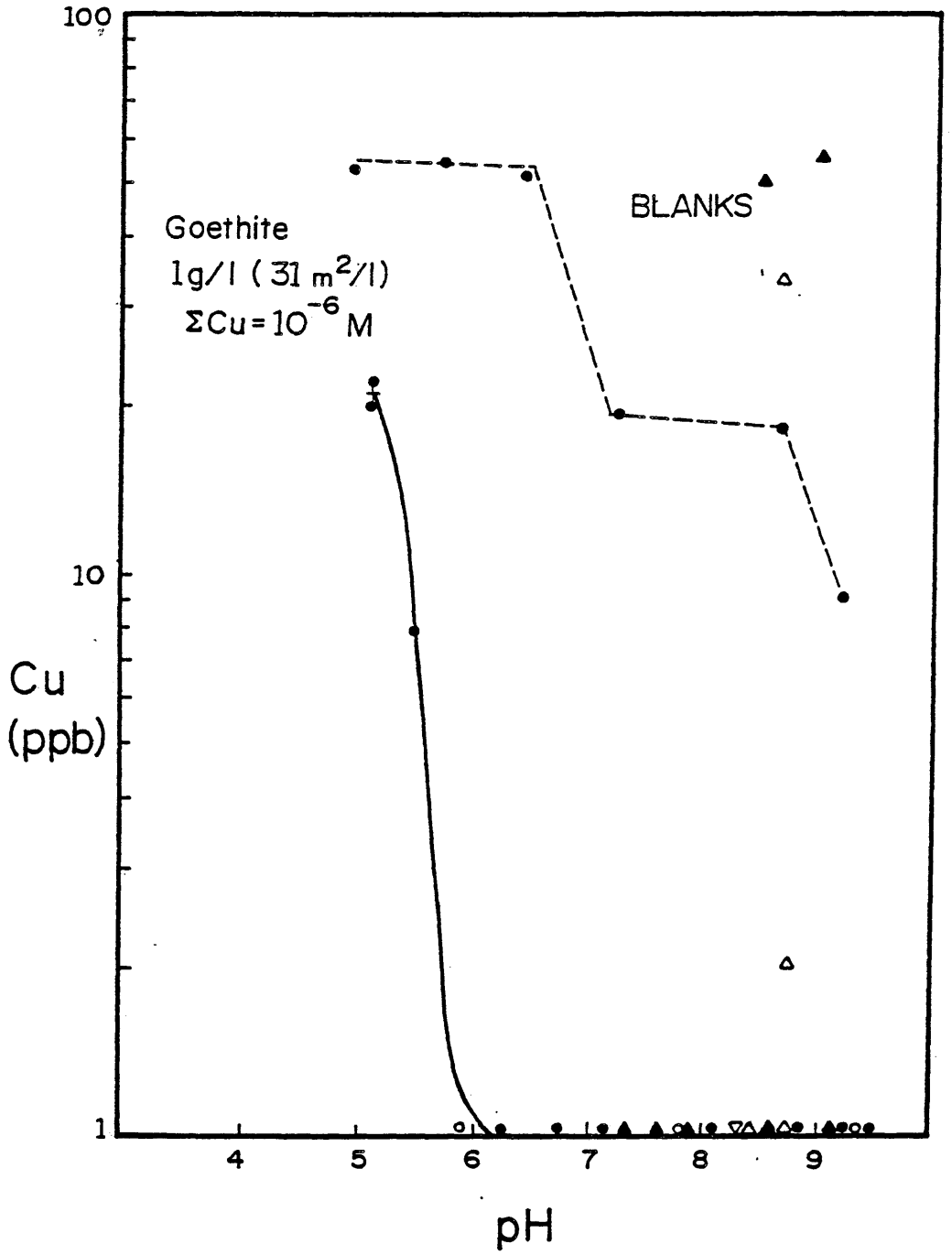

Figure 16: Adsorption of copper onto goethite for $\Sigma Cu = 10^{-6}$ M under a variety of aqueous conditions (see Fig. 14 for key to data symbols).

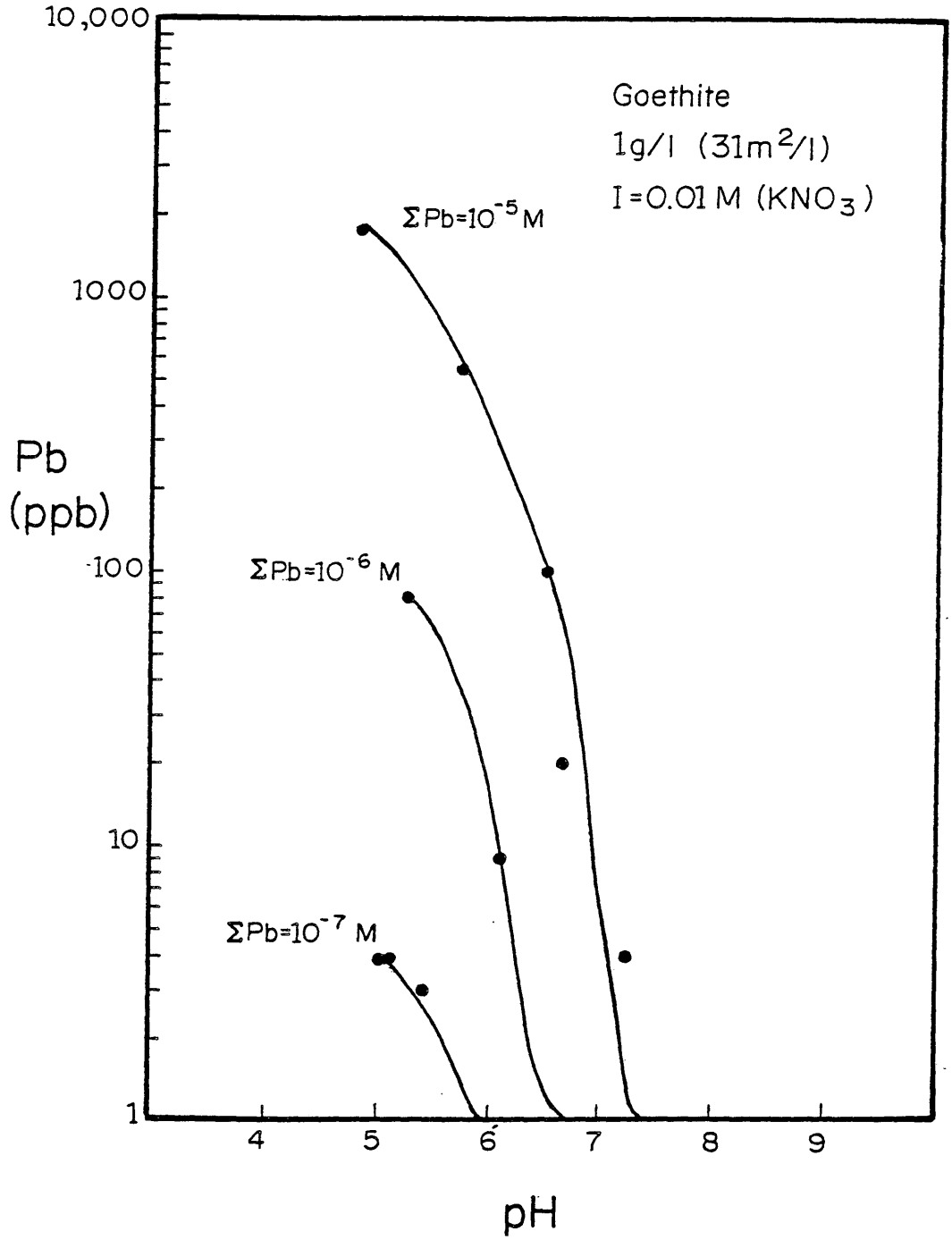

Figure 17: Effect of lead concentration on the pH adsorption edge for lead adsorption onto goethite under atmospheric conditions for I=0.01 M (KNO_3) at 25° C.

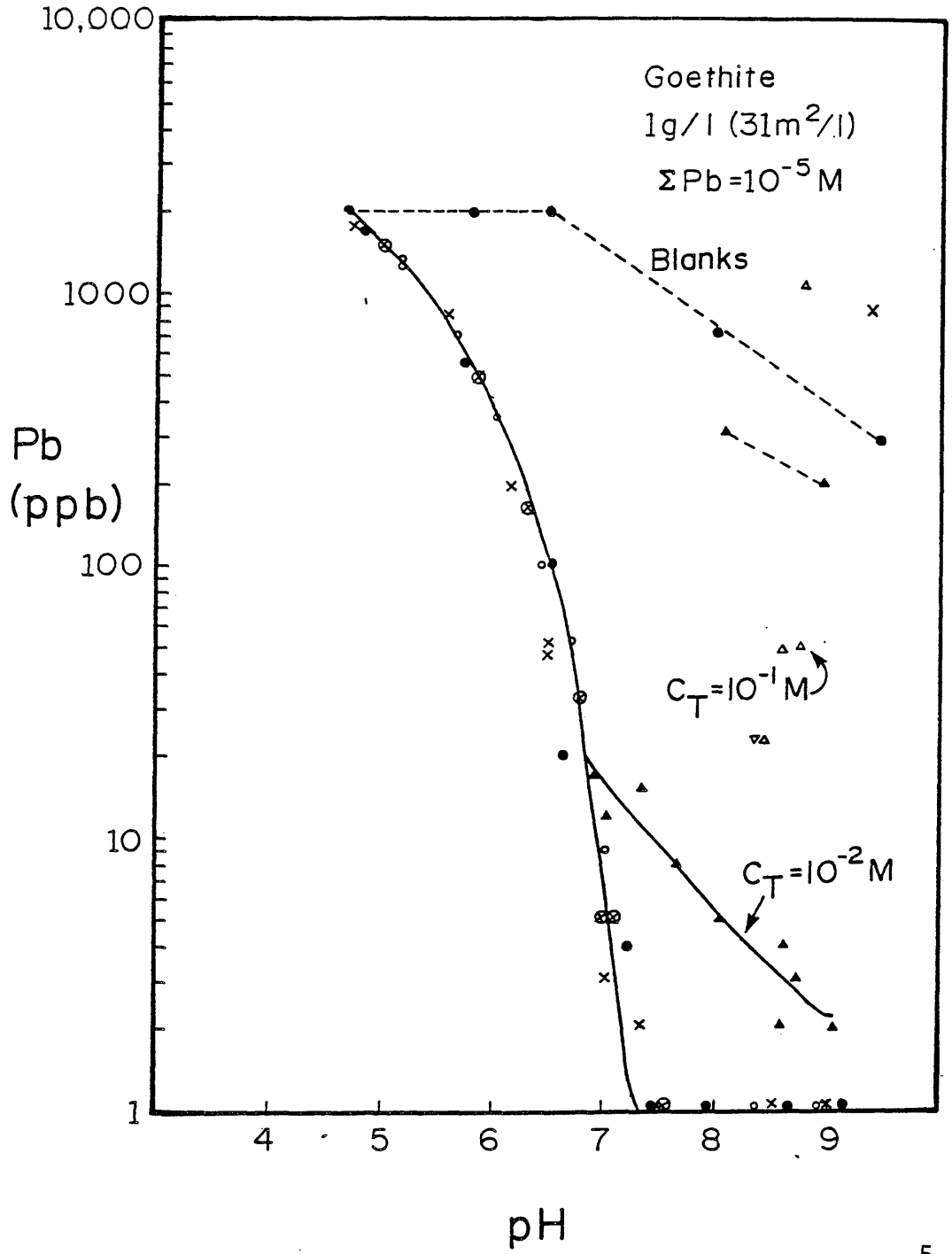

Figure 18: Adsorption of lead onto goethite for $\Sigma Pb = 10^{-5}$ M under a variety of aqueous conditions (see Fig. 14 for key to data symbols).

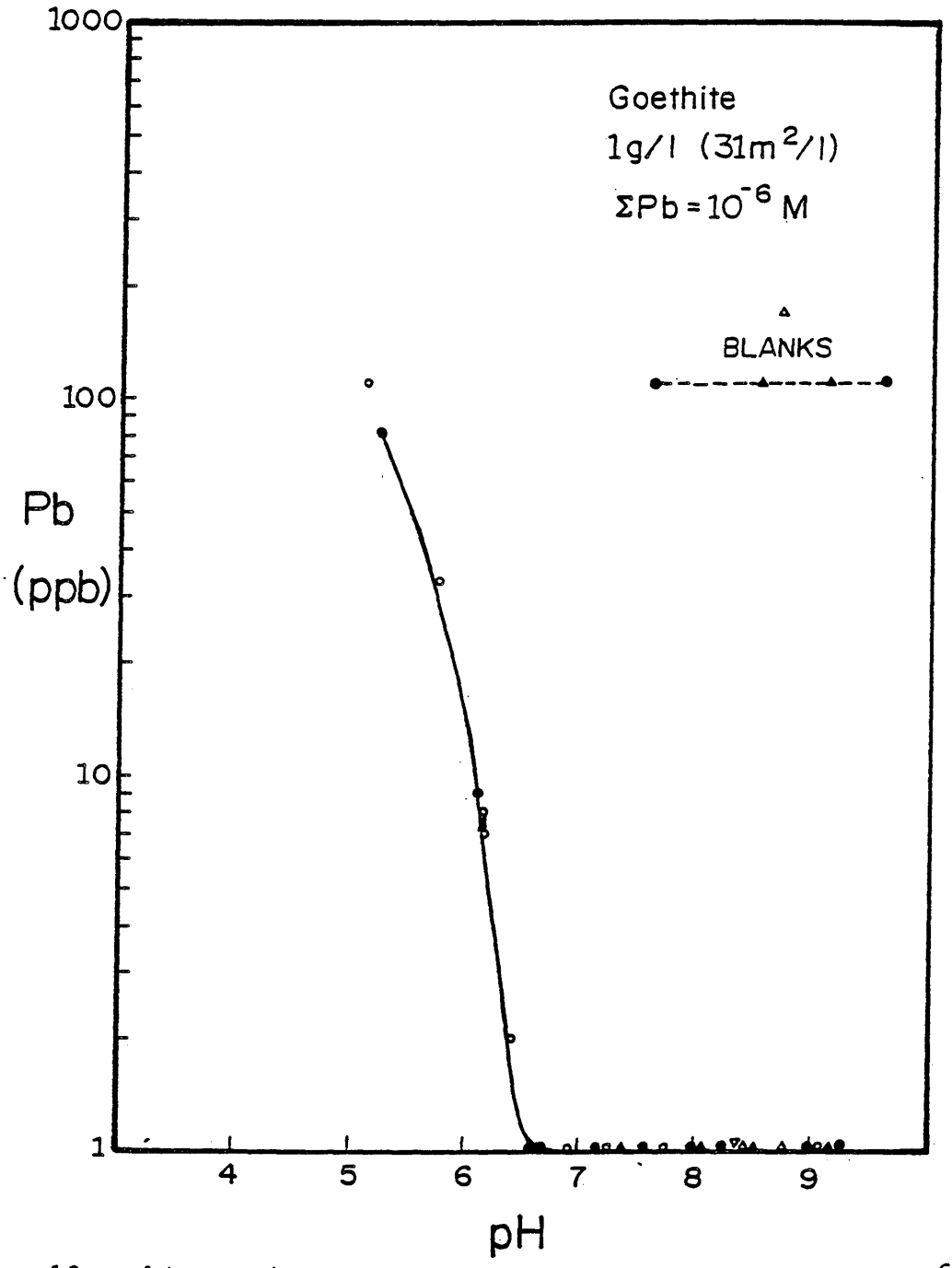

Figure 19: Adsorption of lead onto goethite for $\Sigma Pb=10^{-6}$ M under a variety of aqueous conditions (see Fig. 14 for key to data symbols).

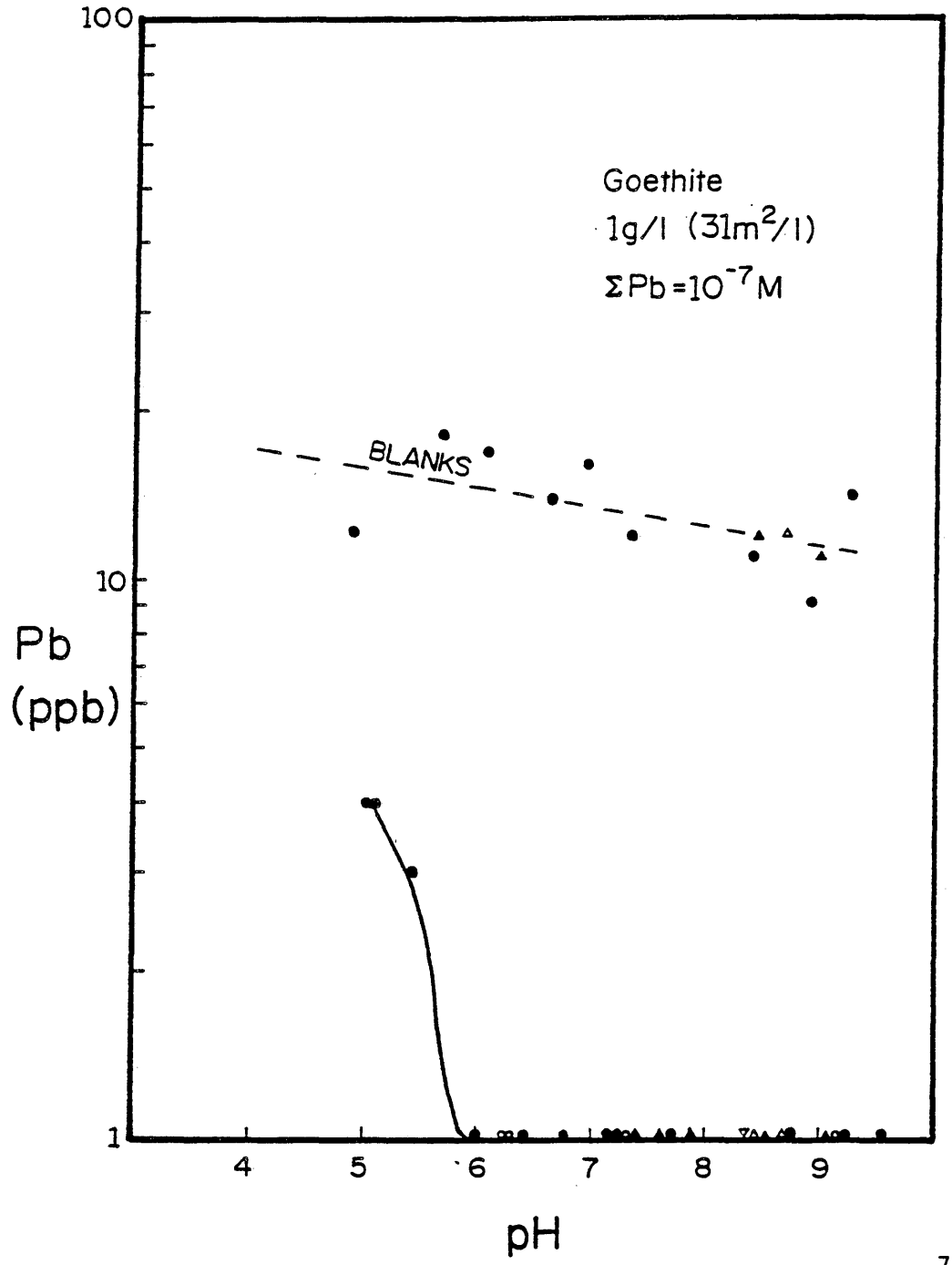

Figure 20: Adsorption of lead onto goethite for $\Sigma Pb = 10^{-7}$ M under a variety of aqueous conditions (see Fig. 14 for key to data symbols).

iron was below the limit of detection (20 ppb). Adsorption density was varied by changing the metal concentration as total surface area remained constant.

Blank experiments (without goethite) were run under the same conditions as the adsorption experiments. Results indicate that there is no significant adsorption of metal to the centrifuge tubes at higher metal concentrations, but there may be some interactions at lower concentrations. In cases where a precipitate appeared in blank solutions, the adsorption edge of the adsorption run occurred prior to the pH of precipitation. This illustrates that dissolved metals in these adsorption experiments are controlled by adsorption reactions rather than solid precipitation reactions.

COPPER

Figure 13 illustrates the pH dependence of adsorption edges at different copper concentrations for a constant goethite surface area of 31 m^2/l in 0.01 M KNO_3. As seen in this figure, there is a shift of the adsorption edges to lower pH regions as the metal concentration is decreased. In all cases, in excess of 99% of the metal is adsorbed at the pH(PZC) of 7.6. This indicates that copper is specifically adsorbed by goethite (assuming that copper is

adsorbed as a positively-charged species). Specific adsorption can be defined as adsorption when both adsorbate and the net surface charge of the adsorbent are similarly charged (Catts, 1982).

Figures 14, 15, and 16 show more detailed adsorption isotherms for copper concentrations of 10^{-4}, 10^{-5}, and 10^{-6} M, respectively. These figures indicate that there is essentially no difference in the results of experiments performed at C_T = 0 or atmospheric CO_2 conditions. Also, there is no effect of either KNO_3 ionic strength (0.01 versus 0.1 M). Figures 14 and 15 imply that there is an inhibitory effect on copper adsorption in the higher C_T experiments. In the $\Sigma Cu = 10^{-4}$ M, $C_T = 10^{-2}$ M experiment, about 80 ppb copper remains in solution at the pH(PZC). This value represents only about 1.3% of the total copper present but could result in environmentally significant amounts of copper mobilized in a natural setting. Futhermore, the degree of adsorption inhibition by carbonate is proportional to C_T (see Fig. 14).

LEAD

Figure 17 illustrates the pH dependence of adsorption edges at different lead concentrations for a constant

goethite surface area of 31 m^2/l in 0.01 M KNO_3. As was the case with copper, there is a shift of the adsorption edges to lower pH regions as the lead concentration is decreased. In all cases, in excess of 99.9% of the lead is adsorbed at the pH(PZC) indicating that lead is specifically adsorbed by goethite.

Figures 18, 19, and 20 show more detailed adsorption isotherms for lead concentrations of 10^{-5}, 10^{-6}, and 10^{-7} M, respectively. As was the case for copper, there is essentially no difference in experimental results for I = 0.01 and I = 0.1 M (as KNO_3), nor for C_T = 0 versus atmospheric conditions. Figure 18 implies a similar inhibitory effect of carbonate on lead adsorption as was true of copper adsorption in higher C_T experiments. In the $C_T = 10^{-2}$ M experiment, about 8 ppb lead remains in solution. This value represents less than 1% of the total lead present. The degree of adsorption inhibition is proportional to C_T.

There was no solid precipitation in the blank experiments at total lead concentrations of 10^{-6} and 10^{-7} M. The variable yet steadily-decreasing blank data points for the 10^{-7} M experiments may be due to lead interaction with container walls.

Copper is specifically adsorbed more strongly than

lead. This is illustrated by the relative positions of their adsorption edges at equal molar concentrations (compare Figs. 17 and 13).

DISCUSSION

Results indicate that there is an inhibitory effect on copper and lead adsorption in the higher C_T experiments. The degree of adsorption inhibition is proportional to C_T and total metal concentration. Adsorption inhibition onto goethite by dissolved carbonate species has previously been reported for the uranium system (Hsi, 1981; Tripathi, 1984; Hsi and Langmuir, 1985) and the plutonium system (Sanchez and others, 1985). This adsorption inhibition is probably due to increased carbonato complexing of the metals. Figure 21 illustrates aqueous speciation for 10^{-4} M total copper under atmospheric conditions (solid lines) and $C_T = 10^{-2}$ M conditions (dashed lines). A comparison of the species distribution for these different C_T conditions shows that there is both an increase in carbonato complexing, at the expense of hydroxo complexing, and a downward pH shift of the carbonato complexes with increasing C_T. These combined effects place the dominant neutral carbonato complex in the pH range of greatest adsorption inhibition, and at a pH

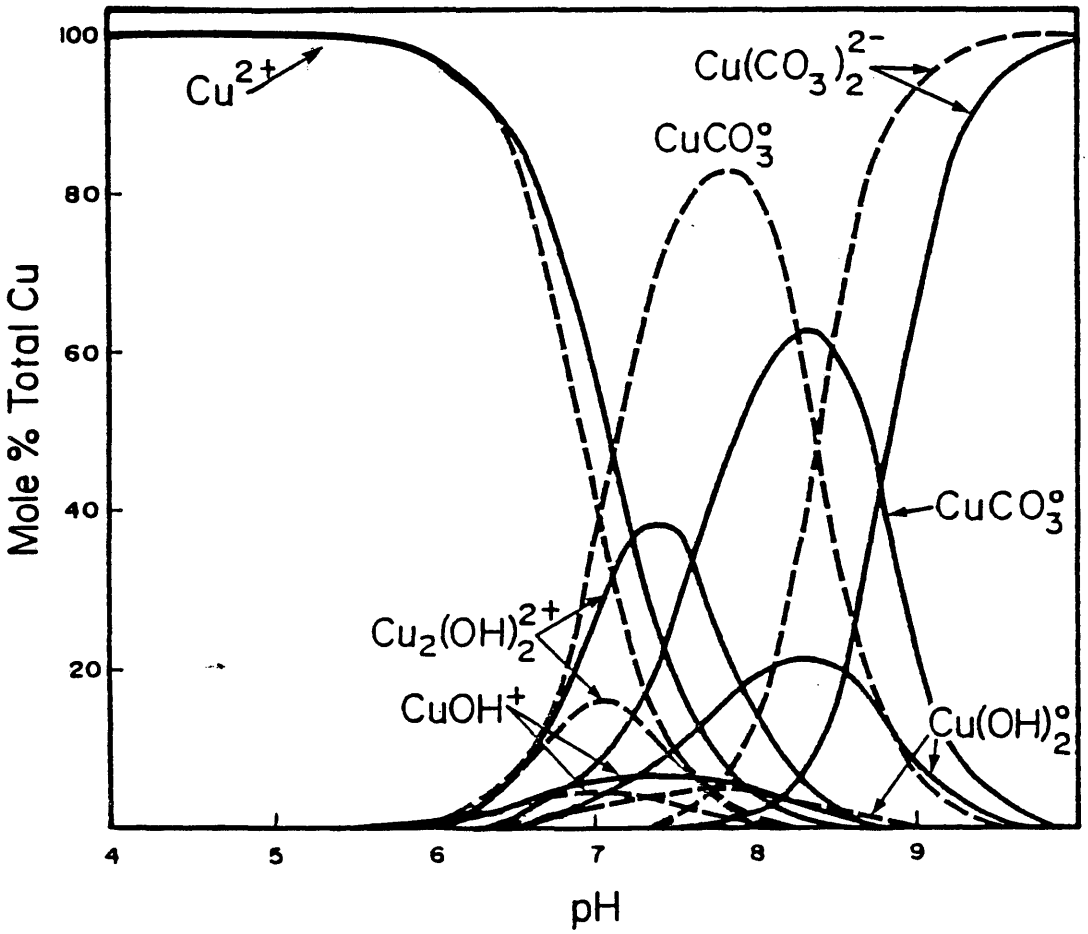

Figure 21: Distribution diagram for copper species as a function of pH for the Cu^{2+}-H_2O-CO_2 system under atmospheric conditions (solid lines) and $C_T=10^{-2}$ M (dashed lines) for $\Sigma Cu=10^{-4}$ M and 25°C.

below completion of the adsorption edge seen in Figure 14. This neutral carbonato complex would be expected to be weakly adsorbed, if at all, compared to free metals and/or hydroxo complexes. The arguments are similar for the lead system (Fig. 22).

As was shown in Figures 13 and 17, there is a shift of the adsorption edges to lower pH regions as the total metal concentration is decreased. Therefore, the lower metal concentration adsorption edges are completed at a pH prior to the neutral carbonato complex region of dominance and no adsorption inhibition by carbonate species would be expected. This correlates with the fact that little or no adsorption inhibition by carbonate was noted at lower metal concentrations in the experimental systems. Hence, adsorption inhibition by carbonate is a function of C_T, pH, and total metal concentration.

Although these experiments were performed in the laboratory, the findings have implications to metal mobility in natural soil systems and aquifers. In neutral to alkaline (especially arid-climate) soils and in groundwater systems that contain calcite and dolomite, carbonato complexing of copper and lead can be expected to increase the mobilities of those metals.

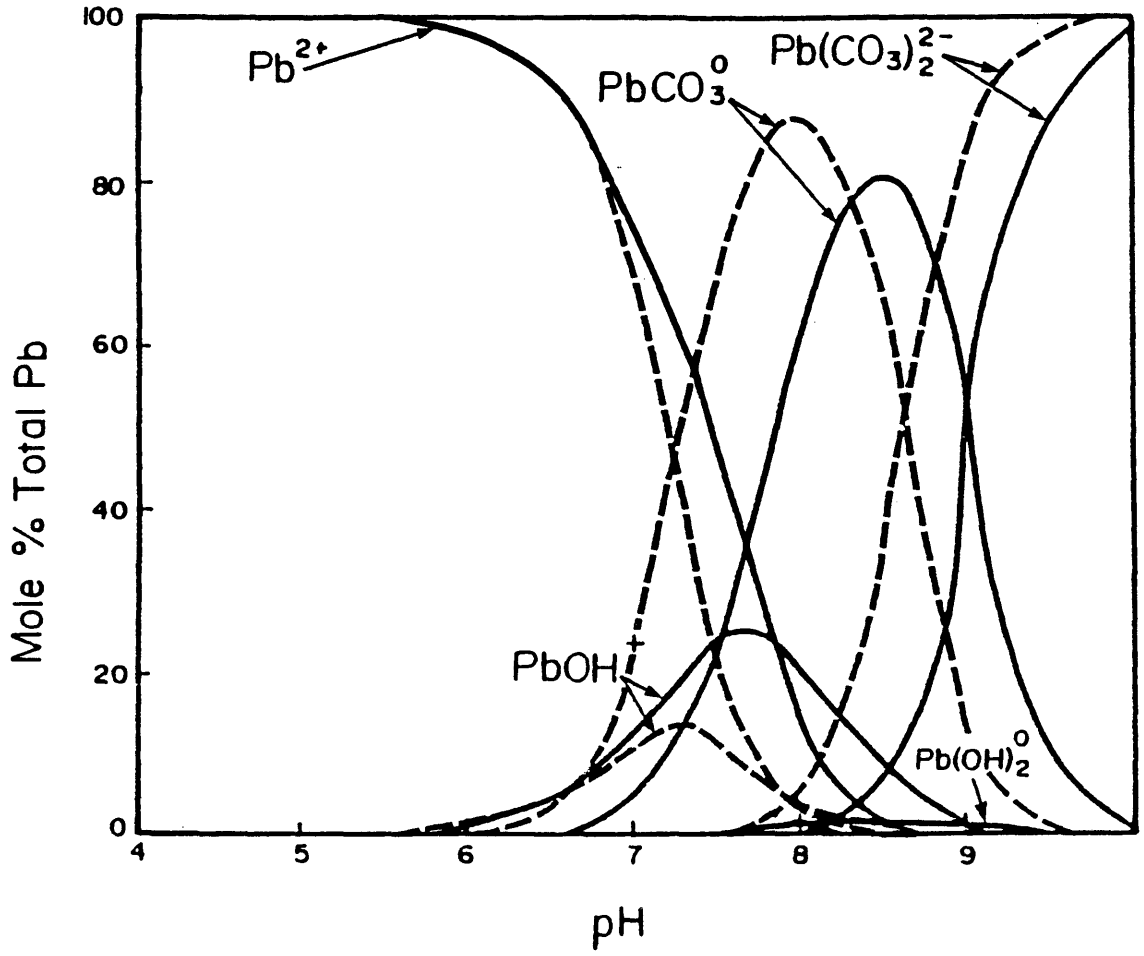

Figure 22: Distribution diagram for lead species as a function of pH for the Pb^{2+}-H_2O-CO_2 system under atmospheric conditions (solid lines) and $C_T=10^{-2}$ M (dashed lines) for $\Sigma Pb=10^{-5}$ M and 25°C.

RESULTS OF SORPTION MODELING

SURFACE COMPLEXATION SITE-BINDING MODEL

The framework of the surface complexation site-binding model is discussed in the Electrostatic Models section of this thesis. Davis and others (1978) have integrated the surface complexation site-binding model into a version of the chemical equilibrium computer program MINEQL (Westall and others, 1976). This program can simultaneously consider solution equilibria and multiple adsorption reactions based on the development of surface charge and potential at the solid/solution interface. Necessary input for the model includes values for intrinsic acidity and complexation constants, inner and outer layer capacitances (C_1 and C_2), specific surface area (A), and surface site density (N_s). The terms [SOH], $\exp(-e\psi_0/kT)$, and $\exp(-e\psi_\beta/kT)$ are treated as independent variables.

Determination of Parameters

Modeling parameters play a significant role in the modeling process. Of the necessary input values, only two are model independent; the surface site density (N_s) and the specific surface area (A). Determination of specific

surface area was discussed in the BET Surface Area section of this thesis. For surface site density the value of 18 sites/nm^2 from Hsi (1981) will be used. Hsi (1981) measured this value using the tritium exchange method of Berube and others (1967) and Yates (1975).

As was discussed in the Electrostatic Models section, neither the intrinsic acidity constants nor the intrinsic complexation constants are directly measureable. However, they can be estimated using apparent stability quotients, Q. James and others (1978) and Davis and others (1978) designed a graphical double extrapolation technique by which intrinsic acidity constants and intrinsic complexation constants for background electrolytes can be evaluated. Their procedure is based on the supposition that apparent stability quotients are related to intrinsic constants through electrostatic field correction terms (Davis and others, 1978). Therefore, intrinsic equilibrium constants can be estimated by extrapolation of the apparent stability quotients to zero charge and zero ionic strength conditions for intrinsic acidity constants, and zero charge and I = 1 M for intrinsic complexation constants. Potentiometric titration data, as discussed previously, are used to construct these plots.

For pH values less than the pH(PZC), it can be

approximated that:

$$[SOH_2^+] = \frac{\sigma_o}{B} \quad \text{and} \quad [SOH] = \frac{N_s - \sigma_o}{B}$$

where $B = 10^6$ F / A (A = specific surface area), N_s is the surface site density (charge / cm^2), and σ_o is the surface charge. The relationship between the intrinsic acidity constant and the apparent stability quotient is:

$$K_{a1}^{int} = \frac{[SOH]\ \{H^+\}}{[SOH_2^+]} \exp\ (-e\psi_o / kT) = Q_{a1} \exp\ (-e\psi_o / kT)$$

where:

$$Q_{a1} = \frac{[SOH]\ \{H^+\}_{(aq)}}{[SOH_2^+]}$$

Upon defining the fractional surface charge as:

$$\alpha_+ = \frac{\sigma_o}{N_s}$$

the logarithmic form of the apparent stability quotient is:

$$pQ_{a1} = pH + \log \frac{\alpha_+}{1 - \alpha_+}$$

An analogous set of computations for pH values greater than

the pH(PZC) leads to a similar equation:

$$pQ_{a2} = pH - \log \frac{\alpha_-}{1 - \alpha_-}$$

When values for pQ are plotted versus $\alpha_\pm + C^{1/2}$ (where C is the electrolyte concentration (M)), potentiometric titration data measured at different ionic strengths can be graphically extrapolated to zero charge and zero ionic strength. Plots for the acidity constants are given in Figures 23 and 24.

When values of pQ versus $\alpha_\pm$ - log C (where C is equal to the concentration of the background electrolyte cation or anion) are graphed, estimates for background electrolyte complexation constants can be obtained (see Figs. 25 and 26).

The inner and outer layer capacitances are adjustable parameters. However, 20 μF / cm^2 has become the accepted value for the outer layer capacitance (C_2) (Stumm and others, 1970; Lyklema and Overbeek, 1961; Davis and others, 1978). The inner layer capacitance (C_1) is estimated by trial and error model fitting of potentiometric titration surface charge data. A value of 280 μF / cm^2 was necessary to fit the data in this study. Balistrieri and Murray (1981) found that a similar inner layer capacitance value of

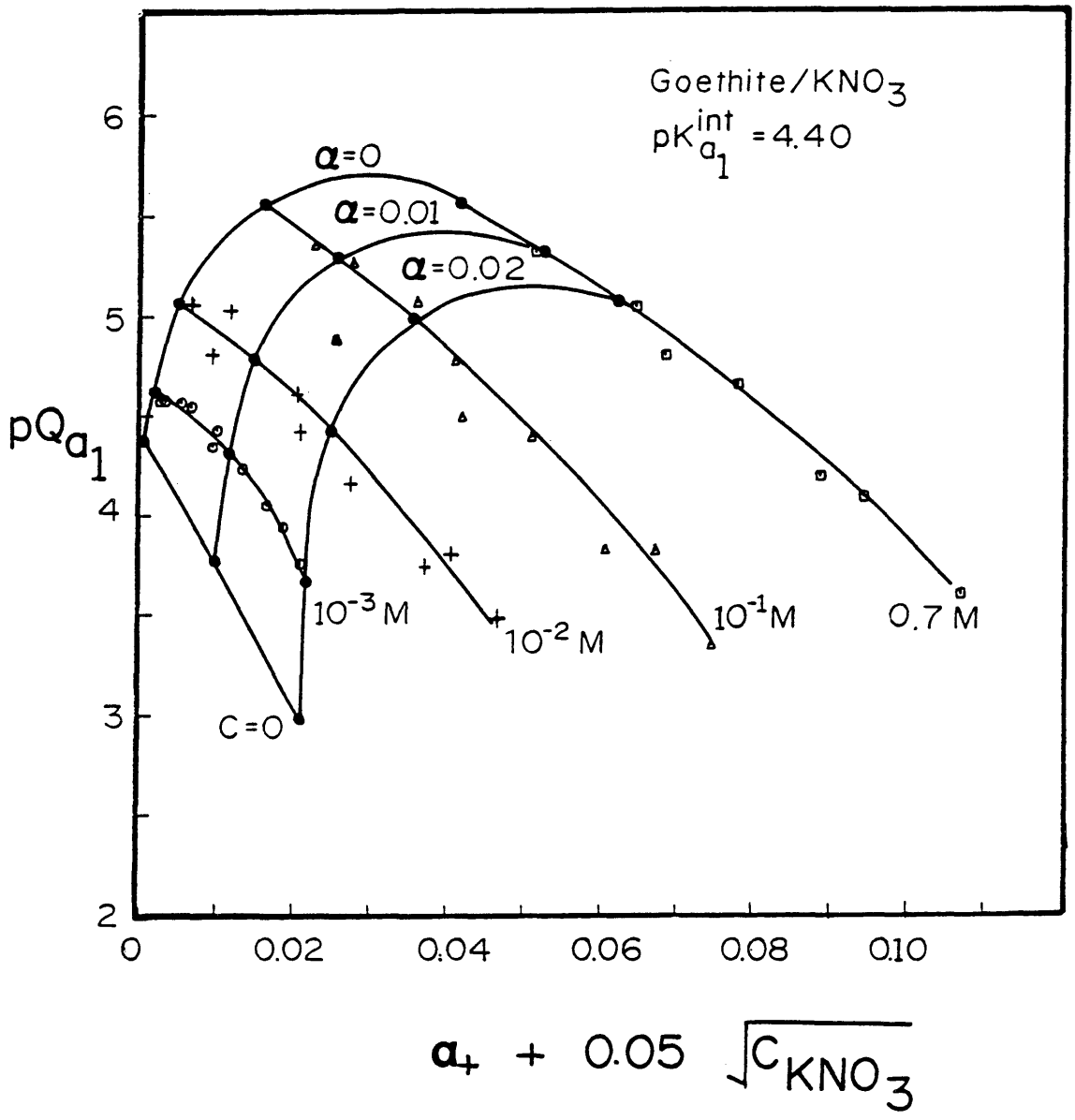

Figure 23: Double extrapolation plot for estimation of the first intrinsic acidity constant in KNO_3 solutions at 25°C. Circles represent potentiometric titration data at $I=10^{-3}$ M, crosses are data at $I=10^{-2}$ M, triangles are data at $I=10^{-1}$ M, and squares are data at $I=0.7$ M (as KNO_3).

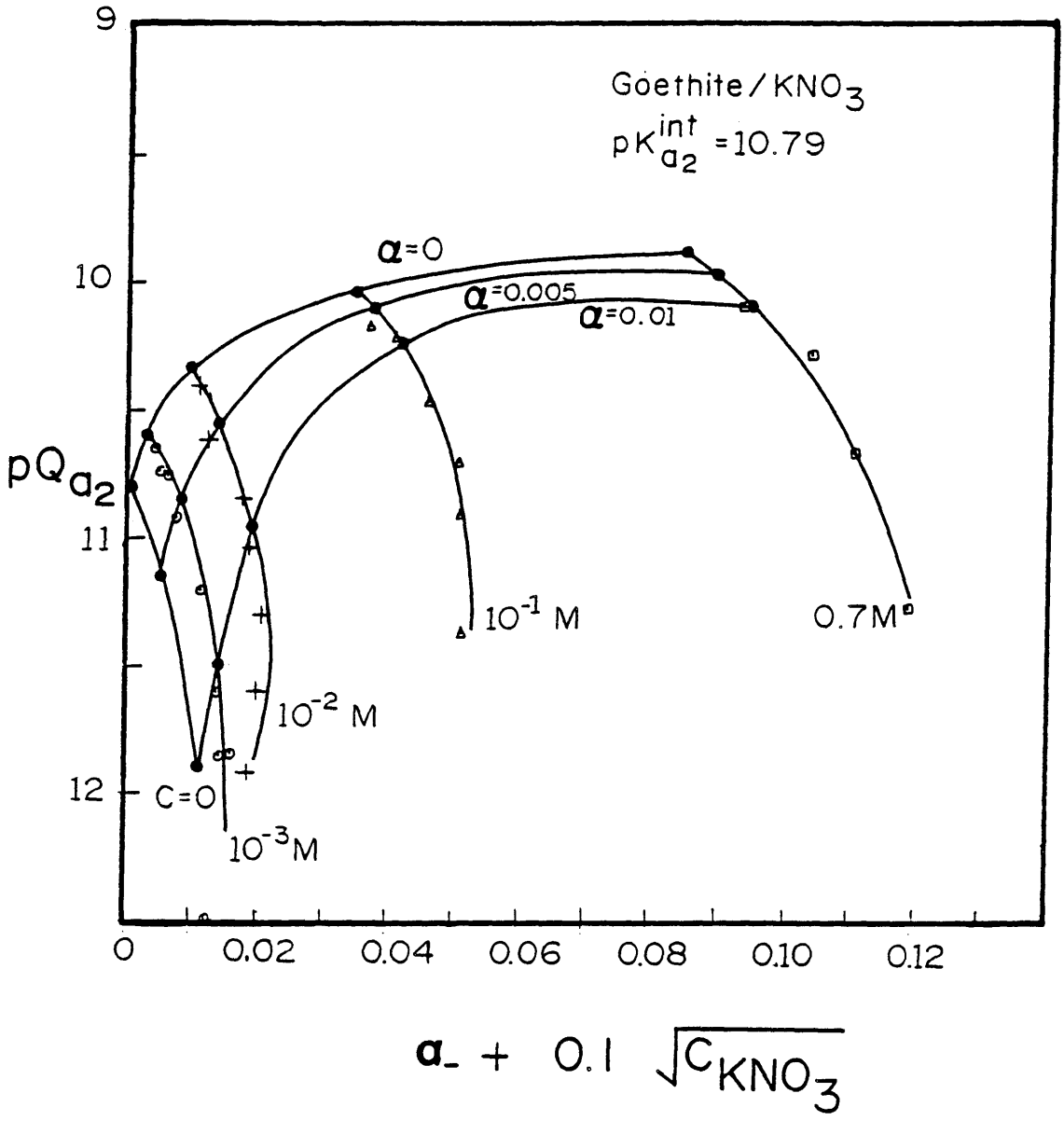

Figure 24: Double extrapolation plot for estimation of the second intrinsic acidity constant in KNO_3 solutions at 25°C. See Fig. 23 for explanation of symbols.

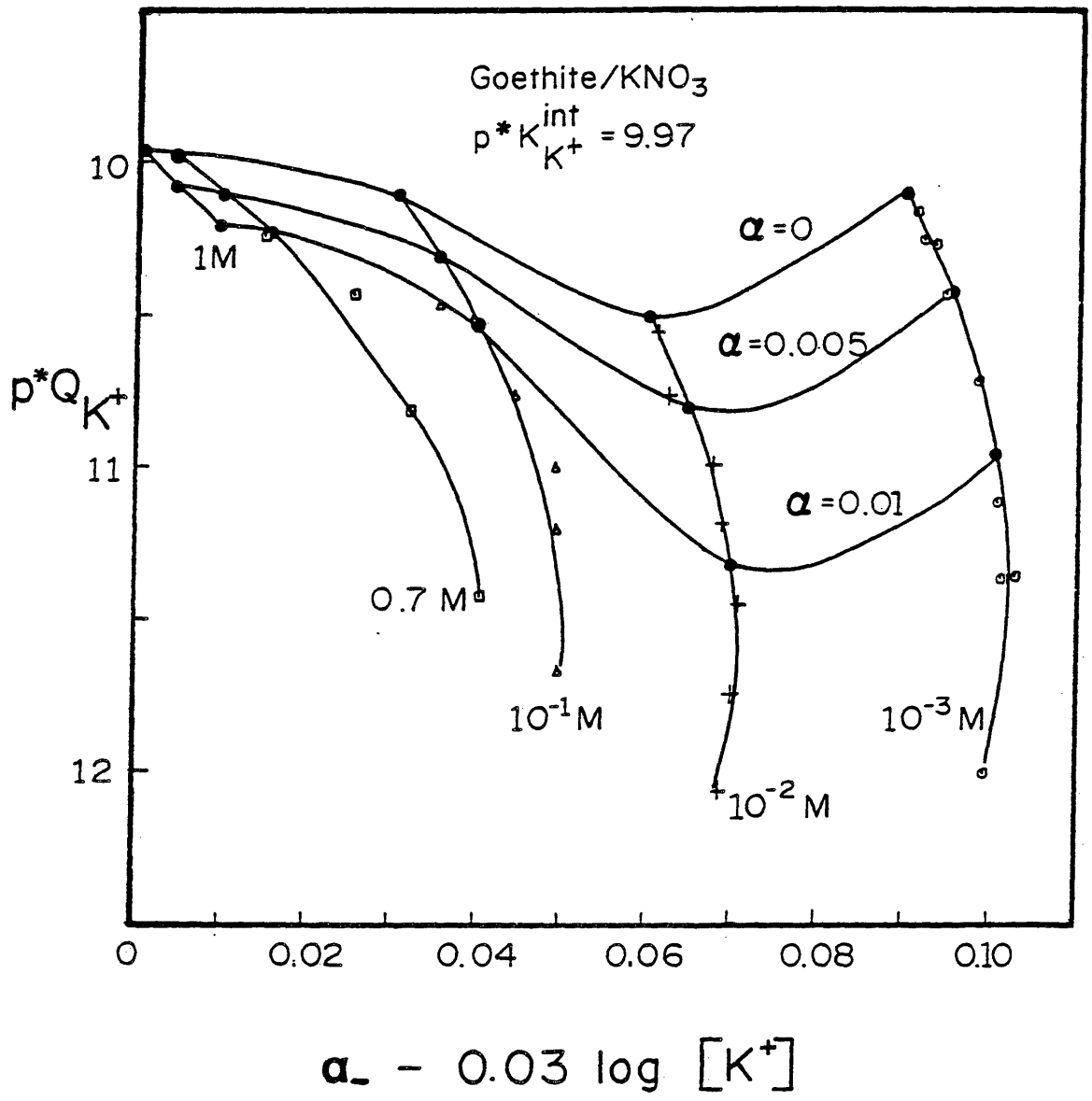

Figure 25: Double extrapolation plot for the estimation of the cationic intrinsic complexation constant in KNO_3 solutions at 25°C. See Fig. 23 for explanation of symbols.

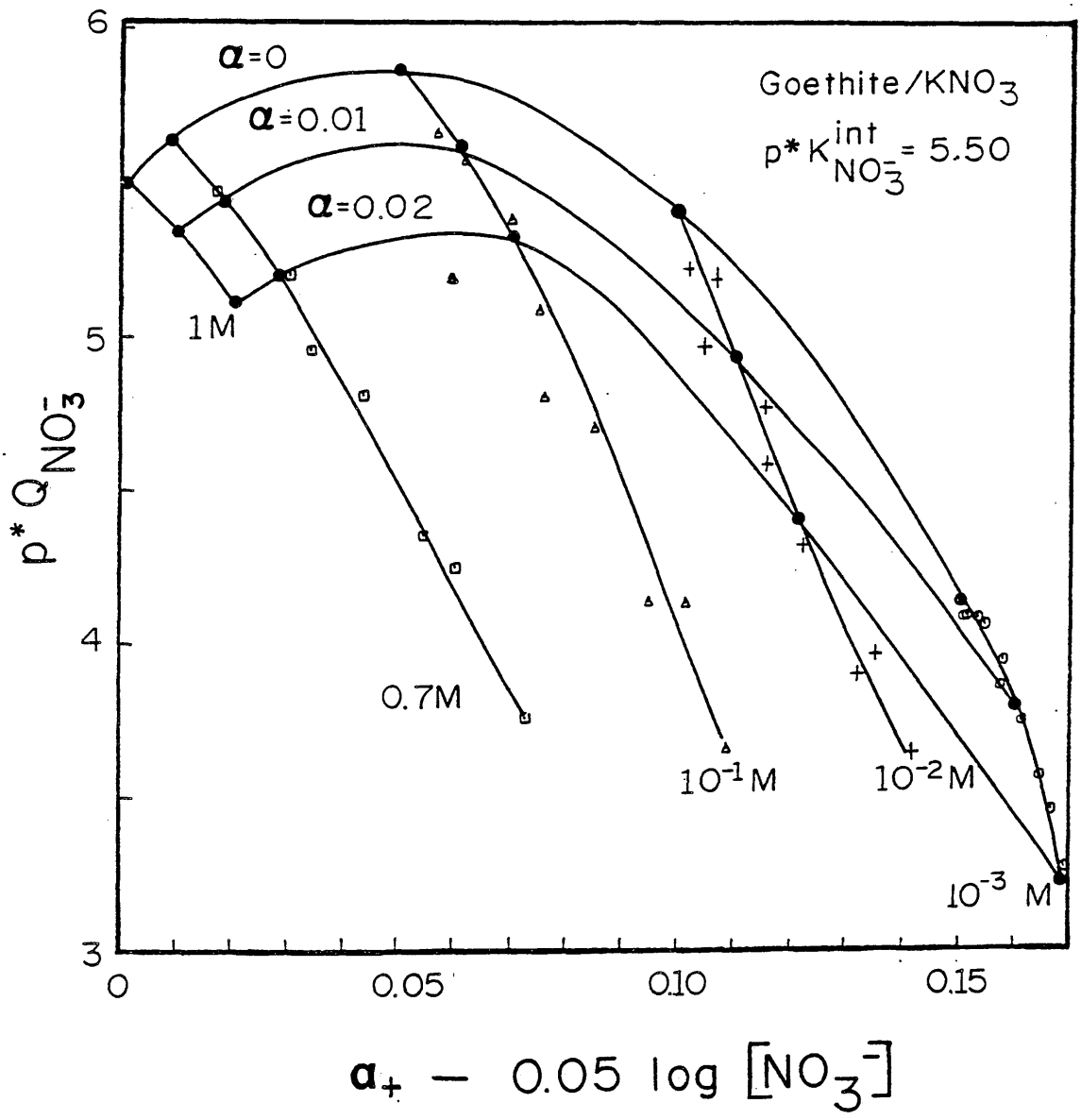

Figure 26: Double extrapolation plot for the estimation of the anionic intrinsic complexation constant in KNO_3 solutions at 25°C. See Fig. 23 for explanation of symbols.

260 μF / cm^2 was needed to fit goethite behavior. However, Davis and others (1978) concluded that C_1 values should range from 100 to 140 μF / cm^2 for oxide surfaces. As a result, Balistrieri and Murray (1981) chose to alter other parameters such that a lower capacitance value could be used in their modeling. Accepting that precedent, the inner layer capacitance was set at 140 μF / cm^2 for this study. As long as a fit of the potentiometric titration surface charge data is obtained, this adjustment will not affect the overall interpretation of the data. The background electrolyte complexation constants were adjusted to obtain a best fit of the experimental surface charge data (Fig. 27). The resulting complexation constants were:

$$p^*K^{int}_{K^+} = 8.75 \text{ and } p^*K^{int}_{NO_3^-} = 6.90$$

Care was taken to adjust the model to best fit the 10^{-2} and 10^{-1} M data as these are the ionic strengths used in the adsorption experiments. Also, it was more important to fit the surface charge below the pH(PZC) of 7.6 because this is the area where the adsorption edges occur. Deviation of the model fits from the experimental values at higher pH's may be due to coagulation of the goethite during the titration experiments. Table 6 summarizes goethite surface parameters used for surface complexation site-binding model calculations in this and other studies.

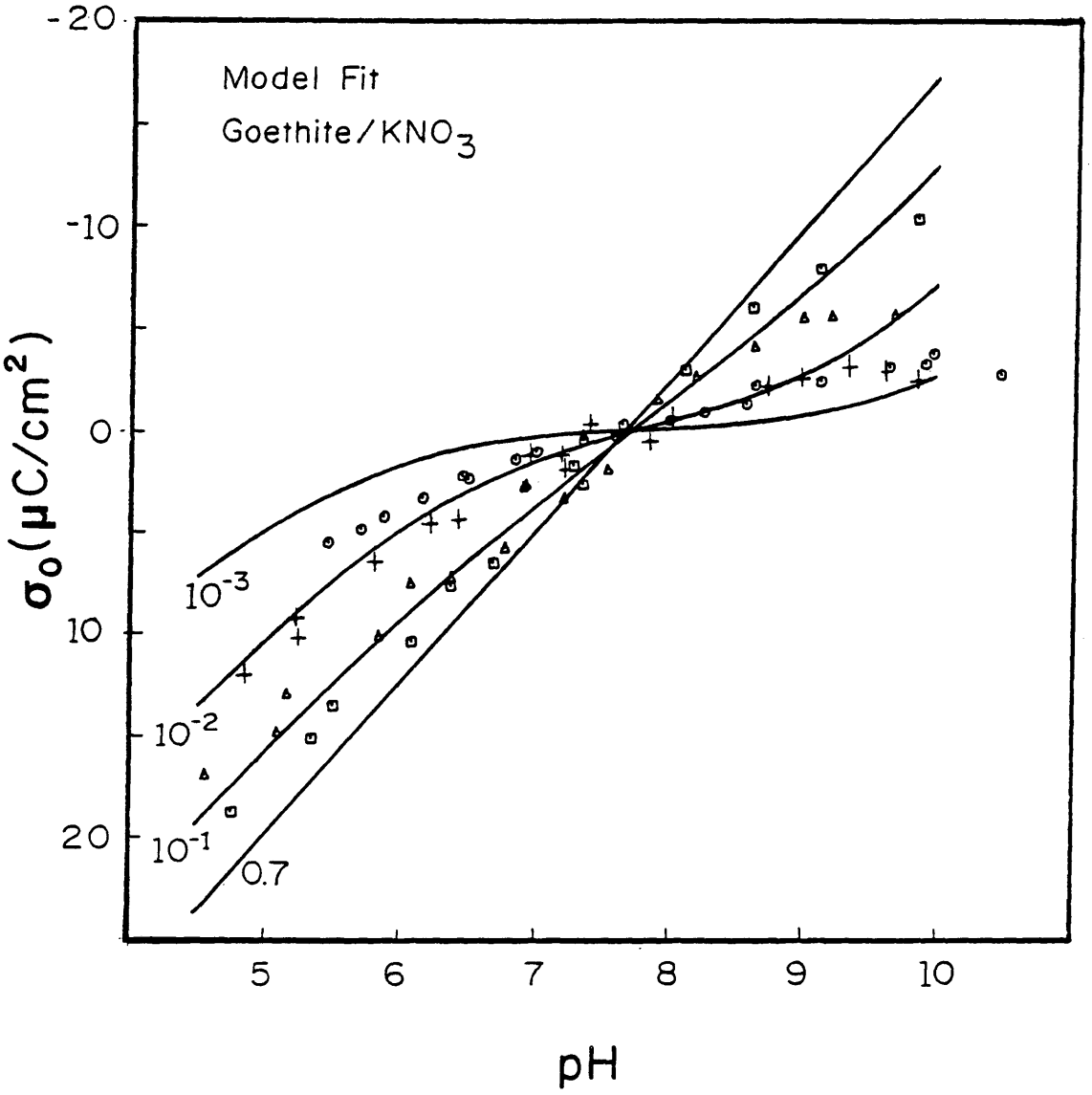

Figure 27: Experimental and computed surface charge density in KNO_3 solutions at 25°C as a function of ionic strength and pH. The solid lines represent model calculations and the symbols are derived from potentiometric titration data. See Fig. 23 for explanation of symbols.

Table 6: Surface parameters of goethite used in model calculations from this and other studies. -- indicates the parameter was not determined in that particular study. All studies assumed C_2 = 20 $\mu F/cm^2$.

Source	a	b	c	d	e	f	g	h
Background Electrolyte	KNO_3	$NaNO_3$	NaCl KCl	NaCl KCl	KCl	NaCl	KNO_3	$NaNO_3$
Surface Area (m^2/g)	30.8	45	48.5	51.8	70.9	32	48	52
Surface Site Density (sites/nm^2)	--	18	--	--	--	--	16.8	7.0
Inner Layer Capacitance (C_1; ($\mu F/cm^2$)	140	140	--	140	--	--	100	110
pH (PZC)	7.6	8.5	7.5	7.5	7.5	7.7	7.5	
pK_{a1}^{int}	4.4	4.5	4.9	5.6	7.0	4.9	4.2	5.8
pK_{a2}^{int}	10.8	12.0	10.4	9.5	8.4	--	10.8	11.1
$p^*K_{cation}^{int}$	8.8	10.1	9.6	8.4	--	6.6	8.9	8.8
$p^*K_{anion}^{int}$	6.9	7.0	5.5	7.0	--	--	6.1	7.6

a This study.
b Hsi (1981).
c Balistrieri and Murray (1979).
d Balistrieri and Murray (1981).
e Atkinson and others (1967) as quoted in Huang (1981).
f Hingston and others (1968) as quoted in James (1981).
g Yates (1975).
h Hayes and Leckie (1986).

Copper and Lead Modeling

Introduction:

As discussed in the Electrostatic Models section of this thesis, the surface complexation site-binding model assumes three layers to be present at the EDL; the surface layer, the β-layer, and the diffuse layer. In the original formulation of this model, the closest that a metal species could come to the surface was the β-layer. In this way, only ion pair complexes between surface sites and metal species in the β-layer were considered (Hayes and Leckie, in press). Recently, the surface complexation site-binding model has been expanded such that metal species are allowed to form surface complexes at either the surface layer or the β-layer (Hachiya and others,1984; Leckie and others, 1986; Hayes and Leckie, in press). Hence, an adsorbed metal species may either form an outer sphere or an inner sphere surface complex. In outer sphere surface complexes, metal species retain their primary hydration sheaths upon adsorption, whereas in inner sphere surface complexes they lose portions of their primary hydration sheaths. This difference can affect both the model stoichiometry of the reaction and the closeness of approach of the adsorbed species to the surface (Hayes and Leckie, in press).

Assuming outer sphere surface adsorption reactions for Cu^{2+} and Pb^{2+}:

$$SOH + Cu_s^{2+} \overset{{}^*K^{int}_{Cu^{2+}}}{\rightleftarrows} SO^-Cu^{2+} + H_s^+$$

and

$$SOH + Pb_s^{2+} \overset{{}^*K^{int}_{Pb^{2+}}}{\rightleftarrows} SO^-Pb^{2+} + H_s^+$$

where the subscript s denotes an ion at or very near the surface, SOH represents a hydrated surface site, SO^- is an ionized surface site, and the ${}^*K^{int}$'s are intrinsic complexation constants. Concentrations of the adsorbed species may be expressed as:

$$[SO^-Cu^{2+}] = {}^*K^{int}_{Cu^{2+}} \frac{[SOH]\,[Cu^{2+}]}{[H^+]} \exp^{[(e\psi_o - 2e\psi_\beta) / kT]}$$

and

$$[SO^-Pb^{2+}] = {}^*K^{int}_{Pb^{2+}} \frac{[SOH]\,[Pb^{2+}]}{[H^+]} \exp^{[(e\psi_o - 2e\psi_\beta) / kT]}$$

Similarly, outer sphere adsorption of the first hydrolysis

species of copper and lead may be described by:

$$SOH + Cu_s^{2+} + H_2O \overset{{}^*K^{int}_{CuOH^+}}{\rightleftarrows} SO^-CuOH^+ + 2H_s^+$$

and

$$SOH + Pb_s^{2+} + H_2O \overset{{}^*K^{int}_{PbOH^+}}{\rightleftarrows} SO^-PbOH^+ + 2H_s^+$$

Concentrations of these adsorbed species are:

$$[SO^-CuOH^+] = {}^*K^{int}_{CuOH^+} \frac{[SOH]\,[Cu^{2+}]}{[H^+]^2} \exp^{[(e\psi_o - e\psi_\beta) / kT]}$$

and

$$[SO^-PbOH^+] = {}^*K^{int}_{PbOH^+} \frac{[SOH]\,[Pb^{2+}]}{[H^+]^2} \exp^{[(e\psi_o - e\psi_\beta) / kT]}$$

Inner sphere surface adsorption reactions may also be tested. The reactions for Cu^{2+} and Pb^{2+} inner sphere surface adsorption may be written as:

$$SOH + Cu_s^{2+} \overset{{}^*K^{int}_{Cu^{2+}}}{\rightleftarrows} SOCu^+ + H_s^+$$

and

$$SOH + Pb_s^{2+} \overset{{}^*K^{int}_{Pb^{2+}}}{\rightleftarrows} SOPb^+ + H_s^+$$

Concentrations of these adsorbed species are then:

$$[SOCu^+] = {}^*K^{int}_{Cu^{2+}} \frac{[SOH]\,[Cu^{2+}]}{[H^+]} \exp^{(-e\psi_o / kT)}$$

and

$$[SOPb^+] = {}^*K^{int}_{Pb^{2+}} \frac{[SOH]\,[Pb^{2+}]}{[H^+]} \exp^{(-e\psi_o / kT)}$$

The difference between inner and outer sphere surface adsorption expressions lies in the treatment of electrostatic potential terms.

The objective of modeling experimental adsorption data with the surface complexation site-binding model is to obtain intrinsic complexation constants for adsorption reactions which fit the data. The predictive ability of the model can then be evaluated via fits of experimental data not used to calibrate intrinsic complexation constants. The

simplest adsorption reactions which best fit the experimental data indicate which metal species are likely to be involved in the adsorption process. Outer and inner sphere metal adsorption analogues are tested and compared.

The strategy used to model experimental data was first to determine intrinsic complexation constants by trial and error for carbonate-free systems. Predominant aqueous species were tested first for adsorption reaction fits and as few reactions as possible were used. The intrinsic complexation constants from these adsorption reaction model fits were then used to model other experimental conditions.

Results:

There was essentially no difference in experimental results obtained under the different conditions of ionic strength (0.01 M and 0.1 M as KNO_3), and carbonate-free versus atmospheric (P_{CO_2} = $10^{-3.5}$ atm) conditions. Hence, the set of experimental points corresponding to I=0.01 M (as KNO_3) and atmospheric conditions was used to evaluate model fits. The highest total metal concentrations (total copper of 10^{-4} M and total lead of 10^{-5} M) were used to calibrate intrinsic complexation constants.

The following conditions were first assumed to calibrate intrinsic complexation constants for the

adsorption of copper and lead onto goethite: P_{CO_2} = 0, I = 0.01 M (as KNO_3), and either $\Sigma Cu = 10^{-4}$ M or $\Sigma Pb = 10^{-5}$ M. Single outer sphere adsorption reactions for Cu^{2+} and Pb^{2+} ions were tested first. As shown in Figs. 28 and 29, model fits using just the divalent ions are in poor agreement with the experimental data. Adjustment of the intrinsic complexation constants moves the curves up and down but does not change their shapes.

Next, outer sphere adsorption of $CuOH^+$ and $PbOH^+$ ions alone was tested. Figure 29 shows that this model reaction provides a good fit of the experimental data for lead with the following intrinsic complexation constant:

$$p^*K^{int}_{PbOH^+} = 8.50$$

It is necessary to include an additional adsorption reaction to model the copper data. Adsorption of $Cu(OH)_2^o$ onto a negative surface site was added to the $CuOH^+$ adsorption model. A good fit of the data resulted with the following intrinsic complexation constants (see Fig. 28):

$$p^*K^{int}_{CuOH^+} = 8.80 \qquad p^*K^{int}_{Cu(OH)_2^o} = 13.60$$

These are the simplest outer sphere adsorption model

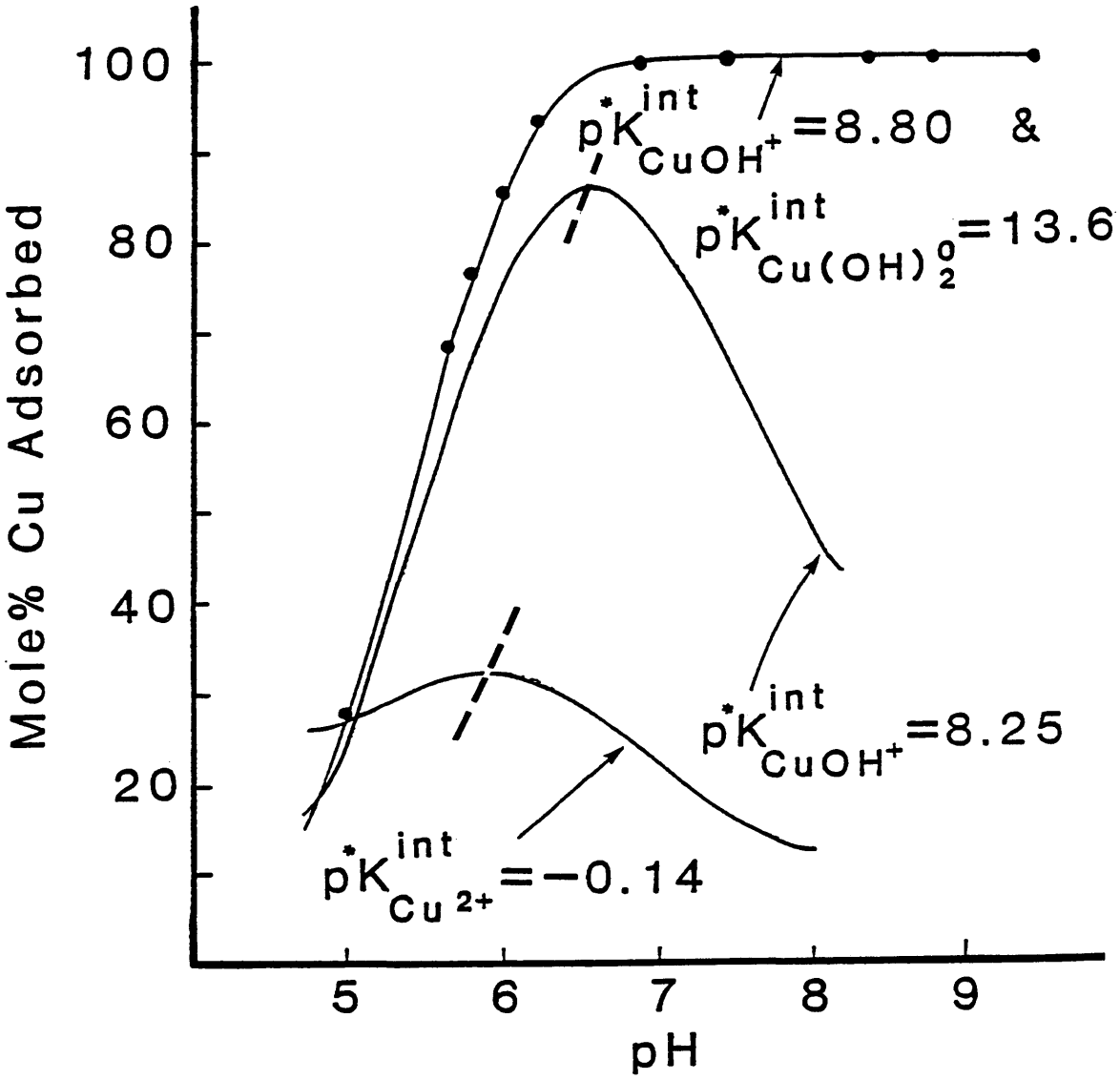

Figure 28: Model-calculated outer sphere surface adsorption of copper by goethite at C_T = 0, I = 0.01 M (as KNO_3), and 25°C for ΣCu = 10^{-4} M. Symbols represent experimental data points and solid lines are calculated model fits of the data. Dashed lines are the points at which solid precipitation took place in the model calculations. The p^*K^{int}'s are model-calculated intrinsic complexation constants.

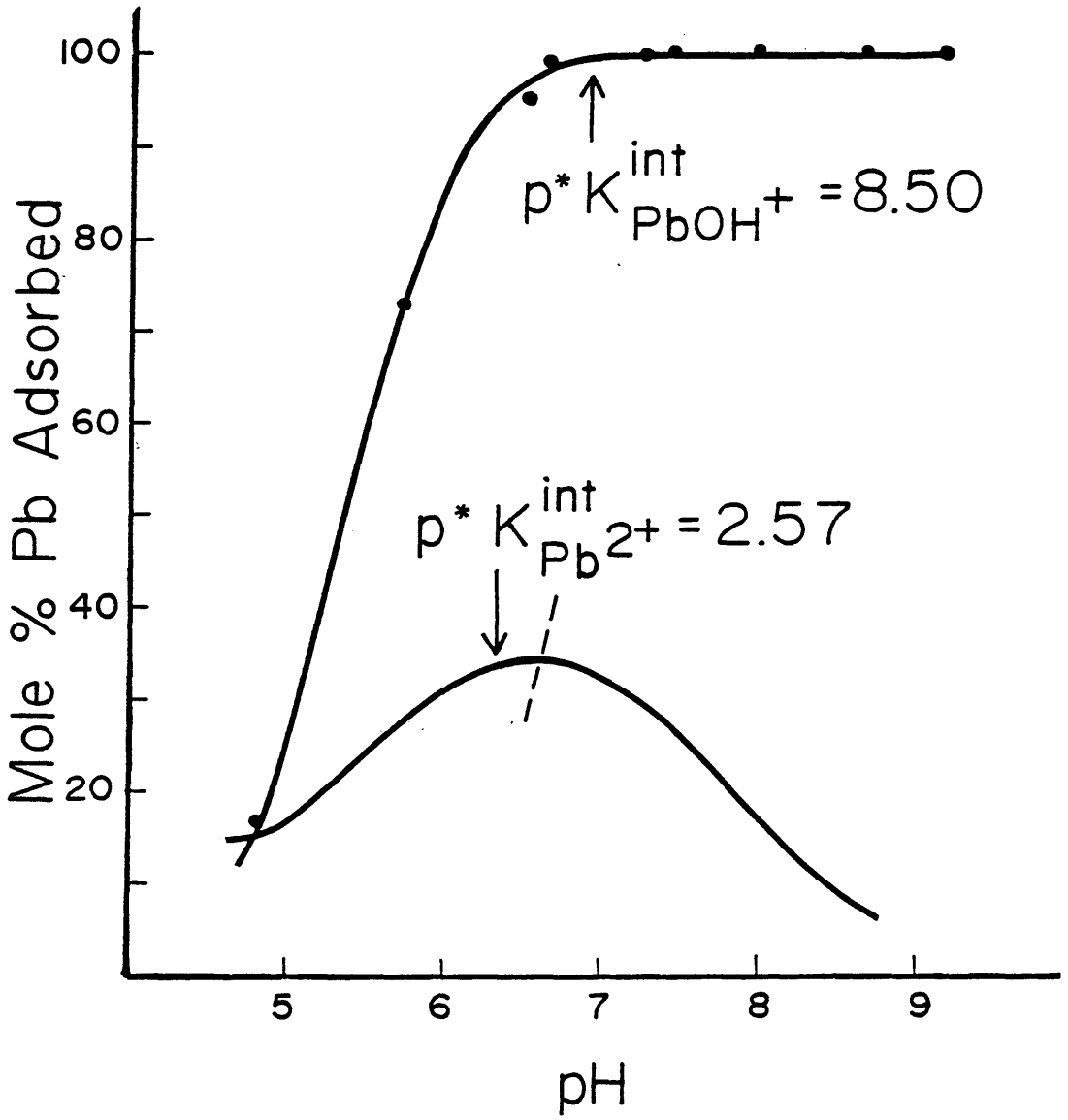

Figure 29: Model-calculated outer sphere surface adsorption of lead by goethite at C_T = 0, I = 0.01 M (as KNO_3), and 25°C for ΣPb = 10^{-5} M. See Fig. 28 for further explanation.

scenarios for copper and lead experimental data under the given conditions. Good model fits of data were also obtained assuming the simultaneous adsorption of a variety of other aqueous species (two or more at a time). However, these other scenarios did no better job of fitting experimental data obtained under different conditions. Intrinsic complexation constants used for model fits appear to be precise to within 0.5 log units for a given adsorption reaction or set of reactions.

Inner sphere adsorption of Cu^{2+} and Pb^{2+} onto goethite was also modeled for $P_{CO_2} = 0$, I = 0.01 M (as KNO_3), and either $\Sigma Cu = 10^{-4}$ or $\Sigma Pb = 10^{-5}$ M. The scenario of inner sphere adsorption of free metal ions yielded good fits for both copper and lead. Adsorption predicted by these reactions is illustrated in Figs. 30 and 31 for the following intrinsic complexation constants:

$$p^*K^{int}_{Cu^{2+}} = -1.85$$

$$p^*K^{int}_{Pb^{2+}} = -0.38$$

Thus far, it is not clear which kind of metal adsorption analogue is better, the outer or the inner sphere. Both do a good job of modeling the experimental

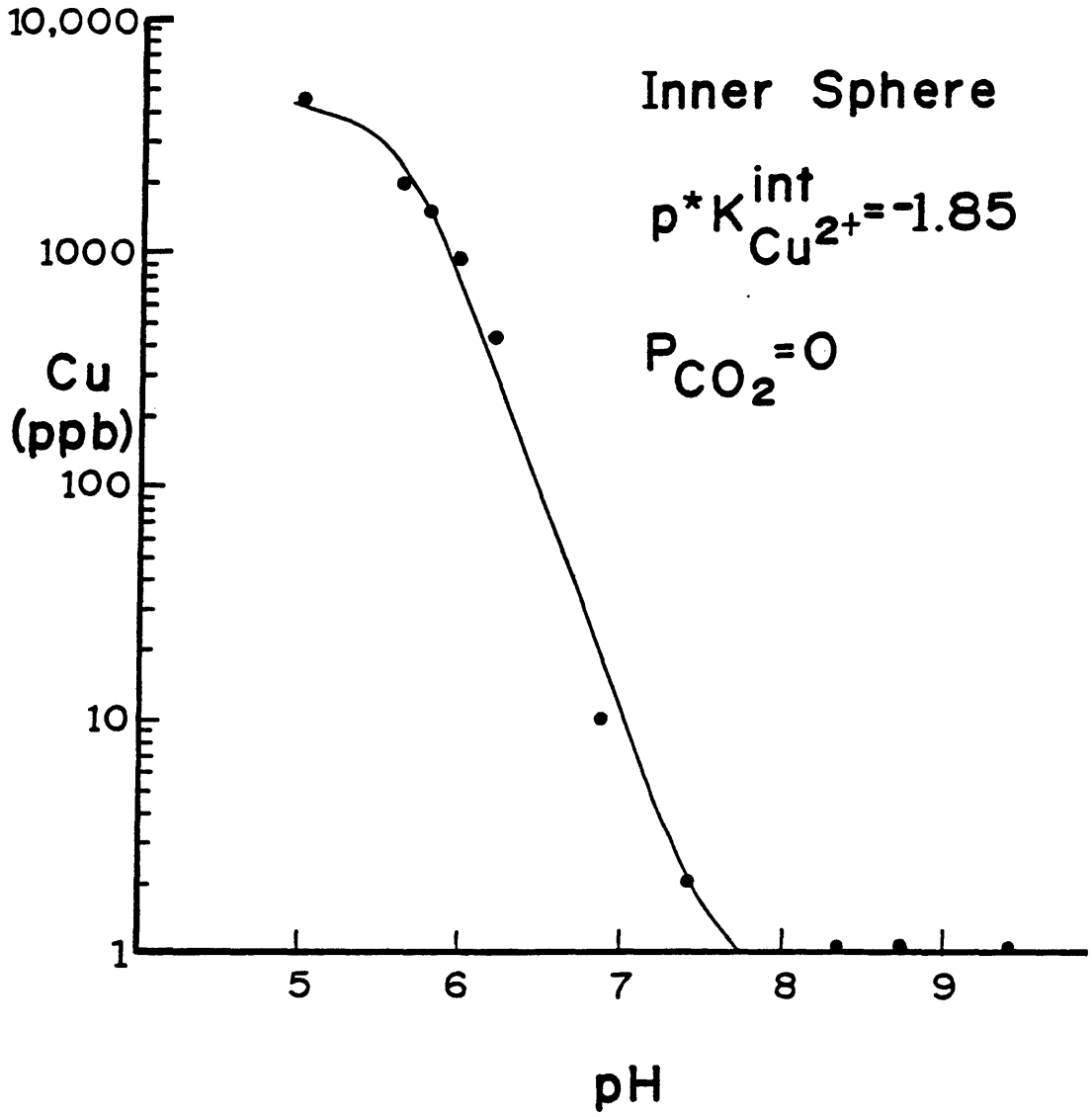

Figure 30: Model-calculated inner sphere surface adsorption of copper by goethite at C_T = 0, I = 0.01 M (as KNO_3), and 25°C for $\Sigma Cu = 10^{-4}$ M. See Fig. 28 for further explanation.

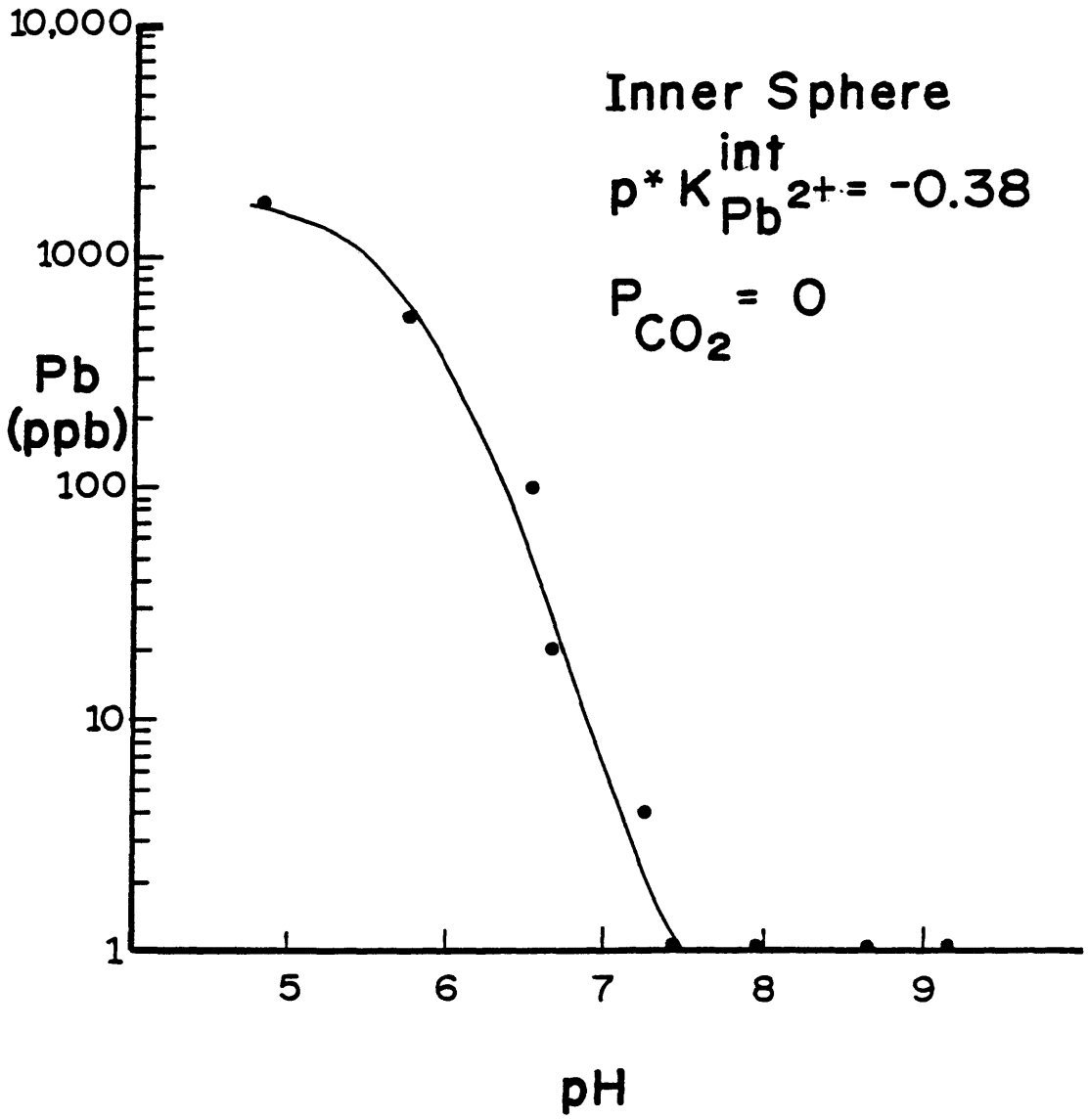

Figure 31: Model-calculated inner sphere surface adsorption of lead by goethite at C_T = 0, I = 0.01 M (as KNO_3), and 25°C for $\Sigma Pb = 10^{-5}$ M. See Fig. 28 for further explanation.

data. These different model analogues suggest contrasting interpretations of the adsorbing metal species; hydroxo species for outer sphere and free ions for inner sphere.

The next step in modeling is to see if the previously determined intrinsic complexation constants for each analogue can be used to model experimental data obtained under a different set of conditions. Experimental data exhibit no significant differences for copper and lead adsorption in solutions with an ionic strength of 0.1 M (as KNO_3). Hence, calculated model fits should show little difference between I = 0.01 and I = 0.1 M (as KNO_3) conditions (with all other experimental conditions being the same as before). Both outer sphere and inner sphere analogues were tested and the results are illustrated in Figures 32 through 35. Inner sphere predictions give good fits for both copper and lead adsorption (Figs. 34 and 35). Both outer sphere fits provide a slight overestimation of adsorption at lower pH values and a very slight underestimation at higher pH values (Figs. 32 and 33). Hence, the inner sphere metal adsorption analogue appears to be slightly better for the prediction of changes in ionic strength.

Next, the ability of the model analogues to predict adsorption under different total dissolved carbonate, C_T,

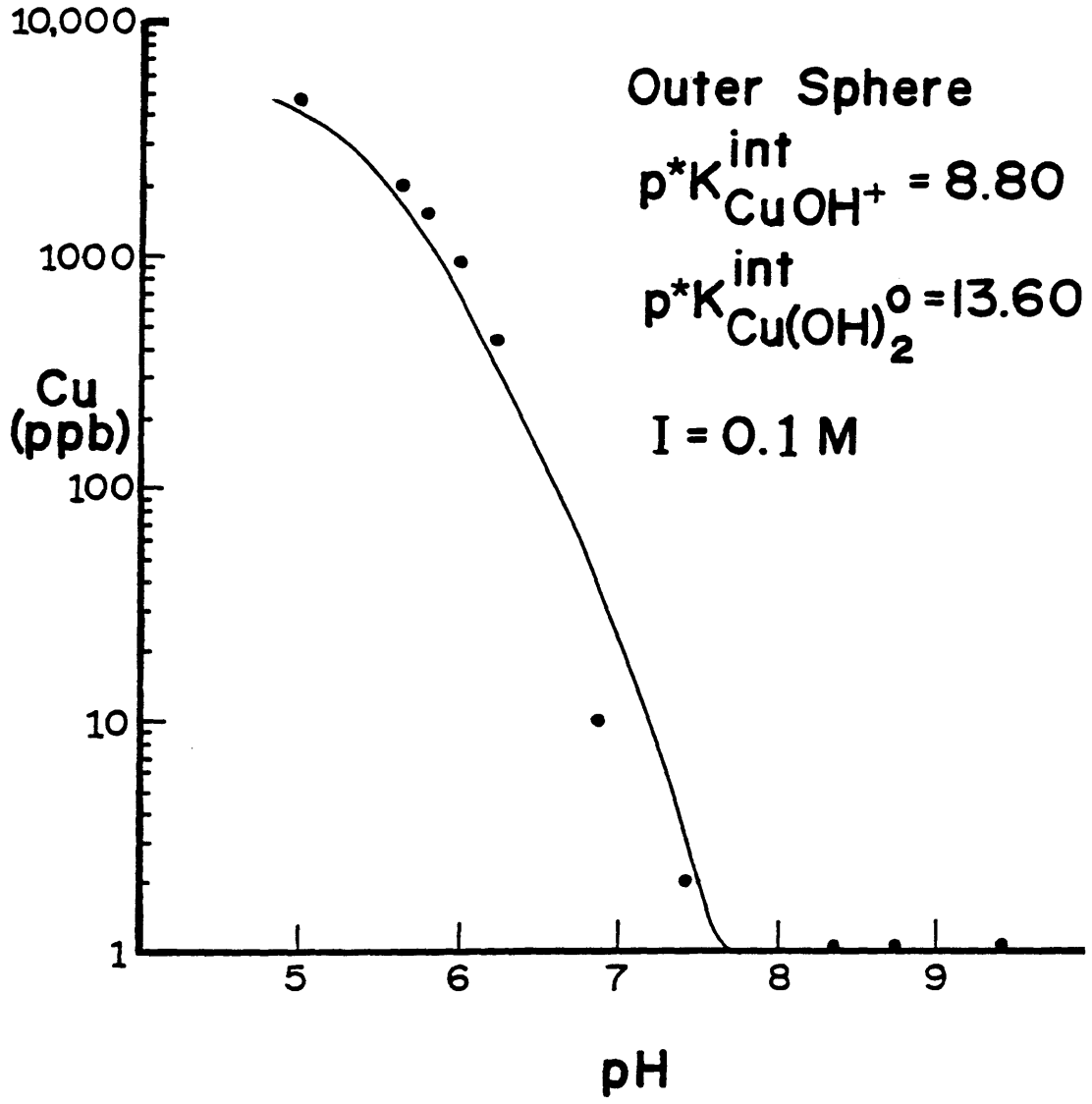

Figure 32: Model-calculated outer sphere surface adsorption of copper by goethite at I = 0.1 M (as KNO_3) and 25°C. See Fig. 28 for further explanation.

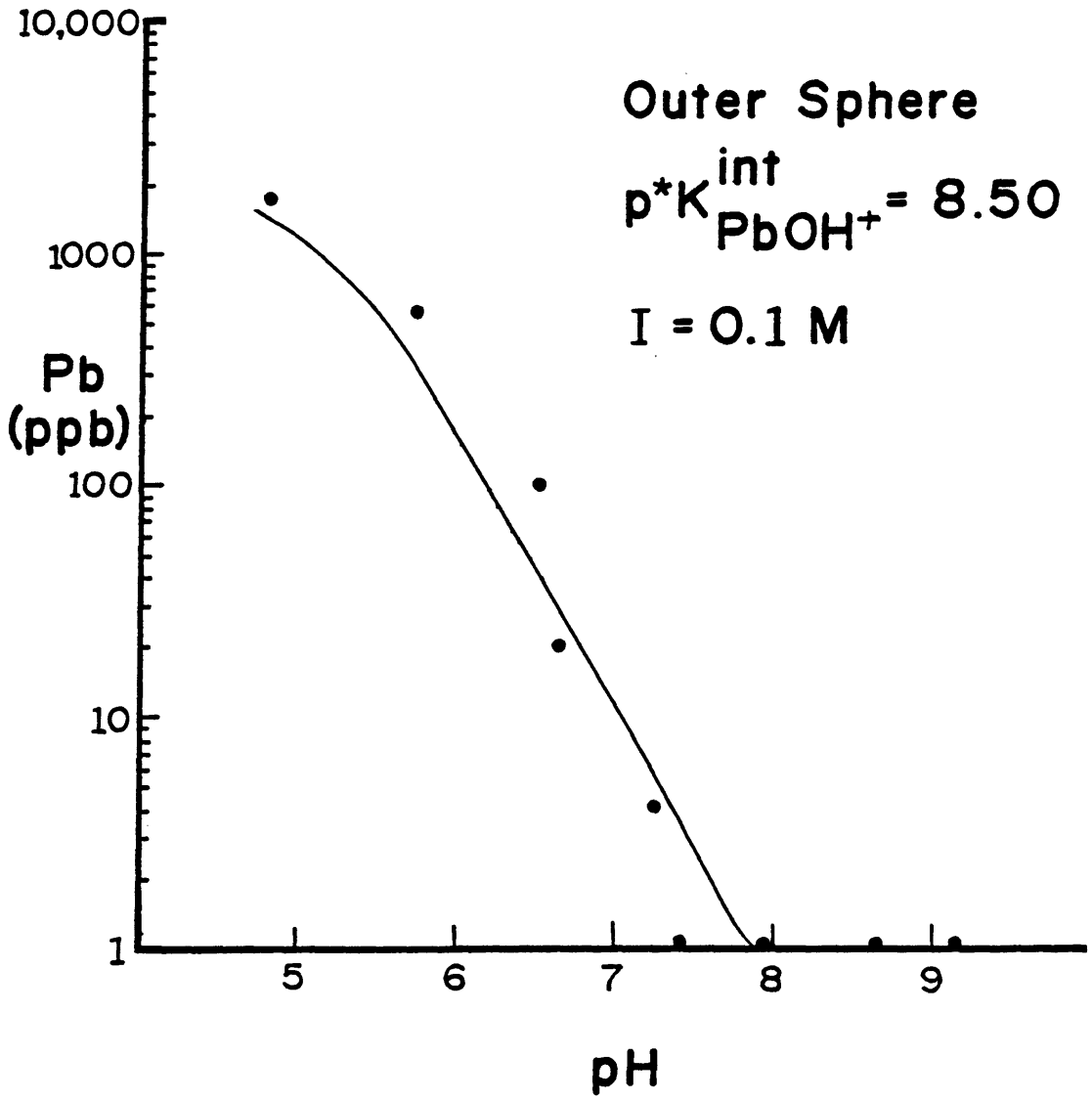

Figure 33: Model-calculated outer sphere surface adsorption of lead by goethite at I = 0.1 M (as KNO_3) and 25°C. See Fig. 28 for further explanation.

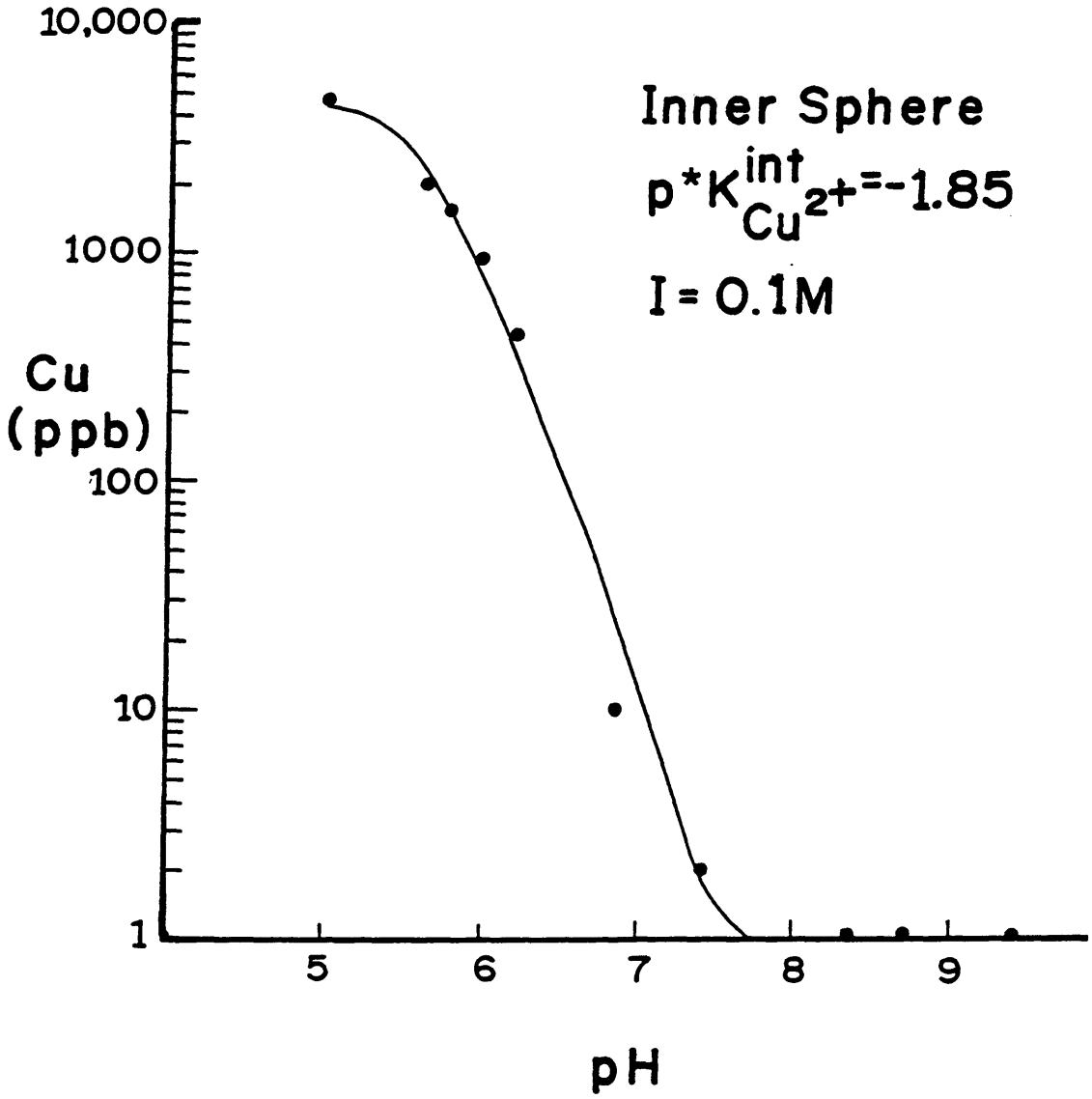

Figure 34: Model-calculated inner sphere surface adsorption of copper by goethite at I = 0.1 M (as KNO_3) and 25°C. See Fig. 28 for further explanation.

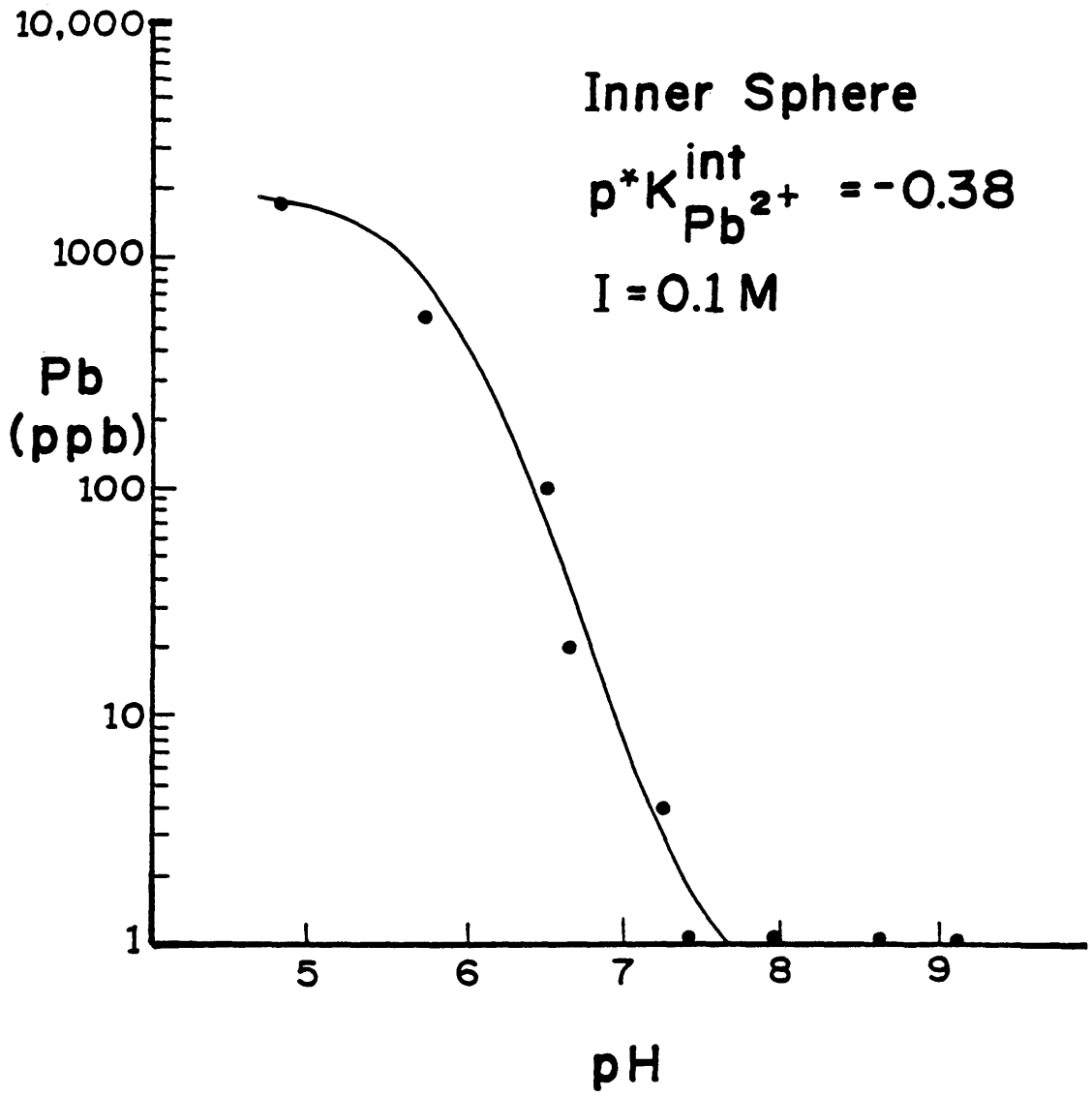

Figure 35: Model-calculated inner sphere surface adsorption of lead by goethite at I = 0.1 M (as KNO_3) and 25°C. See Fig. 28 for further explanation.

conditions will be tested. As was demonstrated in Figs. 14 and 18 of the Results of Sorption Experiments section of this thesis, at $C_T = 10^{-2}$ M there is partial inhibition of aqueous copper and lead adsorption from pH 7 to 9.

Two approaches have been taken with the surface complexation site-binding model in the treatment of varying C_T conditions. The first approach (Hsi, 1981; Hsi and Langmuir, 1985; and Tripathi, 1984) is to neglect the sorption of dissolved carbonate species onto the surface of goethite. This approach was taken due to the lack of information about surface carbonate species, SCS. The second approach (Sanchez and others, 1985) is to estimate binding constants for the dissolved carbonate species onto goethite. Sanchez and others (1985) reported the following estimated intrinsic complexation constants for goethite, calculated from results of Balistrieri and Murray (1982) and Stumm and others (1980):

$$SOH + CO_3^{2-} + H^+ \rightleftarrows SOH_2^+CO_3^{2-} \qquad p^*K^{int}_{CO_3^{2-}} = -15.90$$

$$SOH + CO_3^{2-} + 2H^+ \rightleftarrows SOH_2^+HCO_3^- \qquad p^*K^{int}_{HCO_3^-} = -22.30$$

Zachara and others (in press) measured inorganic carbon adsorption onto amorphous iron oxide ($Fe_2O_3 \cdot H_2O_{(am)}$) and

described the data using the surface complexation site-binding model. Their modeled reaction for HCO_3^- sorption is:

$$SOH_2^+ + HCO_3^- \rightleftarrows SOH_2^+HCO_3^- \qquad pK^{int}_{HCO_3^-} = -5.0$$

When the intrinsic acidity constant for formation of the ionized surface site and the second acidity constant for carbonate are added, this intrinsic complexation constant is similar to that reported by Sanchez and others (1985). Carbonate ion data could not be determined by Zachara and others (in press) because their data were collected below pH 8.

Russell and others (1975) studied the sorption of $CO_2(g)$ onto a moist goethite surface using infrared spectroscopy. Their data indicate the formation of CO_3^{2-} surface complexes. There is also some evidence of an HCO_3^- surface complex. Harrison and Berkheiser (1982) used infrared spectroscopy to examine anion interactions with hydrous iron oxide. They found that carbonate ions coordinate with unidentate surface sites. The preceeding information indicates that sorption of inorganic carbon species directly onto goethite does take place and should probably be considered in modeling calculations. This

carbonate species sorption would presumably make the surface more negative.

For modeling in this study, the HCO_3^- complexation constant determined by Zachara and others (in press) for amorphous iron oxide was used. Anderson and Benjamin (1985) argue that the constants obtained for amorphous iron oxide and goethite should be comparable. The estimated CO_3^{2-} intrinsic complexation constant of Sanchez and others (1985) for goethite was recalculated to be internally consistent with the data of this study and used in goethite modeling calculations. The intrinsic complexation constants for dissolved carbonate species used in this study are:

$$SOH + CO_3^{2-} + H^+ \rightleftarrows SOH_2^+CO_3^{2-} \qquad p^*K^{int}_{CO_3^{2-}} = -14.73$$

$$SOH + CO_3^{2-} + 2H^+ \rightleftarrows SOH_2^+HCO_3^- \qquad p^*K^{int}_{HCO_3^-} = -19.73$$

As demonstrated in the Results of Sorption Experiments section of this thesis, the experimental data were identical for copper and lead adsorption given P_{CO_2} = 0 and atmospheric P_{CO_2} conditions. Likewise, model calculations for copper and lead adsorption given P_{CO_2} = 0 and atmospheric P_{CO_2} conditions. Likewise, model calculations complexation constants previously determined for copper and lead adsorption at P_{CO_2} = 0 were used to model adsorption

under atmospheric conditions. First, the sorption of CO_3^{2-} and HCO_3^- onto goethite was ignored. In both the outer sphere and inner sphere adsorption analogues for copper and lead, the same results were obtained for atmospheric P_{CO_2} conditions as were obtained for $P_{CO_2} = 0$.

Next, the reactions for sorption of CO_3^{2-} and HCO_3^- onto goethite were included, and model calculations redone for atmospheric conditions. The results are given in Figures 36 through 39. As shown in Figures 36 and 38, addition of the surface carbonate species (SCS) to copper systems results in a good fit for the outer sphere model solution and slightly overestimates adsorption at lower pH values for the inner sphere model solution. Figures 37 and 39 illustrate that addition of SCS to lead systems produces model predictions that overestimate lead adsorption for both outer and inner sphere model solutions. To refit the experimental data for the outer sphere system with SCS, a new set of intrinsic complexation constants are necessary:

$$p^*K^{int}_{Pb^{2+}} = 4.0 \qquad p^*K^{int}_{PbOH^+} = 11.4$$

These constants are very different from the original constant for $PbOH^+$ alone. This would indicate that intrinsic complexation constants calibrated to a model with

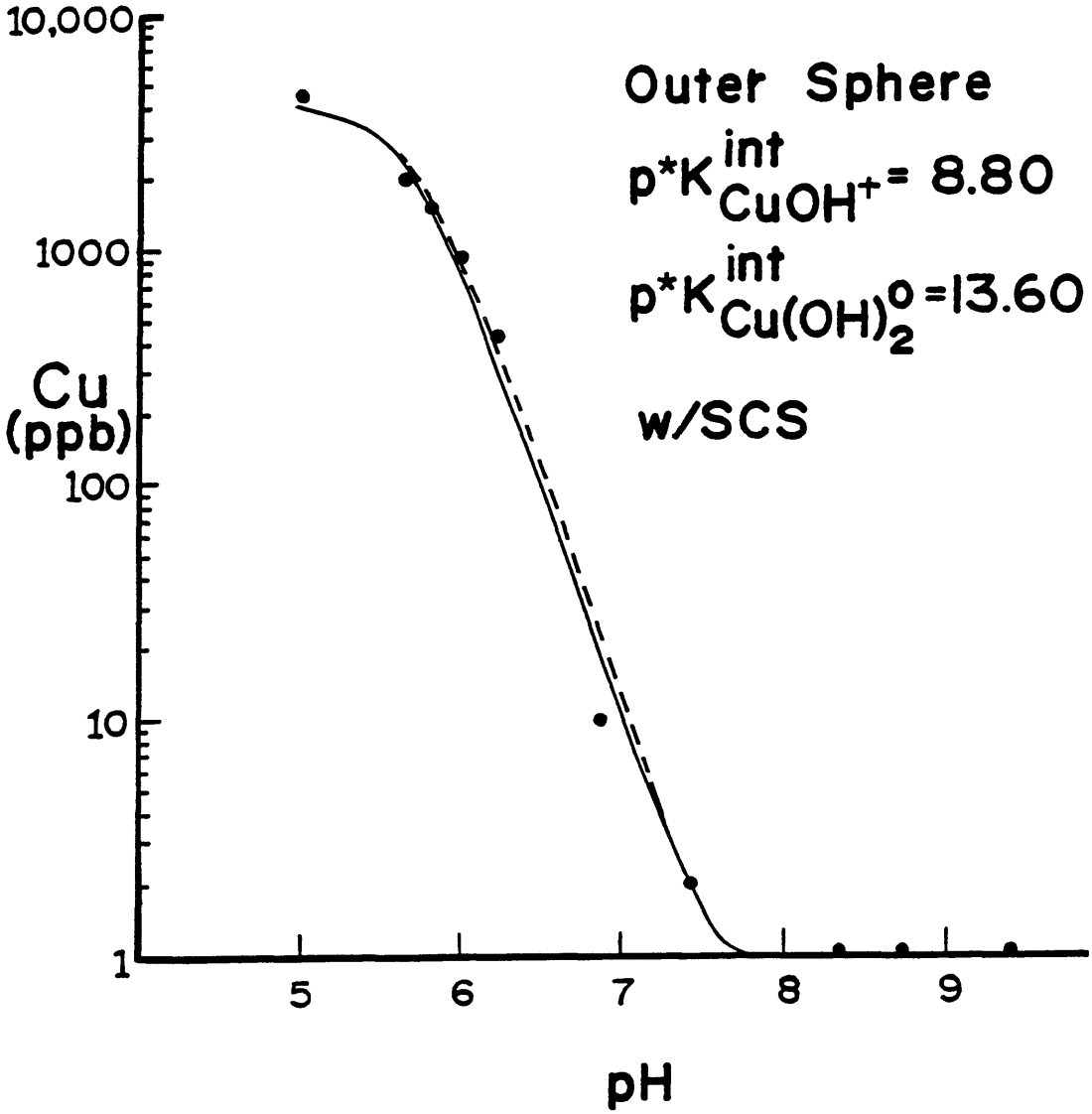

Figure 36: Model-calculated outer sphere surface adsorption of copper by goethite at atmospheric conditions and 25°C with the addition of CO_3^{2-} and HCO_3^- binding constants to the model. The dashed curve shows the model fit without these constants. See Fig. 28 for further explanation.

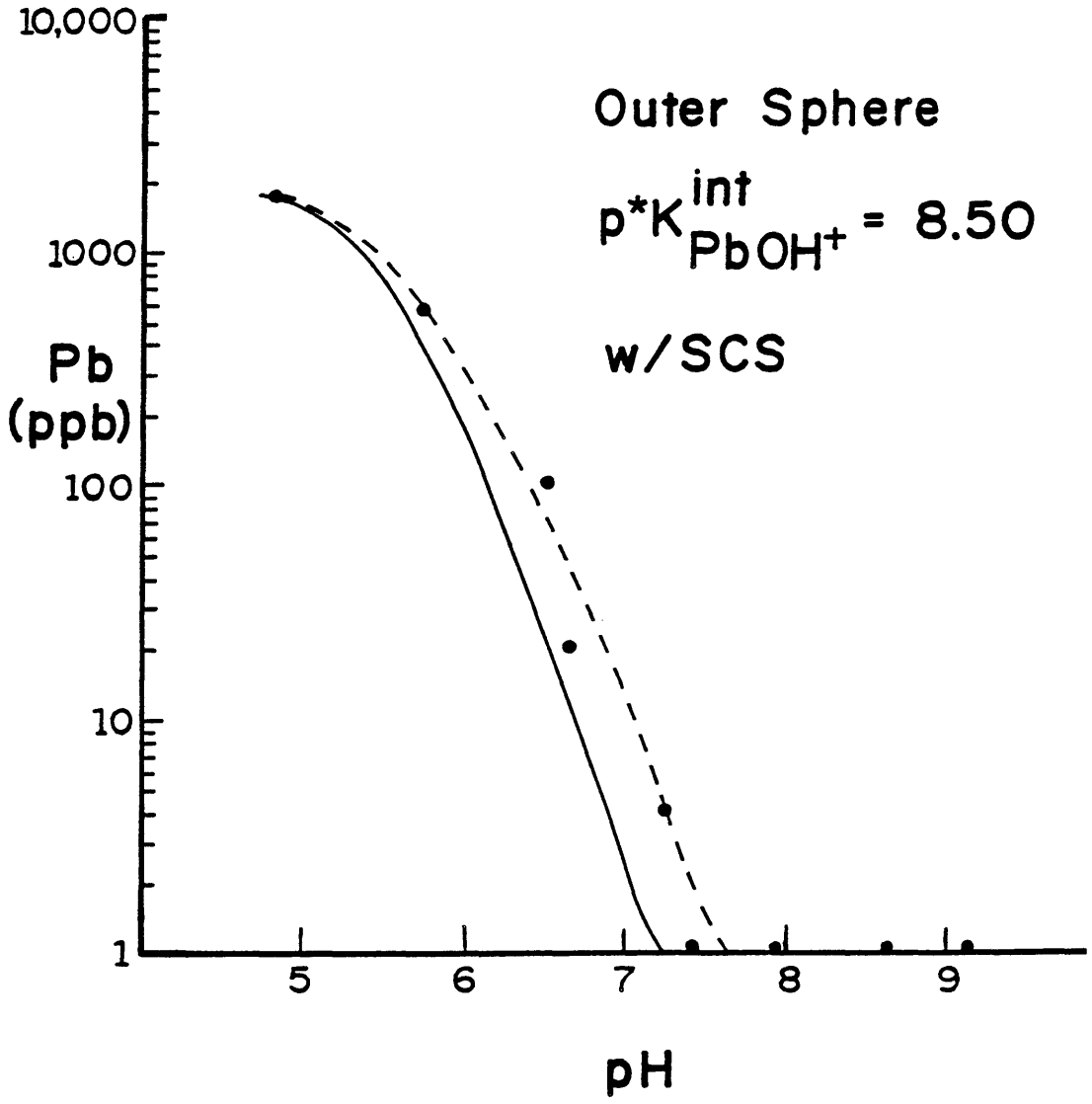

Figure 37: Model-calculated outer sphere surface adsorption of lead by goethite at atmospheric conditions and 25°C with the addition of CO_3^{2-} and HCO_3^- binding constants to the model. The dashed curve shows the model fit without these constants. See Fig. 28 for further explanation.

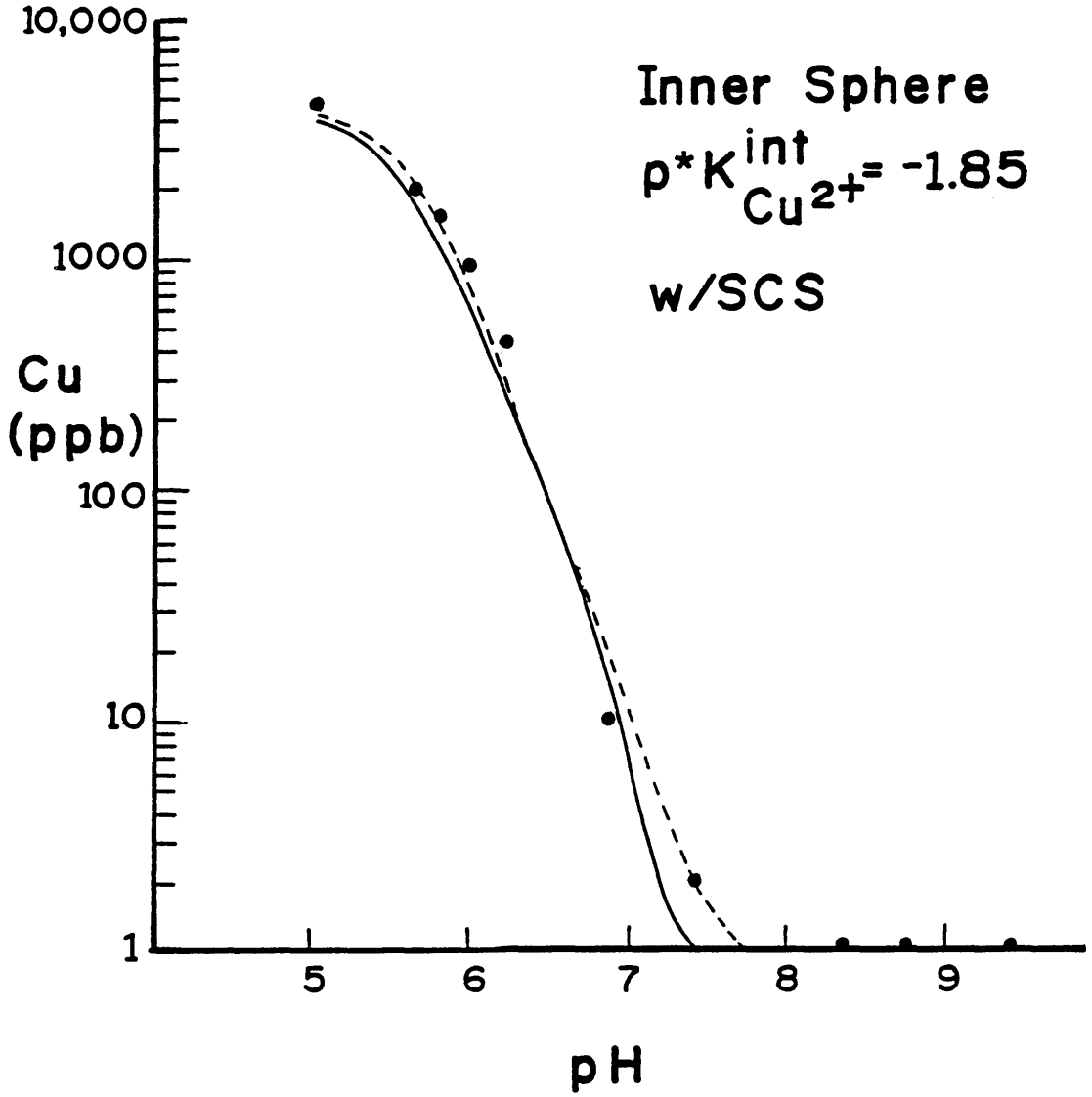

Figure 38: Model-calculated inner sphere surface adsorption of copper by goethite at atmospheric conditions and 25°C with the addition of CO_3^{2-} and HCO_3^{2-} binding constants to the model. The dashed curve shows the model fit without these constants. See Fig. 28 for further explanation.

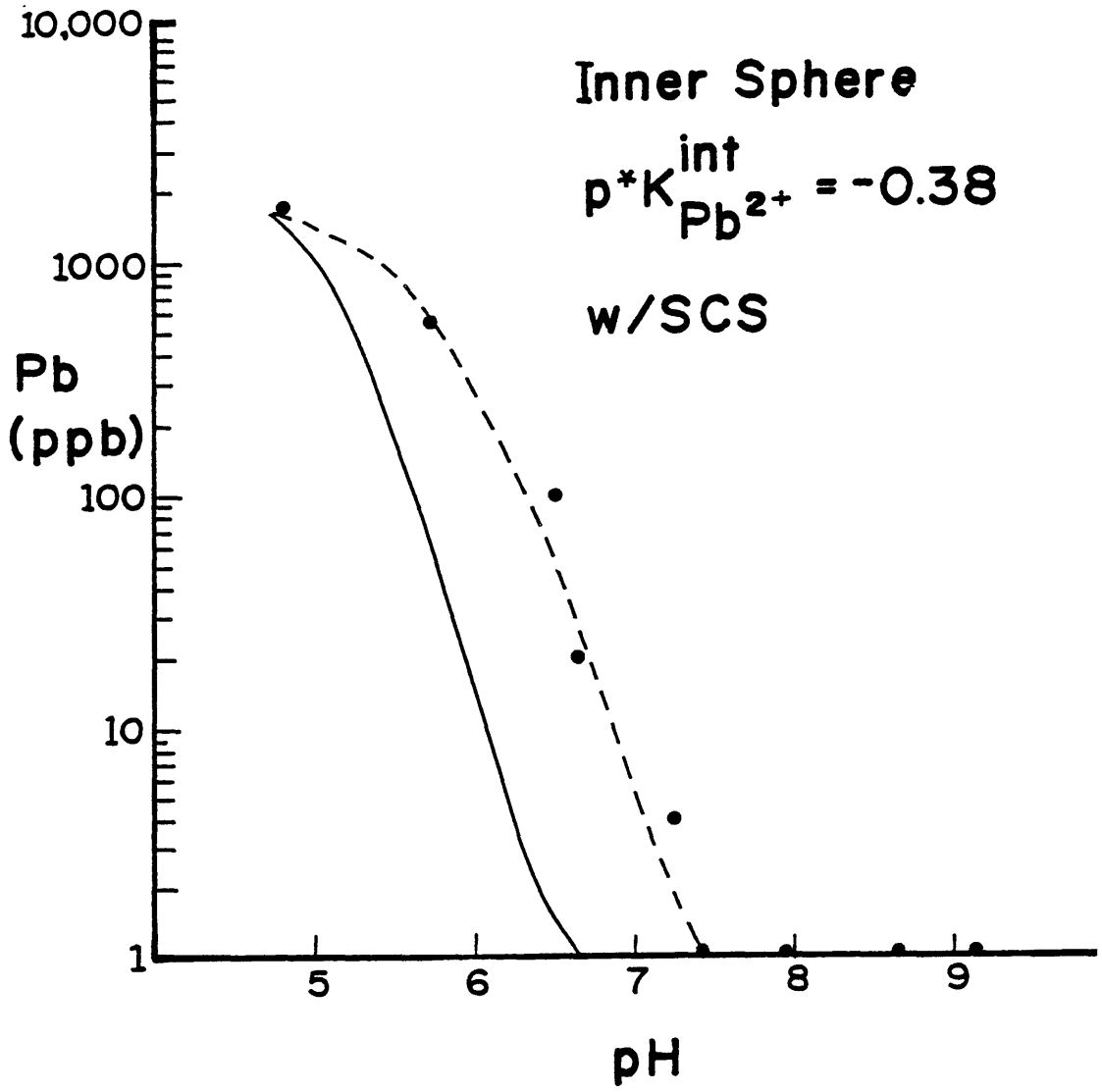

Figure 39: Model-calculated inner sphere surface adsorption of lead by goethite at atmospheric conditions and 25°C with the addition of CO_3^{2-} and HCO_3^- binding constants to the model. The dashed curve shows the model fit without these constants. See Fig. 28 for further explanation.

SCS would yield a different interpretation of the data. A good refit of the inner sphere lead system with SCS was not achieved. None of the single adsorption reactions or group of reactions tried were able to produce a model curve with the correct shape.

Model fits were also attempted for inner sphere CO_3^{2-} and HCO_3^- surface complexes. Model calculations produced underestimation of adsorption for lower pH values in outer sphere adsorption systems. This effect was reversed for inner sphere systems.

Because the inner sphere adsorption model solution of Cu^{2+} with SCS seems to fit the experimental data fairly well (Fig. 38), it is instructive to examine it in more detail. Figure 40 compares speciation diagrams for mole percent of total surface sites versus pH for the inner sphere adsorption of Cu^{2+} under atmospheric conditions with and without the inclusion of SCS (surface complexation reactions for CO_3^{2-} and HCO_3^-). As seen in Figure 40, in the diagram with SCS, the surface CO_3^{2-} species predominates over the surface HCO_3^- with the latter being too insignificant to appear in the diagram. The striking differences between the two diagrams are: 1) the percentage of SO^- sites decreases at pH values greater that 6.6 in the model solution with SCS; 2) K^+ adsorption is greatly enhanced by the inclusion

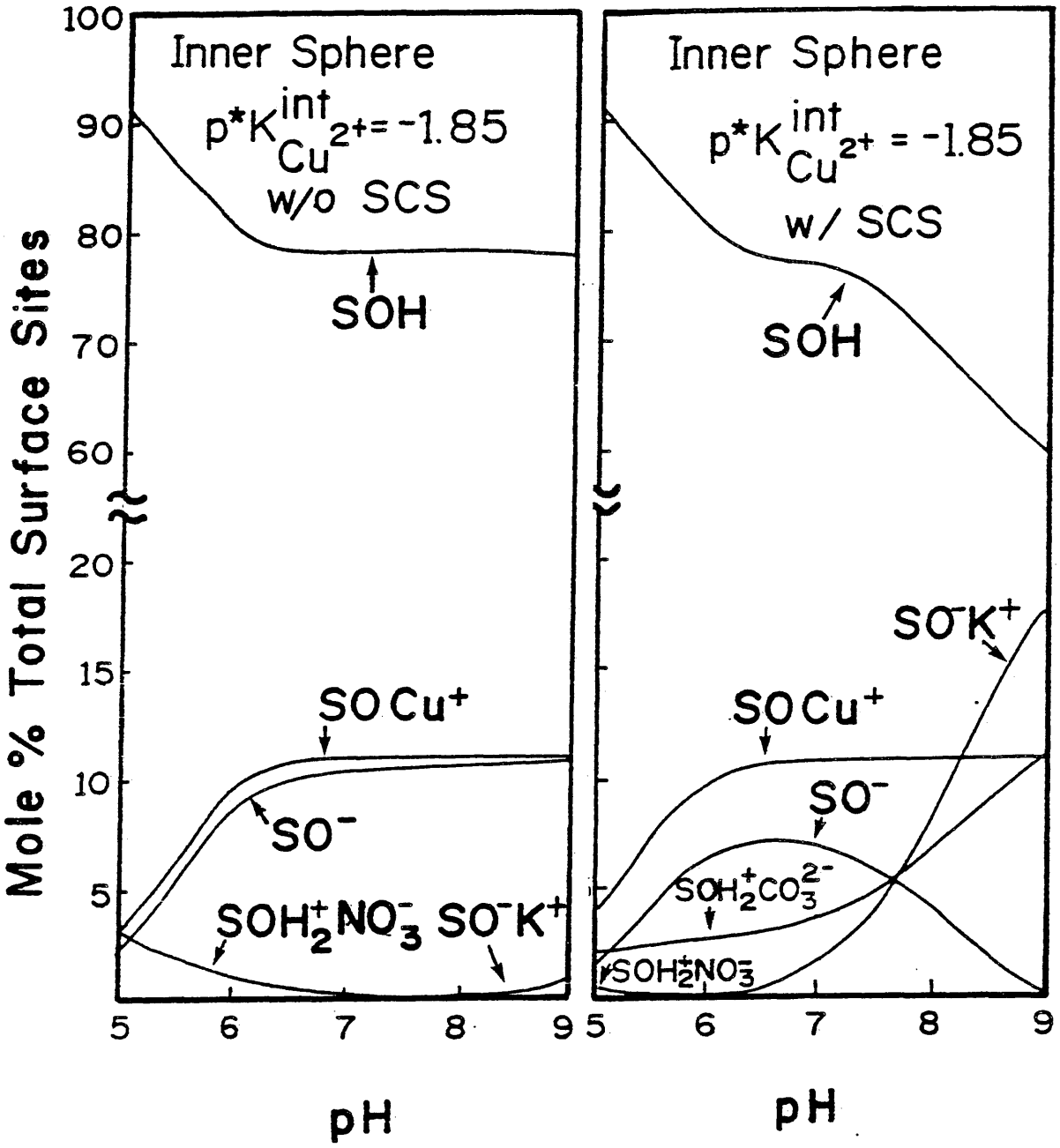

Figure 40: Model-calculated distribution diagrams of inner sphere surface adsorption of copper by goethite with and without binding constants for CO_3^{2-} or HCO_3^- as a function of mole percent total surface sites and pH.

of SCS, and NO_3^- adsorption is somewhat depressed; and 3) the percentage of neutral SOH sites steadily decreases in the model solution with SCS. Hence, CO_3^{2-} seems to sorb to the surface at the expense of the neutral SOH sites, the SO^- sites, and, to a lesser degree, the sorption of NO_3^-. The decrease in SO^- sites corresponds to a large increase in the SO^-K^+ surface complex. The calculated surface charge is more positive (at a given pH) in the model solution with SCS than in the model analogue without SCS.

Next, model calculations were compared with experimental data at $C_T = 10^{-2}$ M. As seen in Figs. 41 through 44, no model solution gives an adequate fit of the experimental data. The same is true for systems with SCS, although figures are not shown. Both copper and lead outer sphere, and copper inner sphere model solutions predict some adsorption inhibition, but the model curves do not follow the experimental data points. There may be several reasons for this. In all cases, the upturn of the curve just before pH 9 is due to the formation of the $M(CO_3)_2^{2-}$ aqueous complex (as indicated by the model calculations). The fact that the experimental data do not show an upturn in this pH range may indicate that the stability constants for these aqueous complexes are too strong. However, model calculations using smaller aqueous complex formation

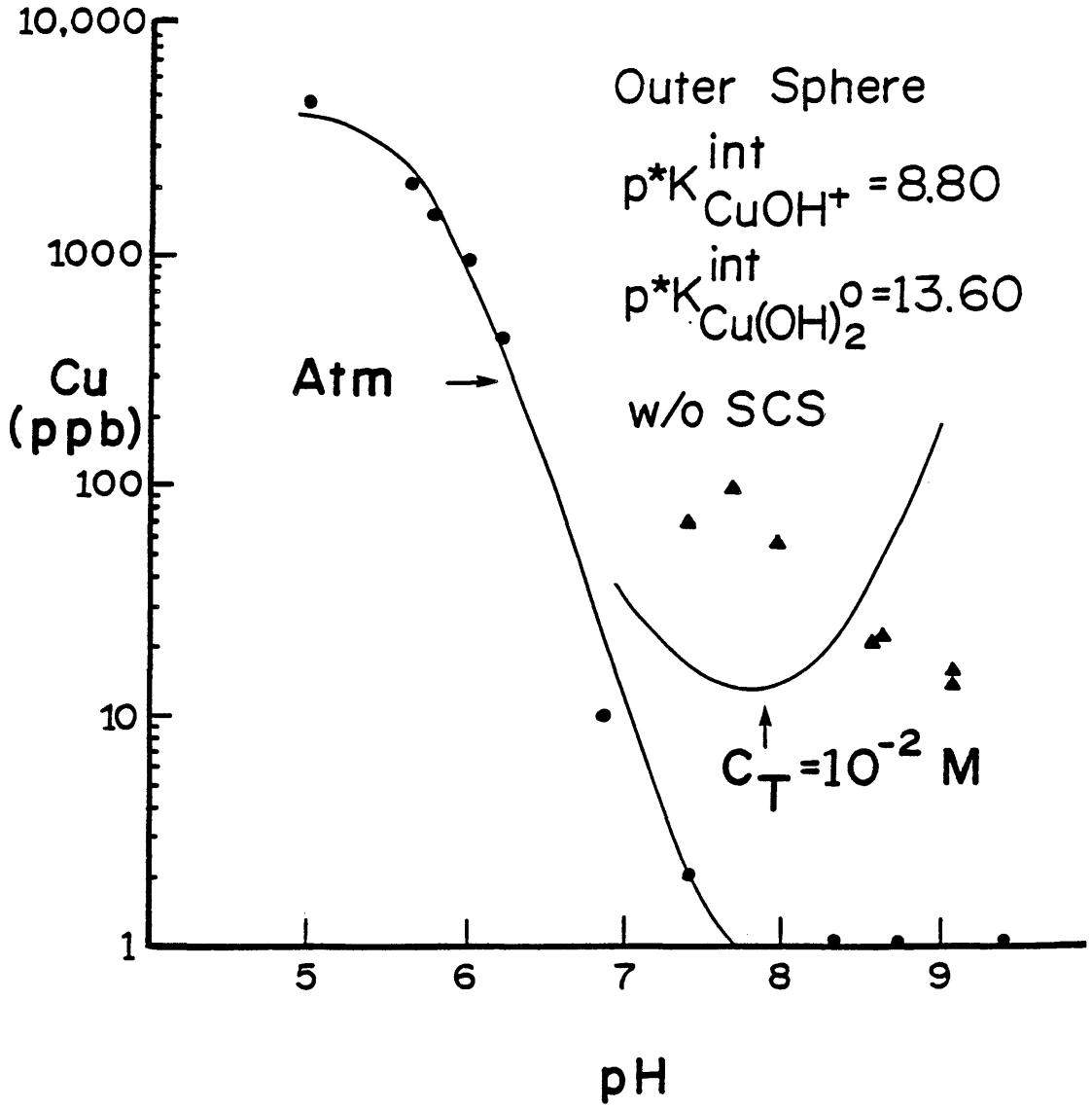

Figure 41: Model-calculated outer sphere surface adsorption of copper by goethite at atmospheric conditions (Atm) and $C_T = 10^{-2}$ M. See Fig. 28 for further explanation.

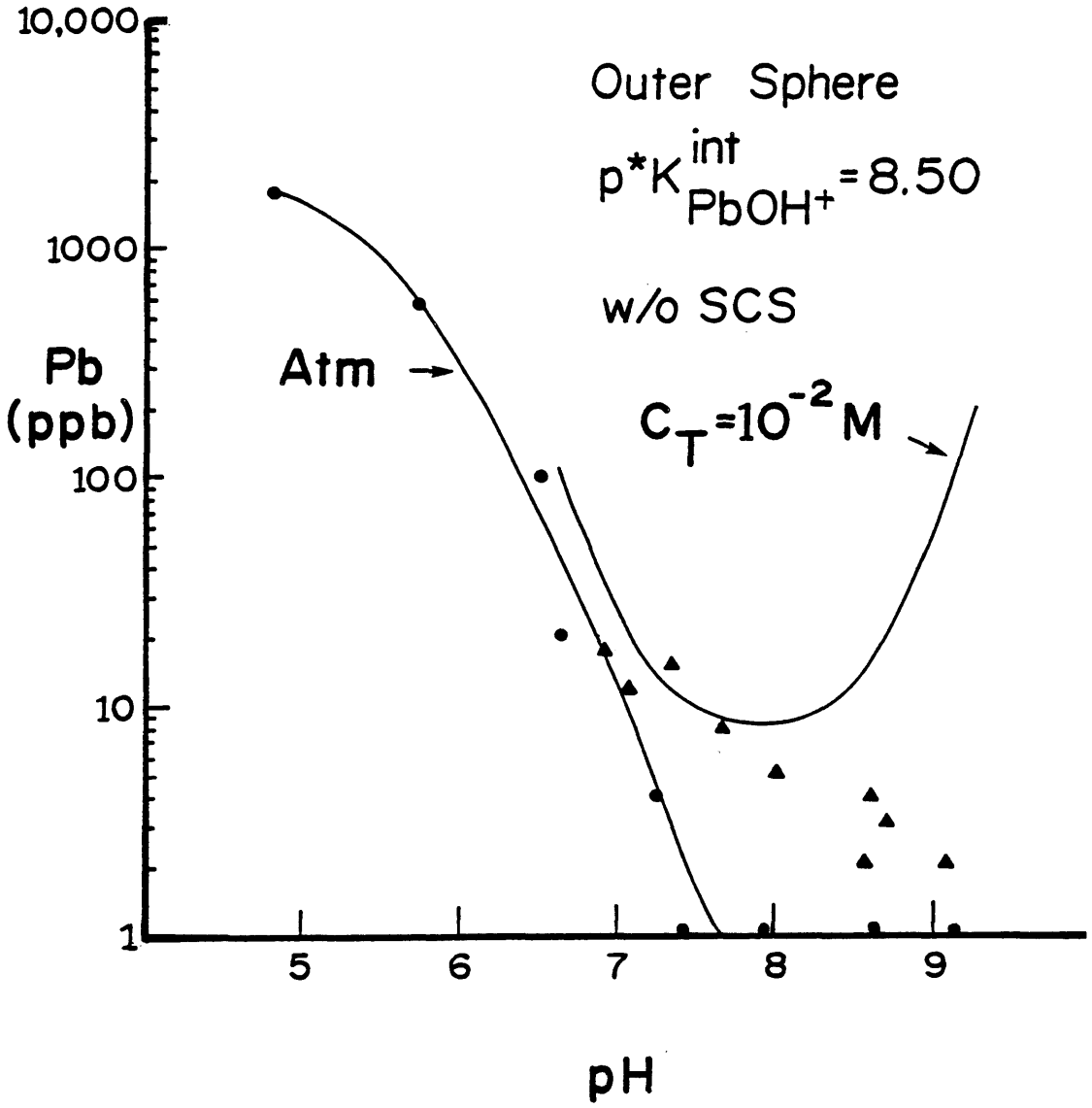

Figure 42: Model-calculated outer sphere surface adsorption of lead by goethite at atmospheric conditions (Atm) and $C_T = 10^{-2}$ M. See Fig. 28 for further explanation.

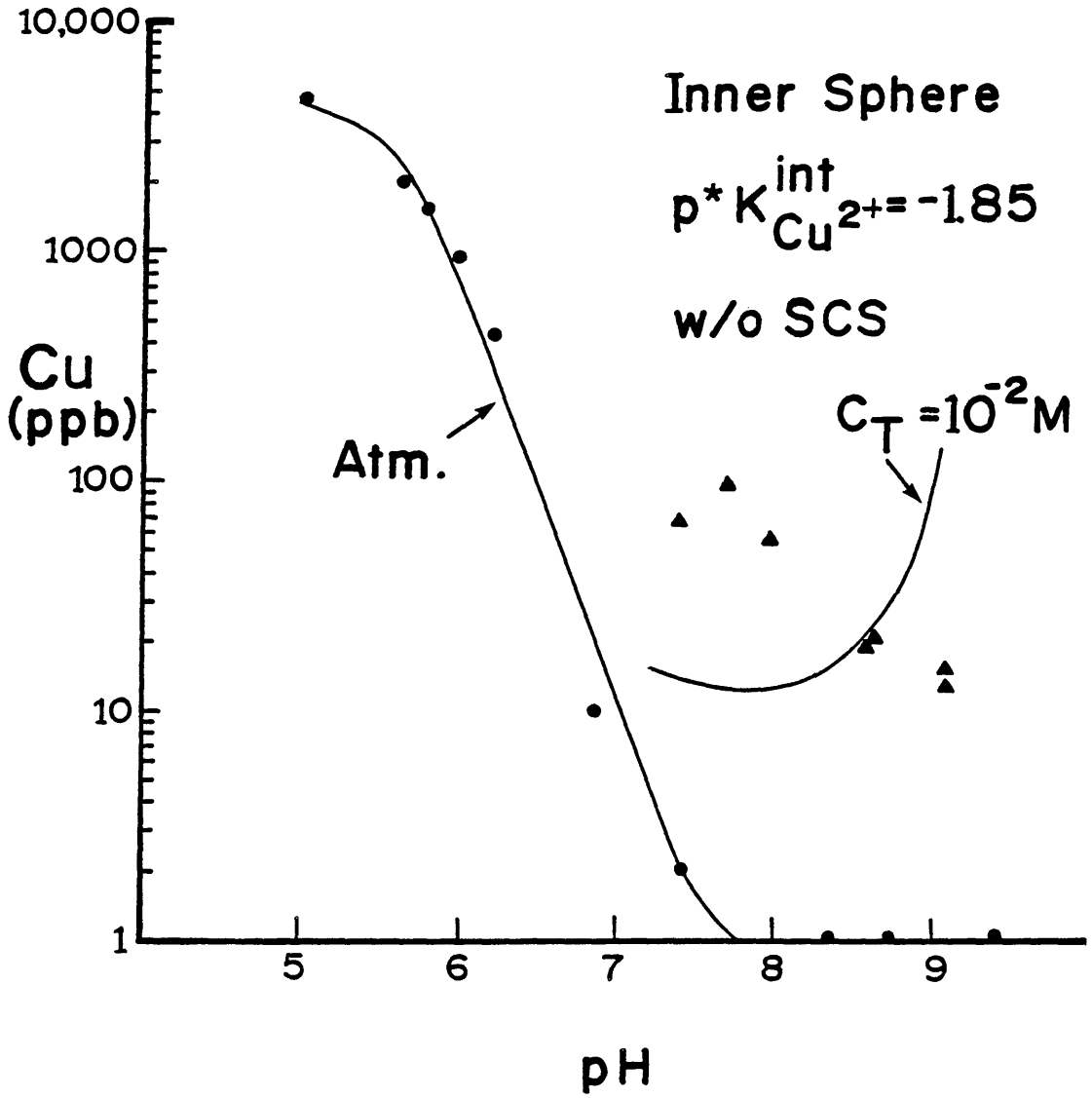

Figure 43: Model-calculated inner sphere surface adsorption of copper by goethite at atmospheric conditions (Atm) and $C_T = 10^{-2}$ M. See Fig. 28 for further explanation.

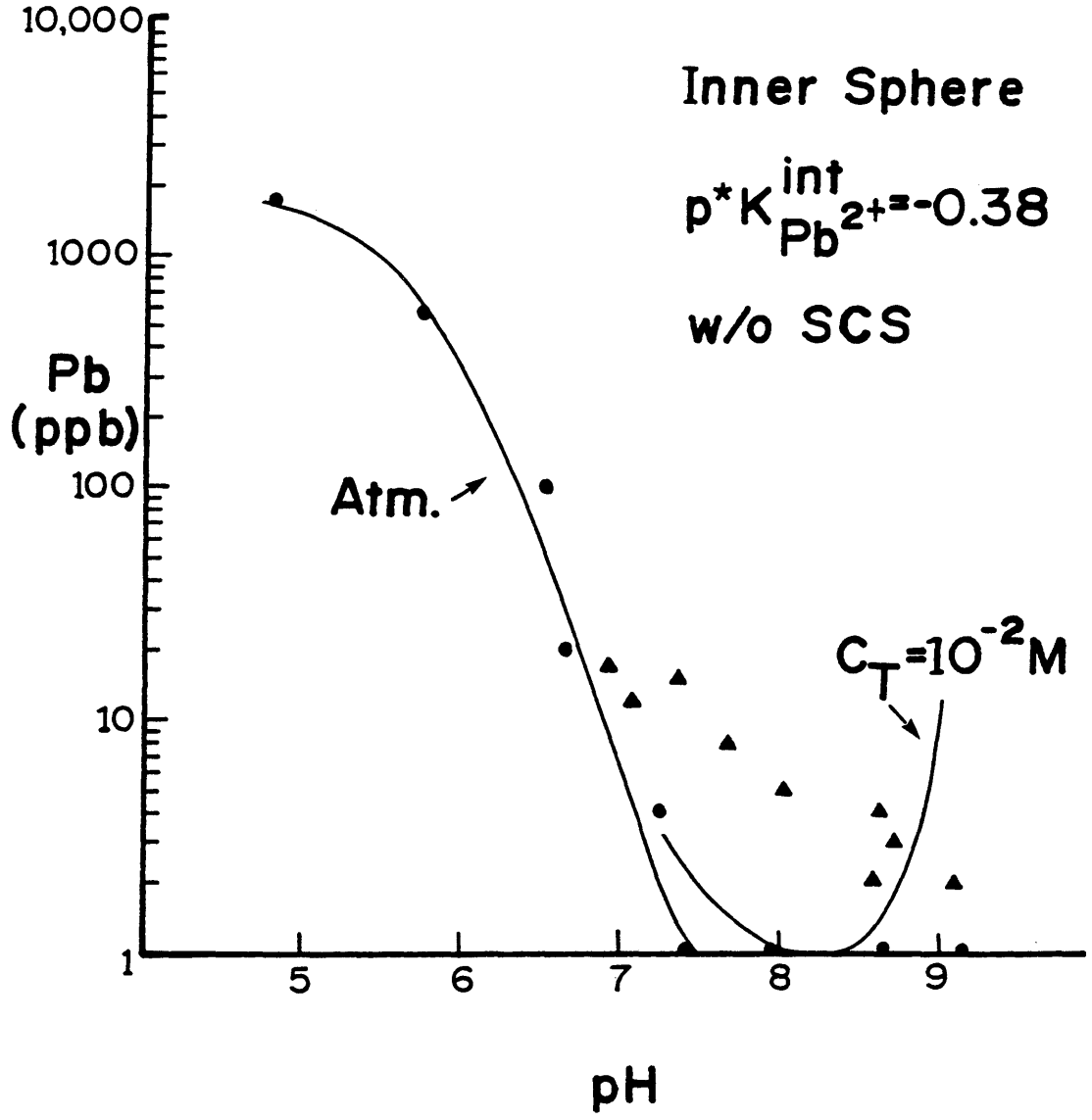

Figure 44: Model-calculated inner sphere surface adsorption of lead by goethite at atmospheric conditions (Atm) and $C_T = 10^{-2}$ M. See Fig. 28 for further explanation.

constants did not improve overall fits. Also, the assumption that $M(CO_3)_2^{2-}$ ions adsorb did not improve overall fits. Another possibility might be that the surface complexation site-binding model is not sensitive enough to model these adsorption inhibition effects since they involve less than 2% of the total metal originally present.

Finally, model fits were determined at lower total metal concentrations but with the same goethite concentration (i.e. at lower adsorption densities). The results are shown in Figs. 45 through 48. The model fits were calibrated at the highest concentrations in all cases. As seen in the figures, model predictions for the lower concentrations vary from being somewhat close to somewhat off. Model predictions are qualitatively correct in all cases. The inclusion of SCS in modeling calculations does not improve model fits.

Discussion:

The predictive ability of the surface complexation site-binding model for both outer sphere and inner sphere surface complex model analogues was tested for different I's, different C_T concentrations, and different N_S values. From this study, it is not clear which kind of surface complex analogue is better. Both do a good job of modeling

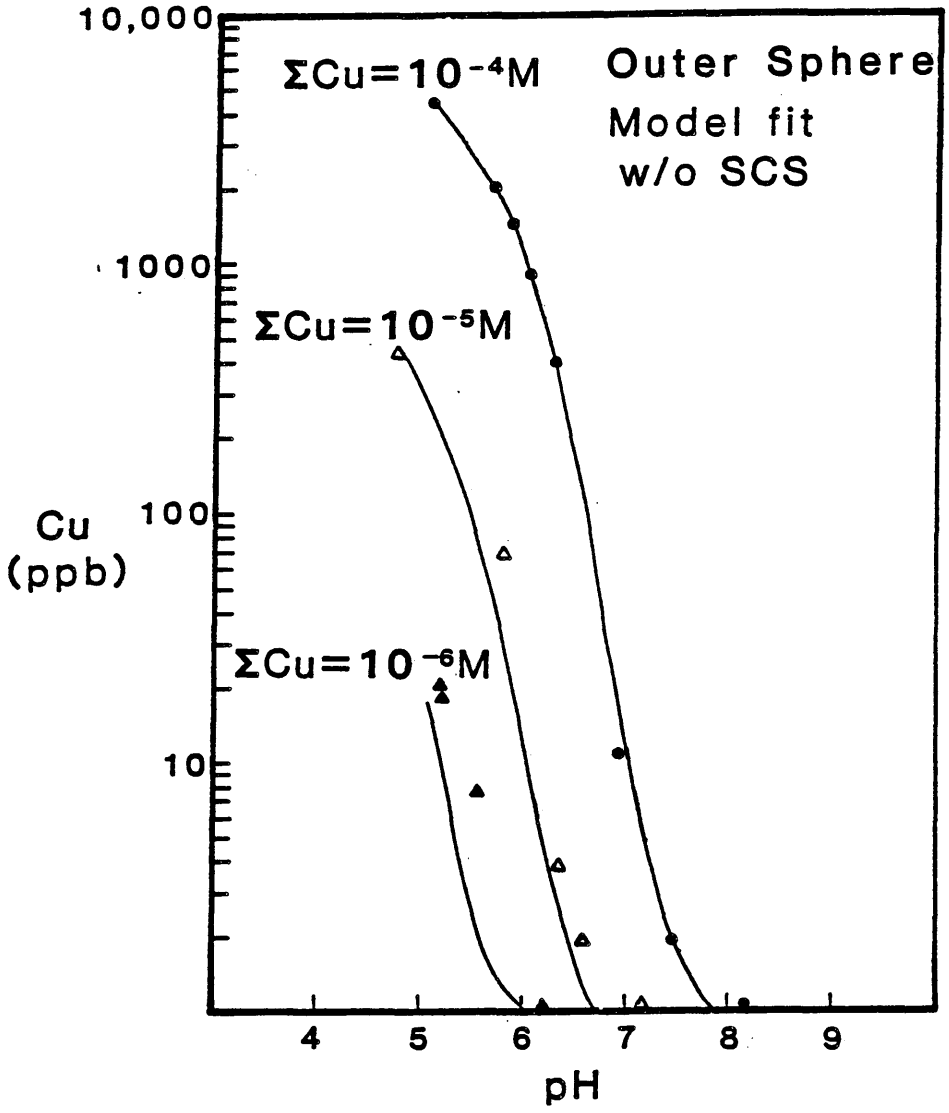

Figure 45: Model-calculated outer sphere surface adsorption of copper by goethite with changing adsorption density. The goethite concentration was 31 g/l in all systems for $p^*K^{int}_{CuOH^+} = 8.80$ and $p^*K^{int}_{Cu(OH)^o_2} = 13.60$ without SCS.

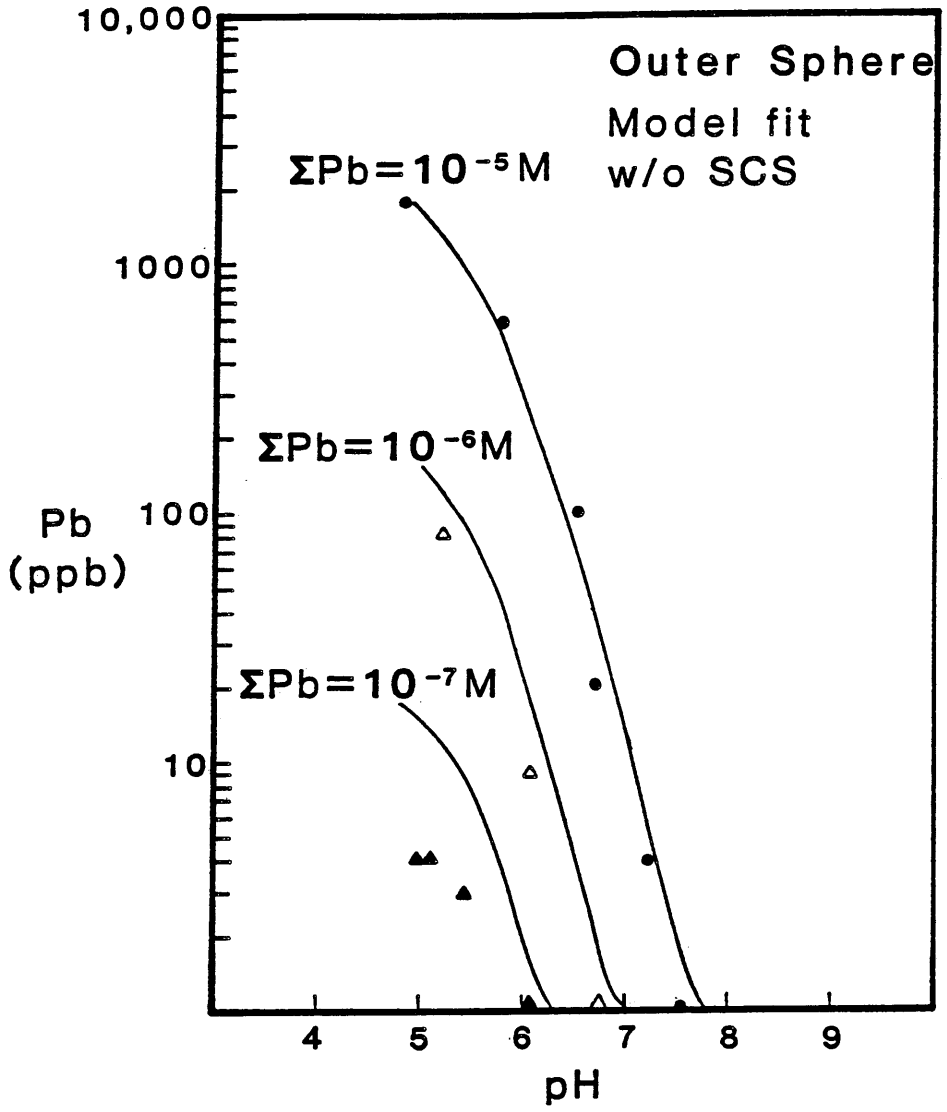

Figure 46: Model-calculated outer sphere surface adsorption of lead by goethite with changing adsorption density. The goethite concentration was 31 g/l in all systems for $p^{*}K^{int}_{PbOH^{+}}$ = 8.50 without SCS.

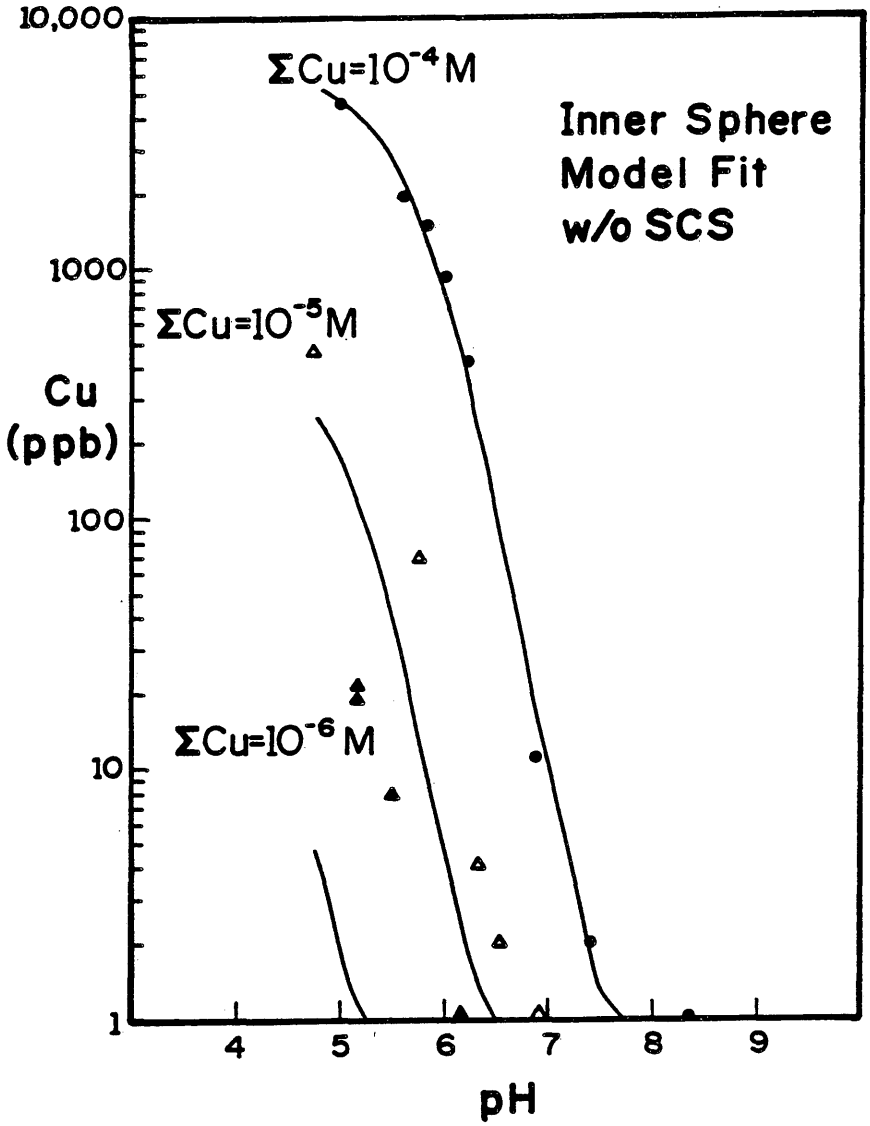

Figure 47: Model-calculated inner sphere surface adsorption of copper by goethite with changing adsorption density. The goethite concentration was 31 g/l in all systems for $p^{*}K^{int}_{Cu^{2+}}$ = -1.85 without SCS.

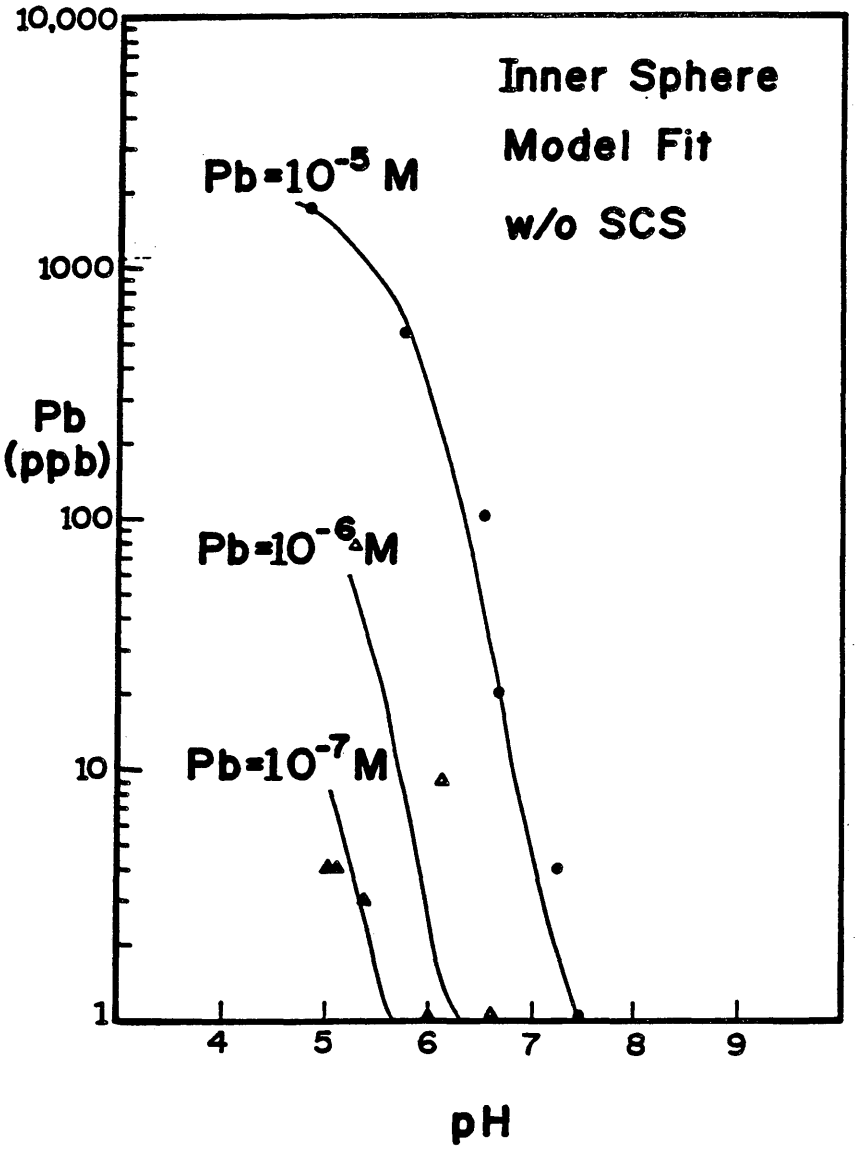

Figure 48: Model-calculated inner sphere surface adsorption of lead by goethite with changing adsorption density. The goethite concentration was 31 g/l in all systems for $p^{*}K^{int}_{Pb^{2+}} = -0.38$ without SCS.

ionic strength differences (up to 0.1 M as KNO_3) and C_T differences up to atmospheric conditions, and both give comparable results for different adsorption densities. Both also have difficulty modeling above atmospheric C_T systems.

These different model analogues suggest contrasting interpretations of the adsorbing metal species. The outer sphere surface complex model indicates that hydroxo species are adsorbed. This finding is consistent with previous thinking that adsorption of hydrolyzed metal ions is favored since secondary hydration waters are more easily removed from hydrolyzed metal ions than from unhydrolyzed metal ions. The inner sphere surface complex analogue suggests that free metal ions are adsorbed.

Hayes and Leckie (1986, in press) used a slightly modified version of the surface complexation site-binding model to study outer sphere and inner sphere lead and cadmium surface complexes on goethite at different ionic strengths. They found that the inner sphere model analogue fit their data much better than did the outer sphere analogue. They also performed potentiometric titrations to determine the number of protons released per lead ion adsorbed. Their results indicate that one proton is released per lead ion adsorbed. This agrees well with inner sphere reaction stoichiometry for the adsorption of free

metal ions. They conclude that treating divalent metal cations as inner sphere surface complexes is more appropriate than as outer sphere surface complexes.

Hachiya and others (1984) found that the inner sphere surface adsorption analogue worked better for Cu^{2+}, Mn^{2+}, Zn^{2+}, Co^{2+}, and Pb^{2+} adsorption onto γ-Al_2O_3. They noted that the equilibrium constants for metal ion adsorption with release of a proton are in the same order as the hydrolysis constants for those metal ions.

Evidence previously presented indicated that CO_3^{2-} and HCO_3^- sorb onto the goethite surface. Based upon modeling simulations in this study, CO_3^{2-} and HCO_3^- probably sorb as outer sphere surface complexes since assumption of inner sphere carbonate sorption resulted in larger discrepancies in model fits. There are some potential problems with the estimated binding constants from Sanchez and others (1985). These constants were originally derived from the data of Stumm and others (1980). Stumm and others compared equilibrium constants for exchange of CO_3^{2-} and HCO_3^- with a goethite hydroxyl group, and equilibrium constants for similar exchange with a water hydroxyl group. Inner sphere surface complexes on goethite were assumed in these comparisons. Hence, the CO_3^{2-} and HCO_3^- estimated binding constants might be somewhat stronger than would be expected

for outer sphere surface complexes. However, decreasing the CO_3^{2-} binding constant in the model did not significantly change model fits until the constant was reduced to such an extent as to almost eliminate its presence.

The inclusion of estimated binding constants for CO_3^{2-} and HCO_3^- in the model does not help predictive modeling capabilities for the parameters tested in this study. Tripathi (1984) did not include adsorption of aqueous carbonate species onto goethite in his modeling efforts. He reported an improvement in model fit with an increase in surface area for carbonate-bearing systems. This suggests that sorption of CO_3^{2-} and HCO_3^- is not responsible for his model fit discrepancies since one would expect a worsening in the fit with an increase in surface area.

Adsorption density experiments have been performed by several researchers and all have noted a pH shift of the adsorption edge with changing adsorption density. Benjamin and Leckie (1981a) concluded that the reason the pH region of the adsorption edge becomes more alkaline as total adsorbate concentration increases (i.e. adsorption becomes less specific) is that the surface has many groups of binding sites. At small adsorbate to adsorbent ratios, all types of sites are available in excess and the higher binding energy sites are filled first. The surface

complexation site-binding model assumes all sites have the same binding energy and should underestimate the amount of adsorption taking place at lower adsorbate concentrations. In the case of copper, the changing dimer ($Cu_2(OH)_2^{2+}$) concentration with total concentration might play a role in the adsorption density modeling results.

Tripathi (1984) points out another factor in adsorption density modeling results. He reports that G. A. Parks has shown that equilibrium constants calculated with the surface complexation site-binding model contain a term which is proportional to the surface area. This dependence results from the use of specific surface area to calculate the concentration of surface sites, [SOH] (Leckie, 1986):

$$[SOH] = \frac{N_s \times A \times W}{6.02 \times 10^{23}}$$

where N_s is the surface site density (sites/cm^2), A the specific surface area (cm^2/g), and W the amount of solid dispersed (g/l). The concentration of surface sites is used as a component to define surface species. Components are effectively "reference species" from which all other species can be formulated (Morel, 1983). This dependency probably makes the constants only valid for the surface area at which they were calibrated. Hence, care should be taken when this

model is to be used to predict conditions at different adsorption densities (Tripathi, 1984). However, because most adsorption studies are performed under the conditions that [SOH] is much greater than site occupancy, [SOH] should remain fairly constant over several orders of magnitude of adsorption density (Leckie, 1986).

ESTIMATION OF APPARENT BINDING CONSTANTS

Introduction

Benjamin (1978), and Benjamin and Leckie (1981a) developed an equation to calculate the apparent or average equilibrium binding constant of a metal on a sorbent material. With this equation, the distribution of site binding energies may be examined. The apparent binding constant is defined as:

$$K_e' = \frac{(\overline{SOMe}_T)\ (H^+)^x}{(\overline{SOH}_T)\ (Me)} \cdot EDL$$

where:

$SOMe_T$ = the sum of the activities of all adsorbed metal species.

SOH_T = the activity of all protonated surface species.

x = the average number of protons released per metal

ion adsorbed.

EDL = a term accounting for coulombic interactions in the double layer.

The EDL term does not vary much over a pH range of 2 to 3 units in the presence of a swamping electrolyte (Benjamin and Leckie, 1981a). If all adsorption data are from a single ionic strength, activity coefficients can be included in the K'_e value. Hence, a new variable K_e is defined:

$$K_e = \frac{K'_e}{EDL}$$

K_e can be determined solely from experimental measurements. Since:

$$\frac{(\overline{SOMe}_T)}{(\overline{SOH}_T)} = \Gamma ,$$

then,

$$K_e = \Gamma \frac{(H^+)^x}{(Me)}$$

This value of K_e can be plotted versus Γ. Benjamin and Leckie (1981a) observed that, for very low surface coverages, K_e is constant. For these conditions the metal

ions bind to an excess of high energy sites. As surface coverage increases, corresponding to lower K_e values, these sites are depleted.

Copper and Lead Apparent Binding Constants

Adsorption data from this study for atmospheric conditions, I = 0.1 M (as KNO_3), total copper of 10^{-4}, 10^{-5}, and 10^{-6} M, total lead of 10^{-5}, 10^{-6}, and 10^{-7} M, and a pH range of 5 to 7 have been plotted. First, the outer sphere scenario in which metal hydroxo species are the adsorbate was considered. For this model, two protons are released for each metal ion adsorbed. These data are plotted in Fig. 49.

Empirical evidence indicates that less than two protons are released per metal ion adsorbed. Benjamin and Leckie (1981a) measured the proton release accompanying adsorption of copper and lead ions onto $Fe_2O_3 \cdot H_2O$. They report 1.88-1.89 protons released per copper ion, and 1.65 protons released per lead ion adsorbed. The use of a slightly smaller proton release value in the apparent binding constant equation does not affect the overall interpretation of the data. Although the apparent binding constant calculation assumes that proton release is independent of pH, it is likely that the number of protons released varies

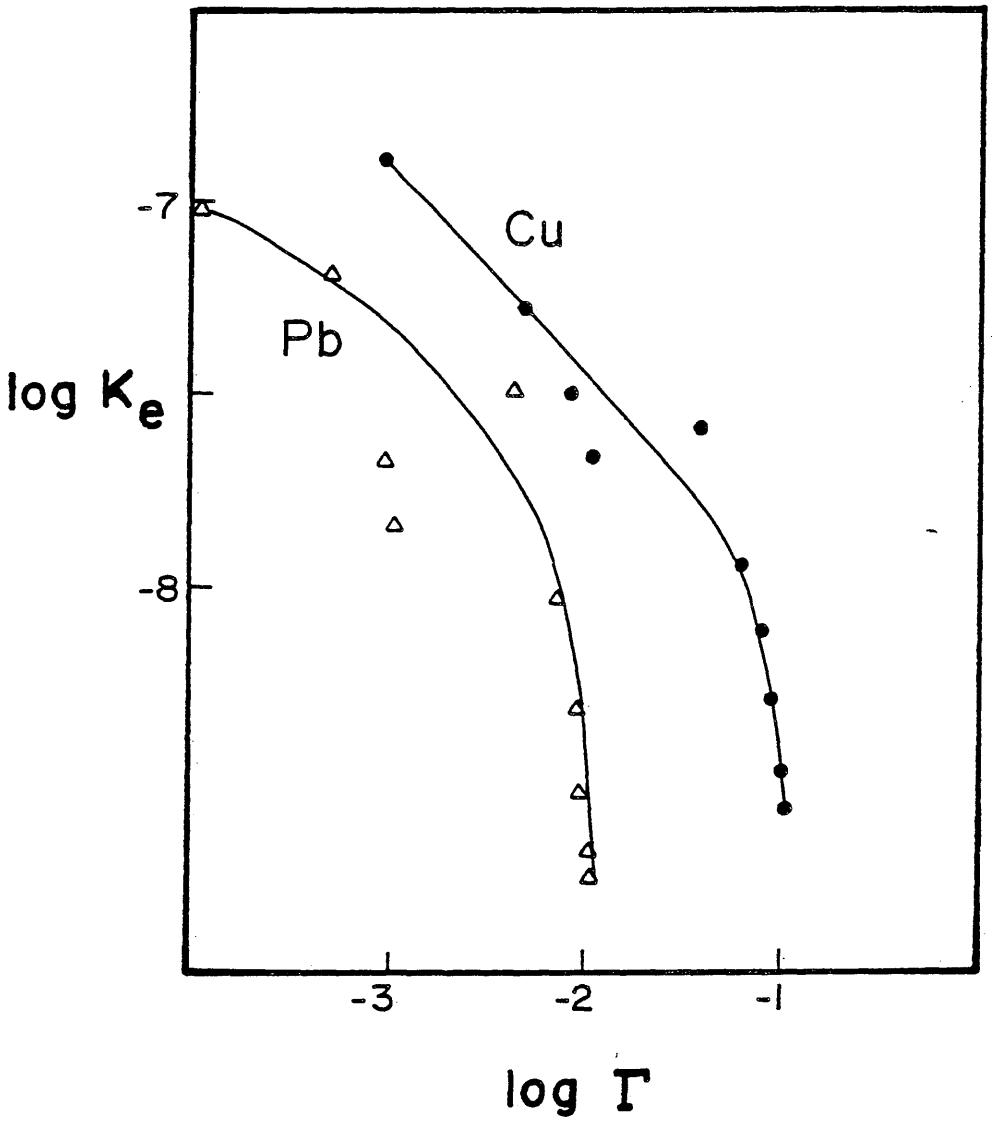

Figure 49: Apparent equilibrium binding constants for copper and lead onto goethite in 0.1 M KNO_3 solution at 25°C assuming that two protons are released for each metal ion adsorbed.

over a wide range of adsorption density and/or pH (Benjamin and Leckie, 1981a). Leckie (1986) reports that the number of protons released per lead ion adsorbed onto goethite changes with pH. The narrow pH range (pH 5-7) used in the apparent binding constant calculations (Fig. 49) of this study should not be subject to much of an effect from changing proton release with changing pH.

Figure 49 shows that there are two general regions for both the copper and lead curves; a portion sloping about 45°, and an almost vertical portion. The regions of changing slope occur at Γ values of about $10^{-1.2}$ and $10^{-2.2}$ for copper and lead, respectively. That neither curve reaches a horizontal slope indicates that the highest binding energy sites are not in excess at any of these surface coverages.

Next, the inner sphere assumption in which free ions are the adsorbate was considered. For this model, one proton is released for each metal ion adsorbed. This proton release corresponds to the findings of Hayes and Leckie (1986, in press) of a reaction stoichiometry of one protnn released per lead ion adsorbed onto goethite. Plotting of this data yielded a graph with no distinguishable curve for either metal. Hence, no site binding information could be obtained for this scenario.

CONCLUSIONS AND RECOMMENDATIONS FOR FUTURE STUDY

CONCLUSIONS

Based on this work, the following conclusions can be drawn:

1. Copper and lead are both specifically adsorbed by goethite with copper being more strongly adsorbed than lead.

2. Copper and lead adsorption reactions equilibrate rapidly, on the order of one hour.

3. Greater than atmospheric amounts of total dissolved carbonate (C_T) reduces adsorption of aqueous copper and lead onto goethite between pH 7 and 9. This adsorption inhibition is proportional to C_T, and is a function of pH and total metal concentration.

4. Copper and lead adsorption are not significantly affected by the change from C_T=0 to atmospheric conditions (P_{CO_2}= $10^{-3.5}$ atm.).

5. Copper and lead adsorption are not significantly affected by an increase in ionic strength up to 0.1 M (as KNO_3).

6. The pH range of copper and lead fractional adsorption is dependent on adsorbate concentration with lower adsorbate concentrations resulting in a shift of the adsorption edges to lower pH regions. This may be attributed to the presence of sites of varying binding energy on the goethite surface.

7. Modeling of experimental data with the surface complexation site-binding model was achieved for simple systems (C_T=0, I=0.01 M (as KNO_3), and $\Sigma Cu=10^{-4}$ M or $\Sigma Pb=10^{-5}$ M). However, the model provides different interpretations of the adsorbate species depending upon whether outer sphere or inner sphere adsorption of the metal is considered. Assumption of outer sphere metal adsorption indicates that hydroxo species are adsorbed whereas assumption of inner sphere metal adsorption indicates that the free ions are the adsorbates.

8. Addition of reactions and intrinsic complexation constants for the adsorption of HCO_3^- and CO_3^{2-} onto goethite results in an overestimation of lead adsorption

when previously determined intrinsic complexation constants are used (for total lead of 10^{-5} M). No improvement in model fits of experimental data was achieved by the addition of carbonate surface reactions.

9. None of the model scenarios used in this study can accurately model metal adsorption inhibition at total dissolved carbonate carbon concentrations of 10^{-2} M. However, the model works well for atmospheric conditions ($P_{CO_2}=10^{-3.5}$ atm.).

10. Order-of-magnitude adsorption density changes can be modeled qualitatively and semi-quantitatively by the model scenarios used in this study. Model fit discrepancies may be attributed to the fact that this model assumes only one type of adsorption site on the goethite surface. Another factor could be the dependence of the model-calculated equilibrium constants on surface area.

DISCUSSION AND RECOMMENDATIONS FOR FUTURE STUDY

There are two main endeavors of adsorption modeling. The first is to gain an understanding of fundamental adsorption processes, and the second is to develop a

predictive model which can be applied to natural systems. Surface complexation models have proved to be valuable tools in fundamental adsorption studies. Natural systems have been successfully modeled by several researchers (Bourg, 1982; Lion and others, 1982; Mouvet and Bourg, 1983; Balistrieri and Murray, 1983). Unfortunately, however, some problems exist in the application of surface complexation models to natural systems. Honeyman (1984) used an adsorptive additivity model and net partitioning coefficients to examine colloidal mixtures of adsorbent materials. He found that the extrapolation of adsorption data derived from single adsorbent systems to heterogeneous systems often results in the improper calculation of solute behavior. He concluded that sorptive behavior in colloidal systems should not be expected to be additive, and recommends caution in the extrapolation of adsorption data to multiple adsorbent systems.

Davis (1980) studied the adsorption of natural dissolved organic matter at the oxide/water interface. His results suggest that, under conditions typical for natural waters, an hydrous iron oxide surface is probably largely covered by adsorbed organic matter. He predicts that the organic coating would have substantial influence on the surface properties of the sorbent material.

The previous discussions indicate that there is a "credibility gap" between fundamental adsorption studies on model systems and their application to natural systems. However, fundamental studies are necessary for the understanding of solid/solution adsorption processes. More research is needed to determine the stoichiometry of solid/solution interfacial reactions. The use of EXAFS (extended X-ray absorption fine structure), an X-ray absorption method, may prove to be useful for this purpose. With direct information about adsorption stoichiometry, appropriate reactions could be included in model predictions, thus eliminating the trial and error approach to adsorption stoichiometry currently required. Another useful addition to adsorption modeling would be the consideration of mineralogical structure such that a reasonable estimation of heterogeneous surface sites could be incorporated.

Alternative approaches to the study of adsorption in natural systems should be investigated. One possibility might be to start with natural materials and obtain bulk adsorption parameters. With this approach, additivity of the individual components is not an issue, but the results are site-specific. Also, determination of metal partitioning in natural samples could be a useful technique

to identify the solid phase in which the metal of interest resides (for example, organic material versus iron oxides).

The proportional adsorption inhibition caused by dissolved carbonate warrants further investigation. This inhibition effect is likely to cause increased mobility of metals in natural systems such as aquifers which contain calcite and dolomite, and arid-climate alkaline soils.

REFERENCES CITED

Adamson, A. W., 1976, Physical Chemistry of Surfaces, 3rd Ed.: John Wiley and Sons, 698 p.

Anderson, P. R., and Benjamin, M. M., 1985, Effects of silicon on the crystallization and adsorption properties of ferric oxides: Environ. Sci. Technol., v. 19, p. 1048-1053.

Atkinson, R. J., Posner, A. M., and Quirk, J. P., 1967, Adsorption of potential-determining ions at the ferric oxide-aqueous electrolyte interface: J. Phys. Chem., v. 71, no. 3, p. 550-558.

Baes, C. F., Jr., and Mesmer, R. E., 1976, The Hydrolysis of Cations: Wiley-Interscience, 489 p.

Baes, C. F., Jr., and Mesmer, R. E., 1981, The thermodynamics of cation hydrolysis: Am. J. Sci., v. 281, p. 935-962.

Balistrieri, L. S., 1977, The basic surface characteristics of goethite: M.S. Thesis, University of Washington, Seattle, Washington.

Balistrieri, L. S., and Murray, J. W., 1979, Surface of goethite in seawater: in E. A. Jenne, ed., Chemical Modeling in Aqueous Systems: Speciation, Sorption, Solubility, and Kinetics: ACS Symposium Series 93, American Chemical Society, Washington, D.C., p. 275-298.

Balistrieri, L. S., and Murray, J. W., 1981, The surface chemistry of goethite in major ion seawater: Am. J. Sci., v. 281, p. 788-806.

Balistrieri, L. S., and Murray, J. W., 1982, The adsorption of Cu, Pb, Zn, and Cd on goethite from major ion seawater: Geochim. Cosmochim. Acta, v. 46, p. 1253-1265.

Balistrieri, L. S., and Murray, J. W., 1983, Metal-solid interactions in the marine environment: Estimating apparent equilibrium binding constants: Geochim. Cosmochim. Acta, v. 47, p. 1091-1098.

Barton, P. B., and Bethke, P. M., 1960, Thermodynamic properties of some synthetic zinc and copper minerals: Am. J. Sci., v. 258A, p. 21-34.

Benjamin, M. M., 1978, Effects of competing metals and complexing ligands on trace metal adsorption at the oxide/solution interface: Ph.D. Thesis, Stanford University, Stanford, California.

Benjamin, M. M., and Leckie, J. O., 1980, Adsorption of metals at oxide interfaces: Effects of the concentrations of adsorbate and competing metals: in Baker, R. A., ed., Contamination and Sediments, Vol. 2, Ann Arbor Science Publishers, Ann Arbor, Michigan.

Benjamin, M. M., and Leckie, J. O., 1981a, Multiple-site adsorption of Cd, Cu, Zn, and Pb on amorphous iron oxyhydroxide: J. Colloid Interface Sci., v. 79, p. 209-221.

Benjamin, M. M., and Leckie, J. O., 1981b, Competitive adsorption of Cd, Cu, Zn, and Pb on amorphous iron oxyhydroxide: J. Colloid Interface Sci., v. 83, p. 410.

Berube, Y. G., Onoda, G. Y., and de Bruyn, P. L., 1967, Proton adsorption at the ferric oxide/aqueous solution interface. II. Analysis of kinetic data: Surface Sci., v. 8, p. 448-461.

Bilinski, H., and Schindler, P., 1982, Solubility and equilibrium constants of lead in carbonate solutions (25°C, I=0.3 mol dm^{-3}): Geochim. Cosmochim. Acta, v. 46, p. 921-928.

Bilinski, H., and Stumm, W., 1973, Pb(II) species in natural waters: Swiss Federal Institute of Technology, EAWAG News, No. 1, Jan. 1973.

Bittel, J. E., and Miller, R. J., 1974, Lead, cadmium, and calcium selectivity coefficients on a montmorillonite, illite, and kaolinite: J. Environ. Quality, v. 3, no. 3, p. 250-253.

Bolt, G. H., 1957, Determination of the charge density of silica sols: J. Phys. Chem., v. 61, p. 1166.

Bourg, A. C. M., 1982, ADSORP, a chemical equilibria computer program accounting for adsorption processes in aquatic systems: Environ. Tech. Letters, v. 3, p. 305-310.

Bowden, J. W., Bolland, M. D. A., Posner, A. M., and Quirk, J. P., 1973, Generalized model for anion and cation adsorption at oxide surfaces: Nature, Phys. Sci., v. 245, p. 81-83.

Bowden, J. W., Posner, A. M., and Quirk, J. P., 1977, Ionic adsorption on variable charge mineral surfaces. Theoretical-charge development and titration curves: Aust. J. Soil Research, v. 15, p. 121-136.

Brunauer, S. C., Emmett, P. H., and Teller, E., 1938, Adsorption of gases in multi-molecular layers: Am. Chem. Soc. J., v. 60, p. 309-319.

Burns, R. G., and Burns, V. M., 1977, Mineralogy of ferromanganese nodules: in Glasby, G. P., ed., Marine Manganese Deposits, Elsevier, Amsterdam, p. 184-248.

Byrne, R. H., and Miller, W. L., 1985, Copper (II) carbonate complexation in seawater: Geochim. Cosmochim. Acta, v. 49, p. 1837-1844.

Catts, J. G., 1982, Adsorption of Cu, Pb, and Zn onto birnessite: Ph.D. Thesis, Colorado School of Mines, Golden, Colorado.

Chapman, D. L., 1913, A contribution to the theory of electrocapillarity: Phil. Mag., v. 25, no. 6, p. 475-481.

CODATA Task Group on Key Values for Thermodynamics, 1976, Recommended key values for thermodynamics, 1975: J. Chem. Thermo., v. 8, p. 603-605.

CODATA Task Group on Key Values for Thermodynamics, 1977, Recommended key values for thermodynamics, 1976: J. Chem. Thermo., v. 9, p. 705-706.

Crock, J. G., and Severson, R. C., 1980, Four reference soil and rock samples for measuring element availability in the Western Energy Regions: U.S. Geological Survey Circular No. 841, 16 p.

Davis, J. A., 1977, Adsorption of trace metals and complexing ligands at the oxide/water interface: Ph.D. Thesis, Stanford University, Stanford, California.

Davis, J. A., 1980, Adsorption of natural organic matter from freshwater environments by aluminum oxide: in Baker, R. A., ed., Contaminants and Sediments, Vol. 2, Ann Arbor Science, p. 279-304.

Davis, J. A., 1982, Adsorption of natural dissolved organic matter at the oxide/water interface: Geochim. Cosmochim. Acta, v. 46, p. 2381-2393.

Davis, J. A., and Gloor, R., 1981, Adsorption of dissolved organics in lake water by aluminum oxide. Effect of molecular weight: Environ. Sci. Tech., v. 15, p. 1223-1229.

Davis, J. A., James, R. O., and Leckie, J. O., 1978, Surface ionization and complexation at the oxide/water interface I. Computation of electrical double layer properties in simple electrolytes: J. Colloid Interface Sci., v. 63, no. 3, p. 480-499.

Davis, J. A., and Leckie, J. O., 1978a, Effect of adsorbed complexing ligands on trace metal uptake by hydrous oxides: Environ. Sci. Tech., v. 12, p. 1309-1315.

Davis, J. A., and Leckie, J. O., 1978b, Surface ionization and complexation at the oxide/water interface II. Surface properties of amorphous iron oxyhydroxide and adsorption of metal ions: J. Colloid Interface Sci., v. 67, p. 90-107.

Davis, J. A., and Leckie, J. O., 1979, Speciation of adsorbed ions at the oxide/water interface: in Jenne, E. A., ed., Chemical Modeling in Aqueous Systems: ACS Symp. Ser. No. 93, American Chemical Society, Washington, D. C., p. 299-317.

Davis, J. A., and Leckie, J. O., 1980, Surface ionization and complexation at the oxide/water interface III. Adsorption of anions: J. Colloid Interface Sci., v. 74, p. 32-43.

Duby, P., 1977, The thermodynamic properties of aqueous inorganic copper systems: INCRA Monograph IV: The Metallurgy of Copper, TN1.A1, I55, No. 4.

Dugger, D. L., Stanton, J. H., Irby, B. N., McConnel, B. L., Cummings, W. W., and Maatman, R. W., 1964, The exchange of twenty metal ions with weakly acidic silanol group of silica gel: J. Phys. Chem., v. 68, p. 757-760.

Feitknecht, W., and Schindler, P., 1963, Principles of the determination of solubility constants of hydroxide precipitates: Pure Appl. Chem., v. 6, p. 130-199.

Forbes, E. A., Posner, A. M., and Quirk, J. P., 1976, The specific adsorption of divalent Cd, Co, Cu, Pb, and Zn on goethite: J. Soil Sci., v. 27, p. 154-163.

Gadde, R. R., and Laitinen, H. A., 1973, Study of the sorption of lead by hydrous ferric oxide: Environ. Letters, v. 5, no. 4, p. 223-235.

Garcia-Miragaya, J., and Page, A. L., 1976, Influence of ionic strength and inorganic complex formation on the sorption of trace amounts of Cd by montmorillonite: Soil Sci. Soc. Am. J., v. 40, no. 5, p. 658-663.

Garrels, R. M., and Christ, C. L., 1965, Solutions, Minerals, and Equilibria: Freeman, Cooper and Company, 450 p.

Gedansky, L. M., Wooley, E. M., and Hepler, L. G., 1970, Thermochemistry of compounds and aqueous ions of copper: J. Chem. Thermo., v. 2, p. 561-576.

Gouy, G., 1910, Sur la constitution de la charge electrique a la surface d'un electrolyte: Ann. Phys. (Paris), v. 9, no. 4, p. 457-468.

Grahame, D. C., 1947, The electrical double layer and the theory of electrocapillarity: Chem. Revs., v. 41, p. 441-501.

Gregg, S. G., and Sing, K. S. W., 1967, Surface Area and Porosity: Academic Press, London.

Grim, R. E., 1968, Clay Mineralogy, 2nd Ed.: McGraw-Hill, Inc., 596 p.

Hachiya, K., Sasaki, M., Saruta, Y., Mikami, N., and Yasunaga, T., 1984, Static and kinetic studies of adsorption-desorption of metal ions on a $-Al_2O_3$ surface. 1. Static study of adsorption-desorption: J. Phys. Chem., v. 88, p. 23-27.

Harmsen, K., 1979, Theories of cation adsorption by soil constituents- Discrete-site models, in Bolt, G. H., ed., Soil Chemistry. B. Physico-Chemical Models: Elsevier Scientific Publishing Co., New York, Chapter 4, p. 77-139.

Harrison, J. B., and Berkheiser, V. E., 1982, Anion interactions with freshly prepared hydrous iron oxides: Clays Clay Minerals, v. 30, no. 2, p. 97-102.

Hayes, K. F., and Leckie, J. O., 1986, Mechanism of lead ion adsorption at the goethite/water interface: in J. A. Davis, and K. F. Hayes, eds., Geochemical Processes at Mineral Surfaces: ACS Symposium Series, American Chemical Society, Washington, D.C., chapter 7.

Hayes, K. F., and Leckie, J. O., in press, Modeling ionic strength effects on cation adsorption at hydrous oxide/solution interfaces: submitted to J. Colloid Interface Sci.

Hem, J. D., 1970, Study and interpretation of the chemical characteristics of natural water, 2nd Ed.: U. S. Geological Survey Water Supply Paper 1473, 363 p.

Hildebrand, E. E., and Blum, W. E., 1974, Lead fixation by clay minerals: Naturwissenschaften, v. 61, p. 169-170.

Hingston, F. J., Posner, A. M., and Quirk, J. P., 1968, Adsorption of selenite by goethite: in Gould, R. F., ed., Adsorption From Aqueous Solution, Advances in Chemistry Series no. 79, American Chemical Society, Washington, D. C., p. 82-90.

Hohl, H., and Stumm, W., 1976, Interaction of Pb^{2+} with hydrous $-Al_2O_3$: J. Colloid Interface Sci., v. 55, no. 2, p. 281-288.

Honeyman, B. D., 1984, Cation and anion adsorption at the oxide/solution interface in systems containing binary mixtures of adsorbents: An investigation of the concept of adsorptive additivity: Ph.D. Thesis, Stanford University, Stanford, California.

Hsi, C-K. D., 1981, Sorption of uranium (VI) by iron oxides: PhD Thesis, Colorado School of Mines, Golden, Colorado.

Hsi, C-K. D., and Langmuir, Donald, 1985, Adsorption of uranyl onto ferric oxyhydroxides: Application of the surface complexation site-binding model: Geochim. Cosmochim. Acta, v. 49, p. 1931-1941.

Huang, C. P., 1981, The surface acidity of hydrous solids: in M. A. Anderson, and A. J. Rubin, eds., Adsorption of Inorganics at Solid-Liquid Interfaces: Ann Arbor Science Publishers, Inc., Ann Arbor Michigan, p. 183-218.

Huang, C. P., and Stumm, W. J., 1972, The specific surface area of α-Al_2O_3: Surface Sci., v. 32, p. 287-296.

Huang, C. P., and Stumm, W. J., 1973, Specific adsorption of cations on hydrous α-Al_2O_3: J. Colloid Interface Sci., v. 43, no. 2, p. 409-420.

Jackson, M. L., 1969, Soil Chemical Analysis Advanced Course: published by Jackson, Madison, Wisconsin, 991 p.

James, R. O., 1981, Surface ionization and complexation at the colloid/aqueous electrolyte interface: in M. A. Anderson, and A. J. Rubin, eds., Adsorption of Inorganics at Solid-Liquid Interfaces: Ann Arbor Science Publishers, Ann Arbor, Michigan, p. 219-262.

James, R. O., Davis, J. A., and Leckie, J. O., 1978, Computer simulation of the conductometric and potentiometric titrations of the surface groups on ionizable latexes: J. Colloid Interface Sci., v. 65, p. 331-344.

James, R. O., and Healy, T. W., 1972a, Adsorption of hydrolyzable metal ions at the oxide-water interface, I. Co(II) adsorption on SiO_2 and TiO_2 as model systems: J. Colloid Interface Sci., v. 40, no. 1, p. 42-52.

James, R. O., and Healy, T. W., 1972b, Adsorption of hydrolyzable metal ions at the oxide-water interface, II. Charge reversal of SiO_2 and TiO_2 colloids by adsorbed Co(II), La(III), and Th(IV) as model systems: J. Colloid Interface Sci., v. 40, no. 1, p. 53-64.

James, R. O., and Healy, T. W., 1972c, Adsorption of hydrolyzable metal ions at the oxide-water interface, III. A thermodynamic model of adsorption: J. Colloid Interface Sci., v. 40, no. 1, p. 65-79.

James, R. O., and MacNaughton, M. G., 1977, The adsorption of aqueous heavy metals on inorganic minerals: Geochim. Cosmochim. Acta, v. 41, p. 1549-1555.

James, R. O., and Parks, G. A., 1982, Characterization of aqueous colloids by their electrical double layer and intrinsic surface chemical properties: in Matijevic, E., ed., Surface and Colloid Science, Vol. 12, Plenum Press, New York, New York, p. 119-216.

James, R. O., Stiglich, P. J., and Healy, T. W., 1975, Analysis of models of adsorption of metal ions at oxide-water interfaces: Disc. Faraday Soc., v. 59, p. 142-156.

James, R. O., Stiglich, P. J., and Healy, T. W., 1981, The TiO_2/aqueous electrolyte system - Applications of colloidal models and model colloids: in Tewari, P. H., ed., Adsorption From Aqueous Solutions, Plenum Press, New York, New York, p. 19-40.

Jenne, E. A., 1968, Controls on Mn, Fe, Co, Ni, Cu, and Zn concentrations in soils and water. The significant role of hydrous Mn and Fe oxides: in Trace Inorganics in Water, Adv. Chem. Ser. No. 73, American Chemical Society, Washington, D. C., p. 337-387.

Jenne, E. A., 1977, Trace element sorption by sediments and soils- Sites and processes: in Chappel, W., and Petersen, K., eds., Symposium on Molybdenum in the Environment, M. Dekker Inc., New York, New York, p. 425-553.

Jenne, E. A., and Luoma, S. N., 1977, The forms of trace elements in soils, sediment, and associated waters: in Wildung, R., and Drucker, H., eds., Biological Implications of Metals in the Environment, CONF-750929, NTIS, Springfield, Virginia, p. 110-143.

Kinniburgh, D. G., and Jackson, M. L., 1981, Cation adsorption by hydrous metal oxides and clay: in Anderson, M. A., and Rubin, A. J., eds., Adsorption of Inorganics at Solid-Liquid Interfaces, Ann Arbor Science Publishers, Ann Arbor, Michigan, p. 91-160.

Krishnamoorthy, C., and Overstreet, R., 1949, Theory of ion exchange relationships: Soil Sci., v. 68, p. 307-315.

Krishnamoorthy, C., and Overstreet, R., 1950, An experimental evaluation of ion exchange relationships: Soil Sci., v. 69, p. 41-53.

Langmuir, Donald, 1981, The power exchange function: A general model for metal adsorption onto geological materials: in Tewari, P. H., ed., Adsorption From Aqueous Solutions, Plenum Press, New York, New York, p. 1-18.

Langmuir, Donald, 1984, Personal Communication (Colorado School of Mines, Golden, Colorado).

Leckie, J. O., 1986, Personal Communication (Stanford University, Stanford, California).

Leckie, J. O., and James, R. O., 1974, Control mechanisms for trace metals in natural waters: in Rubin, A. J., ed., Aqueous-Environmental Chemistry of Metals, Ann Arbor Science Publishers, Ann Arbor, Michigan, p. 1-76.

Leckie, J. O., Tripathi, V. S., and Kent, D. B., 1986, Modeling solute adsorption as surface complexation in porous media: II. Criteria for selecting reaction stoichiometries: lecture given at the 8th Rocky Mountain Regional Meeting of the American Chemical Society, Denver, Colorado, June 8-12, 1986.

Lion, L. W., Altmann, R. S., and Leckie, J. O., 1982, Trace metal adsorption characteristics of estuarine particulate matter: Evaluation of contributions of Fe/Mn oxide and organic surface coatings: Environ. Sci. Tech., v. 16, p. 660-666.

Loganathan, P., and Burau, R. G., 1973, Sorption of heavy metal ions by a hydrous manganese oxide: Geochim. Cosmochim. Acta, v. 37, p. 1277-1293.

Lyklema, J., and Overbeek, J. T. G., 1961, Electrochemistry of silver iodide, the capacity of the double layer at the silver iodide-water interface: J. Colloid Sci., v. 16, p. 595-608.

Maes, A., Peigneur, P., and Cremers, A., 1975, Thermodynamics of transition metal ion exchange in montmorillonite: Proc. International Clay Conference, Madrid, Spain, p. 319-329.

Menzel, R. G., and Jackson, M. L., 1950, Mechanism of sorption of hydroxy cupric ion by clays: Soil Sci. Soc. Am. Proc., v. 15, p. 122-124.

Moody, J. R., and Lindstrom, R. M., 1977, Selection and cleaning of plastic containers for storage of trace element samples: Anal. Chem., v. 49, no. 14, p. 2264-2267.

Morel, F. M. M., 1983, Principles of Aquatic Chemistry: Wiley-Interscience, New York, New York, 446 p.

Mouvet, C., and Bourg, A. C. M., 1983, Speciation (including adsorbed species) of copper, lead, nickel, and zinc in the Meuse River. Observed results compared to values calculated with a chemical equilibrium program: Water Res., v. 17, p. 641-649.

Naumov, G. B., Ryzhenko, B. N., and Khodakovsky, F. L., 1974, Handbook of thermodynamic data: National Technical Information Service, U. S. Dept. of Commerce, Springfield, VA.

Ozsvath, D., 1979, Modelling heavy metal sorption from subsurface water with the n-power exchange function: MS Thesis in Geochemistry, The Pennsylvania State University, University Park, Pennsylvania, 61 p.

Parker, V. B., Wagman, D. D., and Evans, W. H., 1971, Selected values of chemical thermodynamic properties: National Bureau of Standards Technical Note 270-6, National Bureau of Standards, Washington, D. C.

Parker, V. B., Wagman, D. D., and Garvin, D., 1976, Selected thermochemical data compatible with the CODATA recommendations: NBSIR 75-986, Interim Report, Office of Standard Reference Data, National Bureau of Standards, Washington, D. C.

Parks, G. A., 1965, The isoelectric points of solid oxides, solid hydroxides, and aqueous hydroxo complex systems: Chemical Reviews, v. 65, p. 177-198.

Parks, G. A., and de Bruyn P. L., 1962, The zero point of charge of oxides: J. Phys. Chem., v. 66, p. 967.

Posselt, H. S., Anderson, F. J., and Weber, W. J., 1968, Cation sorption on colloidal hydrous manganese dioxide: Current Research, v. 2, no. 12, p. 1087-1093.

Rhoades, J. D., 1982, Cation exchange capacity: in Page, A. L., Miller, R. H., and Keeney, D. R., eds., Methods of Soil Analysis Part 2, American Society of Agronomy, Inc., and Soil Science Society of America, Inc., Publisher, Madison, Wisconsin, p. 149-157.

Rickard, D. T., and Nriagu, J. O., 1978, Aqueous environmental chemistry of lead: in Nriagu, J. O., ed., The Biogeochemistry of Lead in the Environment, Elsevier/North-Holland Biomedical Press, Amsterdam, Ch. 8, p. 219-284.

Riese, A. C., 1982, Adsorption of radium and thorium onto quartz and kaolinite: A comparison of solution/surface equilibria models: PhD Thesis, Colorado School of Mines, Golden, Colorado.

Riffaldi, R., Levi-Minzi, R., and Soldatini, G. F., 1976, Pb adsorption by soils: II. Specific adsorption: Water, Air, Soil Pollution, v. 6, no. 1, p. 119-128.

Robie, R. A., Hemingway, B. S., and Fisher, J. R., 1978, Thermodynamic properties of minerals and related substances at 298.15 K and 1 bar (10^5 Pascals) pressure and at higher temperatures: U. S. Geological Survey Bulletin 1452, 456 p.

Rubin, A. J., and Mercer, D. L., 1981, Adsorption of free and complexed metals from solution by activated carbon: in Anderson, M. A., and Rubin, A. J., eds., Adsorption of Inorganics at Solid-Liquid Interfaces, Ann Arbor Science Publishers, Inc., Ann Arbor, Michigan, p. 295-326.

Russel, J. D., Paterson, E., Fraser, A. R., and Farmer, V. C., 1975, Adsorption of carbon dioxide on goethite surfaces, and its inplications for anion adsorption: J. Chem. Soc. London Faraday Trans., v. 71, p. 1623-1630.

Sadiq, M., and Lindsay, W. L., 1979, Selection of standard free energies of formation for use in soil chemistry: Technical Bulletin 134, Department of Agronomy, Colorado State University, Fort Collins, Colorado.

Sanchez, A. L., Murray, J. W., and Sibley, T. H., 1985, The adsorption of plutonium IV and V on goethite: Geochim. Cosmochim. Acta, v. 49, p. 2297-2307.

Schindler, P. W., 1967, Heterogeneous equilibria involving oxides, hydroxides, carbonates, and hydroxide carbonates: in Gould, R. F., ed., Equilibrium Concepts in Natural Water Systems, Advances in Chemistry Series 67, American Chemical Society, Washington, D. C., p. 196-221.

Schindler, P. W., 1981, Surface complexes at oxide-water interfaces: in Anderson, M. A., and Rubin, A. J., eds., Adsorption at the Solid-Liquid Interface, Ann Arbor Science Publishers, Ann Arbor, Michigan.

Schindler, P. W.,Althaus, H., Hofer, F., and Minder, W., 1965, Loslichkeitsprodukte von Zinkoxid, Kupferhydroxid und Kupferoxid in Abhangigkeit von Teilchengrosse und molarer Oberflache. Ein Beitrag zur Thermodynamik von Grenzflachen fest-flussig: Helvetica Chimica Acta, v. 48, p. 1204-1215.

Schindler, P. W., Fiirst, B., Dick, R., and Wolf, P. B., 1976, Surface complex formation with Fe^{2+}, Cu^{2+}, Cd^{2+}, and Pb^{2+}: J. Colloid Interface Sci., v. 55, no. 2, p. 469-475.

Schindler, P., Reinert, M., and Gamsjager, H., 1968, Loslichkeitskonstanten und Freie Bildungsenthalpien von $Cu_2(OH)_2CO_3$ (Malachit) und $Cu_3(OH)_2(CO_3)_2$ (Azurit) bei 25°C: Helvetica Chimica Acta, v. 51, no. 8, p. 1845-1856.

Shaw, D. J., 1980, Introduction to Colloid and Surface Chemistry, 3rd Ed.: Butterworths.

Silva, R. J., Benson, L. V., Yee, A. W., and Parks, G. A., 1979, Collection and generation of transport data: Theoretical and experimental evaluation of waste transport in selected rocks: Waste Isolation Safety Assessment Program, Annual Progress Report, Battelle/ONWI Subcontract No. 45901AK.

Skoog, D. A., and West, D. M., 1976, Fundamentals of Analytical Chemistry, 3rd Ed.: Saunders College Publishing, Philadelphia, Pennsylvania.

Smith, R. M., and Martell, A. E., 1976, Critical Stability Constants, Vol. 4. Inorganic Complexes: Plenum Press, New York, New York, 257 p.

Soldatini, G. F., Riffaldi, R., and Levi-Minzi, R., 1976, Pb adsorption by soils: I. Adsorption as measured by the Langmuir and Freundlich isotherms: Water, Air, Soil Pollution, v. 6, no. 1, p. 111-118.

Steger, H. F., 1973, On the mechanism of the adsorption of trace copper by bentonite: Clays Clay Minerals, v. 21, no. 6, p. 429-436.

Stern, O., 1924, The theory of the electrolytic double-layer: Z. Elektrochem, v. 30, p. 508-516.

Stumm, W., Huang, C. P., and Jenkins, S. R., 1970, Specific chemical interactions affecting the stability of dispersed systems: Croat. Chem. Acta, v. 42, p. 223-245.

Stumm, W., Kummert, R., and Sigg, L., 1980, A ligand exchange model for the adsorption of inorganic and organic ligands at hydrous oxide interfaces: Croat. Chem. Acta, v. 53, p. 291-312.

Stumm, W., and Morgan, J. J., 1981, Aquatic Chemistry, 2nd Ed.: Wiley-Interscience, New York, 780 p.

Symes, J. L., and Kester, D. R., 1984, Thermodynamic stability studies of the basic copper carbonate mineral, malachite: Geochim. Cosmochim. Acta, v. 48, p. 2219-2229.

Tripathi, V. S., 1984, Uranium (VI) transport modeling: Geochemical data and submodels: Ph.D. Thesis, Stanford University, Stanford, California.

Truesdell, A. H., and Christ, C. L., 1968, Cation exchange in clays interpreted by regular solution theory: Am. J. Sci., v. 266, p. 402-412.

van Olphen, H., 1977, An Introduction to Clay Colloid Chemistry: Wiley-Interscience Publishers, New York, New York, 318 p.

Vuceta, J., and Morgan, J. J., 1978, Chemical modeling of trace metals in fresh water. Role of complexation and adsorption: Environ. Sci. Tech., v. 12, p. 1302-1309.

Wagman, D. D., Evans, W. H., Parker, V. B., Halow, I., Bailey, S. M., and Schumm, R. H., 1968, Selected values of chemical thermodynamic properties: National Bureau of Standards Technical Note 270-3.

Wagman, D. D., Evans, W. H., Parker, V. B., and Schumm, R. H., 1976, Chemical thermodynamic properties of compounds of sodium, potassium and rubidium: An interim tabulation of selected values: U.S. National Bureau of Standards Interim Report 76-1034, National Bureau of Standards, Washington, D. C.

Westall, J. C., 1980, Chemical equilibrium including adsorption on charged surfaces: Adv. Chem. Ser. No. 189 (Part. Water), American Chemical Society, Washington D. C., p. 33-44.

Westall, J. C., and Hohl, H., 1980, A comparison of electrostatic models for the oxide/solution interface: Advances in Colloid and Interface Science, v. 12, p. 265-294.

Westall, J. C., Zachary, J. L., and Morel, F. M., M., 1976, MINEQL, a computer program for the calculation of chemical equilibrium composition of aqueous systems: Water Quality Laboratory, Technical Note 18, Department of Civil Engineering, Massachusetts Institute of Technology, Cambridge, Massachusetts.

Yates, D. E., 1975, The structure of the oxide/aqueous electrolyte interface: Ph.D. Thesis, University of Melbourne, Melbourne, Australia.

Yates, D. E., and Healy, T. W., 1975, Mechanism of anion adsorption at the ferric and chromic oxide/water interface: J. Colloid Interface Sci., v. 52, p. 222-228.

Yates, D. E., and Healy, T. W., 1976, The structure of the silica/electrolyte interface: J. Colloid Interface Sci., v. 55, p. 9-19.

Yates, D. E., Levine, S., and Healy, T. W., 1974, Site-binding model of the electrical double layer at the oxide/water interface: Chem. Soc. Faraday Transactions I., v. 70, p. 1807-1818.

Youden, W. J., 1951, Statistical Methods for Chemists: John Wiley and Sons, Inc., New York, New York, 126 p.

Zachara, J. M., Girvin, D. C., Schmidt, R. L., and Resch, C. T., in press, Chromate adsorption on amorphous iron oxyhydroxide in the presence of major groundwater ions: Submitted to Environ. Sci. Tech.

Zirino, A., and Yamamoto, S., 1972, A pH-dependent model for the chemical speciation of copper, zinc, cadmium, and lead in seawater: Limnology and Oceanography, v. 17, no. 5, p. 661-671.

APPENDIX I

Computer Programs Used for Data Analysis

```
C       NORMV IS USED TO NORMALIZE POTENTIOMETRIC
C       TITRATION VOLUMES TO STRONG ACID AND BASE CONCENTRATIONS
C       OF 0.1000 M.  IT THEN DETERMINES THE DIFFERENCE BETWEEN
C       VOLUME OF ACID AND BASE ADDED TO THE SYSTEM AT A GIVEN
C       POINT IN THE TITRATION.  INPUT AND OUTPUT FILES ARE
C       INTERACTIVE.  THREE OUTPUT FILES ARE WRITTEN:
C              1. ALL THE PH AND VOLUME DATA.
C              2. DATA INTENDED FOR USE BY A PLOT PROGRAM.
C              3. DATA INTENDED FOR REVISION FOR THE PROGRAM SIGMA.
C       INPUT VOLUMES ARE IN MLS. THERE MUST BE A 0 AT THE END OF
C       THE INPUT DATA SET.         K. SMITH
C
        DOUBLE PRECISION FILIN, ALL, GRAPH, SIGMA
2       WRITE (4,3)
3       FORMAT(5X,'ENTER INPUT FILE NAME',/)
        READ (4,4) FILIN
        OPEN (UNIT=21, FILE=FILIN)
4       FORMAT (A10)
        WRITE (4,5)
5       FORMAT(/,5X,'ENTER 3 OUTPUT FILE NAMES (1 PER LINE)',/)
        READ (4,4) ALL
        READ (4,4) GRAPH
        READ (4,4) SIGMA
        OPEN (UNIT=10, FILE=ALL)
        OPEN (UNIT=11, FILE=GRAPH)
        OPEN (UNIT=12, FILE=SIGMA)
        READ (21,9) CONAC, CONBA
9       FORMAT (2G)
C
C       READ IN EACH INCREMENT OF TITRATION DATA:
        WRITE (10,40)
        DVOLN = 0.0
        VOLACN = 0.0
        VOLBAN = 0.0
        DVOLNX = 0.0
20      READ (21,30) INDEX, PHINAL, VOLAC, VOLBA
        IF (INDEX .EQ. 0) GO TO 60
30      FORMAT (4G)
C
C       NORMALIZE TITRATION VOLUMES:
        VOLACN = (VOLAC * CONAC) / 0.1000
        VOLBAN = (VOLBA * CONBA) / 0.1000
        DVOLN = VOLBAN - VOLACN
C
        WRITE (10,50) INDEX, PHINAL, DVOLN, VOLACN, VOLBAN
        WRITE (11,55) DVOLN, PHINAL
        DVOLNX = -DVOLN
        WRITE (12,56) INDEX, PHINAL, VOLACN, VOLBAN, DVOLNX
40      FORMAT('INDEX',4X,'PH',4X,'VOLUME DIFFERENCE',
     1  4X,'NORM. VOL. ACID',4X,'NORM. VOL. BASE')
50      FORMAT(/, I3, 1X, F8.3, 3X, F9.3, 12X, F9.3, 10X, F9.3)
55      FORMAT (2F)
56      FORMAT (I3, 4F)
        GO TO 20
        CONTINUE
C
60      CLOSE (UNIT=10)
        CLOSE (UNIT=11)
        CLOSE (UNIT=12)
70      WRITE (4,75)
75      FORMAT(//,5X,'ANOTHER SET OF DATA? ("Y" OR "N")',/)
        READ (4,80) ANS
80      FORMAT (A1)
        IF (ANS .EQ. 'Y') GO TO 2
        IF (ANS .NE. 'N') GO TO 70
        STOP
        END
```

```
C       SIGMA DETERMINES THE SURFACE CHARGE OF A SOL FROM
C       POTENTIOMETRIC TITRATION DATA.  VOLUMES ARE AS
C       ML'S, SURFACE AREA IS IN TERMS OF SQUARE METERS, AND
C       SIGMA IS IN UNITS OF MICRO C/SQUARE CMS.  INPUT AND
C       OUTPUT FILES ARE INTERACTIVE.  TWO OUTPUT FILES ARE
C       WRITTEN:  ONE GIVES ALL THE DATA, AND THE OTHER IS
C       INTENDED FOR USE BY A PLOT PROGRAM. THERE MUST BE A 0 AT
C       THE END OF THE INPUT FILE.  INPUT DATA MUST BE NORMALIZED
C       TO ACID AND BASE CONCENTRATIONS OF 0.1 M, HAVE THE EFFECTS
C       OF THE BLANK TITRATION REMOVED, AND HAVE HAD AN ORIGINAL
C       VOLUME OF 50 ML.      K. SMITH
C
        DOUBLE PRECISION FILIN, ALL, PLOT
2       WRITE (4,3)
3       FORMAT(5X,'ENTER INPUT FILE NAME',/)
        READ (4,4) FILIN
        OPEN (UNIT=21, FILE=FILIN)
4       FORMAT (A10)
        WRITE (4,5)
5       FORMAT(/,5X,'ENTER 2 OUTPUT FILE NAMES (1 PER LINE)',/)
        READ (4,4) ALL
        READ (4,4) PLOT
        OPEN (UNIT=11, FILE=ALL)
        OPEN (UNIT=12, FILE=PLOT)
C
C       READ IN INITIAL DATA:
        READ(21,6)PHINT,VOLINT,GAMMAH,GAMMOH,AREA
6       FORMAT (5G)
C
C       CALCULATE THE CONCENTRATION OF H AND OH:
        PHX = 0.0
        ACTH = 0.0
        CONCHI = 0.0
        POHP = 0.0
        POHX = 0.0
        ACTOH = 0.0
        CONOHI = 0.0
        PHX = -PHINT
        ACTH = 10.0**PHX
        CONCHI = ACTH / GAMMAH
        POHP = 14.0 - PHINT
        POHX = -POHP
        ACTOH = 10.0**POHX
        CONOHI = ACTOH / GAMMOH
        WRITE (11,7)
        WRITE (11,8) PHX, ACTH, CONCHI, GAMMAH
        WRITE (11,9)
        WRITE (11,8) POHX, ACTOH, CONOHI, GAMMOH
7       FORMAT (30X, 'H DATA')
8       FORMAT (/, G, 5X, G, 5X, G, 5X, G)
9       FORMAT (//, 30X, 'OH DATA')
C
C       READ IN EACH INCREMENT OF THE DATA:
        WRITE (11,16)
        PHY = 0.0
        ACTHY = 0.0
        CONCHT = 0.0
        POHY = 0.0
        POHZ = 0.0
        ACTOHT = 0.0
        CONOHT = 0.0
        GAMMA = 0.0
        SIGMA = 0.0
10      READ (21,15) INDEX, PHINAL, VOLACN, VOLBAN, DVOLNX
        IF (INDEX .EQ. 0) GO TO 20
15      FORMAT (5G)
C
```

```
C       CALCULATE THE CONCENTRATION OF H AND OH:
        PHY = -PHINAL
        ACTHY = 10.0**PHY
        CONCHT = ACTHY / GAMMAH
        POHY = 14.0 - PHINAL
        POHZ = -POHY
        ACTOHT = 10.0**POHZ
        CONOHT = ACTOHT / GAMMOH
C
C       CALCULATE SURFACE CHARGE:
        GAMMA=((CONCHI-CONOHI)*(VOLINT/1000.0))+(0.1*(DVOLNX/1000.0))
     1  -((CONCHT-CONOHT)*((VOLINT+VOLACN+VOLBAN)/1000.0))
        SIGMA=(1000000.0 * 96487.0 * GAMMA) / (AREA * 10000.0)
C
        WRITE (12,17) PHINAL, SIGMA
        WRITE (11,18) INDEX, SIGMA, PHINAL, GAMMA, CONCHT, CONOHT
16      FORMAT(///,12X,'INDEX',7X,'SIGMA',8X,'PH',10X,'GAMMA',
     1  15X,'CONC H',13X,'CONC OH')
17      FORMAT (2F)
18      FORMAT (/,G,4X,F10.3,4X,F8.3,4X,G,4X,G,4X,G)
        GO TO 10
        CONTINUE
C
20      CLOSE (UNIT=11)
        CLOSE (UNIT=12)
25      WRITE (4,30)
30      FORMAT(//,5X,'ANOTHER SET OF DATA? ("Y" OR "N")',/)
        READ (4,35) ANS
35      FORMAT (A1)
        IF (ANS .EQ. 'Y') GO TO 2
        IF (ANS .NE. 'N') GO TO 25
        STOP
        END
```

```
C       PKA1 CALCULATES THE PARAMETERS FOR A DOUBLE EXTRAPOLATION
C       DIAGRAM FOR A POSITIVELY-CHARGED SURFACE.  NECESSARY INPUT
C       IS THE TOTAL NUMBER OF SITES AS MICRO C/SQ CM, AND THE IONIC
C       STRENGTH.  THE INPUT FILE OF PH AND SIGMA VALUES MUST HAVE A
C       0 AT THE END.  INPUT AND OUTPUT FILES ARE INTERACTIVE.
C       TWO OUTPUT FILES ARE WRITTEN:  ONE GIVES THE PARAMETERS AND
C       THE OTHER IS INTENDED FOR USE BY A PLOT PROGRAM.   K. SMITH
C
        DOUBLE PRECISION FILIN, ALL, PLOT, IONICS, LSUBT
2       WRITE (4,3)
3       FORMAT(5X,'ENTER INPUT FILE NAME',/)
        READ (4,4) FILIN
        OPEN (UNIT=21, FILE=FILIN)
4       FORMAT (A10)
        WRITE (4,5)
5       FORMAT(/,5X,'ENTER 2 OUTPUT FILE NAMES (1 PER LINE)',/)
        READ (4,4) ALL
        READ (4,4) PLOT
        OPEN (UNIT=11, FILE=ALL)
        OPEN (UNIT=12, FILE=PLOT)
C
C       READ IN INITIAL DATA:
        WRITE (4,6)
6       FORMAT(/,1X,'ENTER VALUE FOR TOTAL SITES (MICRO C/SQ.CM.)',/)
        READ (4,7) TSITES
7       FORMAT (G)
        WRITE (4,8)
8       FORMAT(/,1X,'ENTER VALUE FOR IONIC STRENGTH (MOLS/L)',/)
        READ (4,9) IONICS
9       FORMAT (G)
C
C       READ IN EACH INCREMENT OF THE DATA:
        WRITE (11,16)
        FRAC = 0.0
        SUBT = 0.0
        LSUBT = 0.0
        PKA1 = 0.0
        FION = 0.0
10      READ (21,15) PHINAL, SIGMA
        IF (PHINAL .EQ. 0) GO TO 20
15      FORMAT (2F)
C
C       CALCULATE THE PARAMETERS:
        FRAC = SIGMA / TSITES
        SUBT = FRAC / (1.0 - FRAC)
        LSUBT = LOG10(SUBT)
        PKA1 = PHINAL + LSUBT
        FION = FRAC + (0.05 * (SQRT(IONICS)))
C
        WRITE (12,17) FION, PKA1
        WRITE (11,18) PKA1, FION, FRAC
16      FORMAT(///,2X,'PKA1',7X,'I TERM',4X,'FRACTIONAL SURF. CHARGE')
17      FORMAT (2F)
18      FORMAT (/,F7.3,4X,G10.3,9X,G10.3)
        GO TO 10
        CONTINUE
C
20      CLOSE (UNIT=11)
        CLOSE (UNIT=12)
25      WRITE (4,30)
30      FORMAT(//,5X,'ANOTHER SET OF DATA? ("Y" OR "N")',/)
        READ (4,35) ANS
35      FORMAT (A1)
        IF (ANS .EQ. 'Y') GO TO 2
        IF (ANS .NE. 'N') GO TO 25
        STOP
        END
```

```
C       PKA2 CALCULATES THE PARAMETERS FOR A DOUBLE EXTRAPOLATION
C       DIAGRAM FOR A NEGATIVELY-CHARGED SURFACE.  NECESSARY INPUT
C       IS THE TOTAL NUMBER OF SITES AS MICRO C/SQ CM, AND THE IONIC
C       STRENGTH.  THE INPUT FILE OF PH AND SIGMA VALUES MUST HAVE A
C       0 AT THE END.  INPUT AND OUTPUT FILES ARE INTERACTIVE.
C       TWO OUTPUT FILES ARE WRITTEN:  ONE GIVES THE PARAMETERS AND
C       THE OTHER IS INTENDED FOR USE BY A PLOT PROGRAM.   K. SMITH
C
        DOUBLE PRECISION FILIN, ALL, PLOT, IONICS, LSUBT
2       WRITE (4,3)
3       FORMAT(5X,'ENTER INPUT FILE NAME',/)
        READ (4,4) FILIN
        OPEN (UNIT=21, FILE=FILIN)
4       FORMAT (A10)
        WRITE (4,5)
5       FORMAT(/,5X,'ENTER 2 OUTPUT FILE NAMES (1 PER LINE)',/)
        READ (4,4) ALL
        READ (4,4) PLOT
        OPEN (UNIT=11, FILE=ALL)
        OPEN (UNIT=12, FILE=PLOT)
C
C       READ IN INITIAL DATA:
        WRITE (4,6)
6       FORMAT(/,1X,'ENTER VALUE FOR TOTAL SITES (MICRO C/SQ.CM.)',/)
        READ (4,7) TSITES
7       FORMAT (G)
        WRITE (4,8)
8       FORMAT(/,1X,'ENTER VALUE FOR IONIC STRENGTH (MOLS/L)',/)
        READ (4,9) IONICS
9       FORMAT (G)
C
C       READ IN EACH INCREMENT OF THE DATA:
        WRITE (11,16)
        FRAC = 0.0
        SUBT = 0.0
        LSUBT = 0.0
        PKA2 = 0.0
        FION = 0.0
10      READ (21,15) PHINAL, SIGMA
        IF (PHINAL .EQ. 0) GO TO 20
15      FORMAT (2F)
C
C       CALCULATE THE PARAMETERS:
        FRAC = (-SIGMA) / TSITES
        SUBT = FRAC / (1.0 - FRAC)
        LSUBT = LOG10(SUBT)
        PKA2 = PHINAL - LSUBT
        FION = FRAC + (0.1 * (SQRT(IONICS)))
C
        WRITE (12,17) FION, PKA2
        WRITE (11,18) PKA2, FION, FRAC
16      FORMAT(///,2X,'PKA2',7X,'I TERM',4X,'FRACTIONAL SURF. CHARGE')
17      FORMAT (2F)
18      FORMAT (/,F7.3,4X,G10.3,3X,G10.3)
        GO TO 10
        CONTINUE
C
20      CLOSE (UNIT=11)
        CLOSE (UNIT=12)
25      WRITE (4,30)
30      FORMAT(//,5X,'ANOTHER SET OF DATA? ("Y" OR "N")',/)
        READ (4,35) ANS
35      FORMAT (A1)
        IF (ANS .EQ. 'Y') GO TO 2
        IF (ANS .NE. 'N') GO TO 25
        STOP
        END
```